

2011

Finite Element Simulation of Fire Induced Spalling in High Strength Concrete Slabs

Shunan Bo
Lehigh University

Follow this and additional works at: <http://preserve.lehigh.edu/etd>

Recommended Citation

Bo, Shunan, "Finite Element Simulation of Fire Induced Spalling in High Strength Concrete Slabs" (2011). *Theses and Dissertations*. Paper 1195.

This Thesis is brought to you for free and open access by Lehigh Preserve. It has been accepted for inclusion in Theses and Dissertations by an authorized administrator of Lehigh Preserve. For more information, please contact preserve@lehigh.edu.

**Finite Element Simulation of Fire Induced Spalling in High
Strength Concrete Slabs**

By

Shunan Bo

A Thesis

Presented to the Graduate and Research Committee

Of Lehigh University

In Candidacy for the Degree of

Master of Science

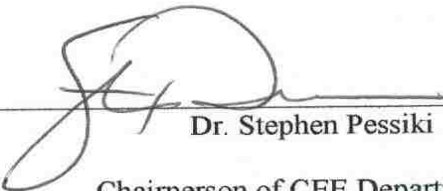
In Civil and Environmental Engineering

Lehigh University

May 2011

This thesis is accepted and approved in partial fulfillment of the requirements for the Master of Science.

Shuman Bo
May 6th, 2011
May 6th, 2011


Dr. Stephen Pessiki

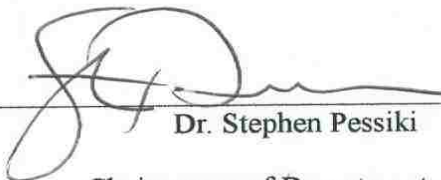
Chairperson of CEE Department
Lehigh University

Thesis Advisor

Nicole Leo Braxtan
Dr. Nicole Leo Braxtan

Assistant Professor of CEE Department
Manhattan College

Thesis Co-Advisor


Dr. Stephen Pessiki
Chairperson of Department

Acknowledgements

I would like to express my thanks to Professor Stephen Pessiki who served as my thesis director. He promoted the interesting topic and discussed with my about the perspectives to carry out the analyses. He always inspired me by asking questions, each time I found the problems were clearer and finally I organized all the analyses together and got this thesis done. Researching and learning with Professor Pessiki was a rewarding and enjoyable time. Also I would like to thank Dr. Nicole Leo, it was she who brought all the background knowledge I needed for my research and patiently discussed with me about the simulation of heat transfer in ABAQUS. She dedicated her time to meet me almost every week to check how my modeling goes. I really appreciate her support and her research experience shared with me.

I would like to thank my parents for always supporting me and having faith in me. And to Fei, without your encourage and support, I could not get through all that depressed time and started over to archive my goals.

Contents

Certificate of Approval	ii
Acknowledgements.....	iii
List of Tables	viii
List of Figures	xi
Abstract.....	1
1 Introduction	2
1.1 Introduction	2
1.1.1 Research objective.....	2
1.1.2 Summary of approach.....	2
1.2 Organization of report	3
1.3 Summary of findings.....	3
1.4 Notation.....	4
2 Background.....	6
2.1 Introduction	6
2.2 Spalling phenomenon.....	6
2.2.1 Definition of spalling.....	6
2.2.2 Parameters influencing spalling.....	6
2.3 Previous research.....	9
2.3.1 Kodur.....	9

2.3.2	Others.....	12
2.4	Fire scenarios.....	13
2.4.1	Fire I	13
2.4.2	Compartment fires	14
2.4.2.1	Compartment description	14
2.4.2.2	Fire II.....	14
2.4.2.3	Fire III	14
2.4.3	Comparison of fire scenarios	15
2.5	Thermal properties of the concrete used in analyses.....	15
2.6	Yield Strength of Reinforced Steel Bars	17
3	Finite element analysis procedure	25
3.1	Introduction	25
3.2	Geometry.....	25
3.3	Simulation of spalling rates.....	28
3.4	Text matrix	30
3.5	Boundary conditions	30
3.6	Loads	30
3.7	Analysis methods	31
4	Analysis Results-Temperatures	36
4.1	Introduction	36

4.2	Nodal temperature	37
4.2.1	Specimens exposed to fire I.....	37
4.2.1.1	Model 100 develops spalling rate I	37
4.2.1.2	Model 100 develops spalling rate II.....	38
4.2.1.3	Model 100 develops no spalling	39
4.2.1.4	Model 300 develops spalling rate I	39
4.2.1.5	Model 300 develops spalling rate II.....	39
4.2.1.6	Model 300 develops no spalling	40
4.2.2	Specimens exposed to fire II	40
4.2.2.1	Model 100 develops spalling rate I	40
4.2.2.2	Model 100 develops spalling rate II.....	40
4.2.2.3	Model 100 develops no spalling	41
4.2.2.4	Model 300 develops spalling rate I	41
4.2.2.5	Model 300 develops spalling rate II.....	41
4.2.2.6	Model 300 develops no spalling	41
4.2.3	Specimens exposed to fire III	42
4.2.3.1	Model 100 develops spalling rate I	42
4.2.3.2	Model 100 develops spalling rate II.....	42
4.2.3.3	Model 100 develops no spalling	43
4.2.3.4	Model 300 develops spalling rate I	43
4.2.3.5	Model 300 develops spalling rate II.....	43
4.2.3.6	Model 300 develops no spalling	43
4.3	Summary of results.....	44

4.3.1	Nodal temperature comparison of the spalling case and no spalling case.....	44
4.3.1.1	Model 100 exposed to fire I	45
4.3.1.2	Model 100 exposed to fire II.....	45
4.3.1.3	Model 100 exposed to fire III.....	45
4.3.1.4	Model 300 exposed to fire I	46
4.3.1.5	Model 300 exposed to fire II.....	46
4.3.1.6	Model 300 exposed to fire III.....	46
4.3.2	Reduction of reinforcement strength	46
4.3.3	Observation.....	51
4.3.4	Conclusion.....	53
5	Conclusions and Future Work	100
5.1	Introduction	100
5.2	Conclusions	100
5.3	Future Work	101
6	References	102
7	Vita	104

List of Tables

Table 2-1	Properties and Results for Tested RC Beams.....	18
Table 2-2	Spalling Rates from Tests.....	18
Table 2-3	Fire I, Fire II, and Fire III.....	18
Table 2-4	Thermal conductivity of the concrete used in analyses.....	19
Table 2-5	Specific heat of the concrete used in analyses.....	19
Table 3-1	Spalling depth I.....	31
Table 3-2	Spalling depth II.....	32
Table 3-3	Analysis Scenarios.....	32
Table 3-4	Boundary conditions--convection and radiation	32
Table 3-5	Coordinates of corner points of Model 100 and Model 300	33
Table 4-1	Nodal coordinates of symbolic points on the path for spalling rate I case, spalling rate II case and no spalling case	56
Table 4-2	Heat transfer procedure of Model 100 with spalling rate I exposed to fire I	56
Table 4-3	Heat transfer procedure of Model 100 with spalling rate II exposed to fire I	57
Table 4-4	Peak values moment of temperature distribution of Model 100 exposed to fire I	57
Table 4-5	Heat transfer procedure of Model 300 with spalling rate I exposed to fire I	58
Table 4-6	Heat transfer procedure of Model 300 with spalling rate II exposed to fire I	59
Table 4-7	Peak values moment of temperature distribution of Model 300 exposed to fire I	60
Table 4-8	Heat transfer procedure of Model 100 with spalling rate I exposed to Fire II	60
Table 4-9	Heat transfer procedure of Model 100 with spalling rate II exposed to fire II.....	61
Table 4-10	Peak values moment of temperature distribution of Model 100 exposed to fire II..	61
Table 4-11	Heat transfer procedure of Model 300 with spalling rate I exposed to fire II.....	62

Table 4-12	Heat transfer procedure of Model 300 with spalling rate II exposed to fire II.....	63
Table 4-13	Peak values moment of temperature distribution of Model 300 exposed to fire II..	64
Table 4-14	Heat transfer procedure of Model 100 with spalling rate I exposed to fire III.....	64
Table 4-15	Heat transfer procedure of Model 100 with spalling rate II exposed to fire III	65
Table 4-16	Peak values moment of temperature distribution of Model 100 exposed to fire III.	65
Table 4-17	Heat transfer procedure of Model 300 with spalling rate I exposed to fire III.....	66
Table 4-18	Heat transfer procedure of Model 300 with spalling rate II exposed to fire III	67
Table 4-19	Peak values moment of temperature distribution of Model 300 exposed to fire III.	68
Table 4-20	Comparison of maximum temperature for Model 100 and Model 300 with all spalling rate cases exposed to fire I.....	68
Table 4-21	Moments when nodal temperature researches maximum for Model 100 and Model 300 exposed to fire I	69
Table 4-22	Comparison of maximum temperature for Model 100 and Model 300 with all spalling rate cases exposed to fire II.....	69
Table 4-23	Moments when nodal temperature researches maximum for Model 100 and Model 300 exposed to fire II.....	69
Table 4-24	Comparison of maximum temperature for Model 100 and Model 300 with all spalling rate cases exposed to fire III	70
Table 4-25	Moments when nodal temperature researches maximum for Model 100 and Model 300 exposed to fire III	70
Table 4-26	Peak temperature of the steel bars for Model 100 and Model 300 exposed to fire I and the reinforcing steel yield strength.....	70

Table 4-27 Peak temperature of the steel bars for Model 100 and Model 300 exposed to fire II and the reinforcing steel yield strength.....	71
Table 4-28 Peak temperature of the steel bars for Model 100 and Model 300 exposed to fire III and the reinforcing steel yield strength.....	71

List of Figures

Figure 2-1	Experimental spalling results: (a) Spalling in NSC beam B2 and HSC beam B5; and (b) cross section showing spalling in HSC beam.	19
Figure 2-2	Experimental result of the normalized spalling volume of Beam B5	20
Figure 2-3	Experimental result of normalized spalling volume of Beam B6	20
Figure 2-4	Development of spalling depth I with time	21
Figure 2-5	Development of spalling depth II with time	21
Figure 2-6	Fire I—ASTM-E119 standard fire	22
Figure 2-7	Fire II—Concrete fire.....	22
Figure 2-8	Fire III—Gypsum fire	23
Figure 2-9	Fire I, Fire II and Fire III.....	23
Figure 2-10	Strength of reinforcement decreases with temperature	24
Figure 3-1	3D Specimens taken from experiments.....	33
Figure 3-2	Idealized 2-D Models for FEA.....	33
Figure 3-3	Stepped spalling depth I for Analysis	34
Figure 3-4	Stepped spalling depth II for Analysis	34
Figure 3-5	Illustration of fire happens to the models.....	35
Figure 3-6	Model 100 and Model 300	35
Figure 4-1	Temperature distribution.....	71
Figure 4-2	Nodal Temperature of the symbolic points of Model 100 with spalling rate I exposed to fire I	72
Figure 4-3	Nodal Temperature of the symbolic points of Model 100 with spalling rate II exposed to fire I	73

Figure 4-4	Nodal Temperature of the symbolic points of Model 100 with no spalling exposed to fire I	74
Figure 4-5	Nodal Temperature of the symbolic points of Model 300 with spalling rate I exposed to fire I	75
Figure 4-6	Nodal Temperature of the symbolic points of Model 300 with spalling rate II exposed to fire I	76
Figure 4-7	Nodal Temperature of the symbolic points of Model 300 with no spalling exposed to fire I	76
Figure 4-8	Nodal Temperature of the symbolic points of Model 100 with spalling rate I exposed to fire II	77
Figure 4-9	Nodal Temperature of the symbolic points of Model 100 with spalling rate II exposed to fire II	78
Figure 4-10	Nodal Temperature of the symbolic points of Model 100 with no spalling exposed to fire II	79
Figure 4-11	Nodal Temperature of the symbolic points of Model 300 with spalling rate I exposed to fire II	80
Figure 4-12	Nodal Temperature of the symbolic points of Model 300 with spalling rate II exposed to fire II	81
Figure 4-13	Nodal Temperature of the symbolic points of Model 300 with no spalling exposed to fire II	81
Figure 4-14	Nodal Temperature of the symbolic points of Model 100 with spalling rate I exposed to fire III	82

Figure 4-15	Nodal Temperature of the symbolic points of Model 100 with spalling rate II exposed to fire III	83
Figure 4-16	Nodal Temperature of the symbolic points of Model 100 with no spalling exposed to fire III.....	84
Figure 4-17	Nodal Temperature of the symbolic points of Model 300 with spalling rate I exposed to fire III	85
Figure 4-18	Nodal Temperature of the symbolic points of Model 300 with spalling rate II exposed to fire III	86
Figure 4-19	Nodal Temperature of the symbolic points of Model 300 with no spalling exposed to fire III.....	86
Figure 4-20	Nodal temperature comparison for Model 100 with all spalling rate cases exposed to fire I	89
Figure 4-21	Nodal temperature comparison for Model 100 with all spalling rate cases exposed to fire II.....	91
Figure 4-22	Nodal temperature comparison for Model 100 with all spalling rate cases exposed to Fire III.....	93
Figure 4-23	Nodal temperature comparison for Model 300 with all spalling rate cases exposed to fire II.....	97
Figure 4-24	Nodal temperature comparison for Model 300 with all spalling rate cases exposed to fire III.....	99

Abstract

Spalling is a common phenomenon of high strength concrete composites that are exposed to fires. Prediction of spalling is not reliable due to the complex combined nature of the influencing parameters. However, two series of idealized finite element models were built to analyze how parameters influence spalling. The finite elements models simulate the performance of high strength concrete slabs against fires. Previous research and tests provide critical parameters that would influence spalling, such as concrete strength, concrete density, moisture content, heating rate and fire profiles. All the parameters were taken to be critical enough to cause explosive spalling by combination. This paper aims to give a general understanding of the influence of these factors on spalling and how concrete temperatures respond to spalling.

Keywords: high strength concrete, finite element model, critical parameters, concrete slab, explosive spalling

1 Introduction

1.1 Introduction

1.1.1 Research objective

Fire induced spalling is a primary characteristic of high strength concrete components when considering of structural fire safety. The fire performance of structural members depends on many interdependent factors, such as properties of materials and fire properties. After reviewing a volume of research in the behavior of structural members exposed to fire, six important parameters are summarized as the leading factors influence fire induced spalling: (1) moisture content; (2) heating rate; (3) specimen dimension and shape; (4) aggregate type; (5) concrete density; and (6) compressive strength. This research, simulated Kodur's tests (Kodur V. K., 2000) in finite element analysis, aim to find a numerical result of how these parameters influence spalling.

1.1.2 Summary of approach

Experimental tests were performed to investigate spalling in concrete beams exposed to fire (Kodur V. K., 2000) . The experimental fire duration, spalling volume and specimen dimensions are used to make numerical approximations to convert the spalling volumes into spalling rates which are treated as a parameter in the following finite element analysis. Finite element models based on the material properties used in the tests by Kodur are created in ABAQUS. Test parameters include thickness of the concrete and potential spalling rates. Results are compared for temperature distribution in the concrete.

1.2 Organization of report

This paper introduces fire induced spalling and shows the necessity of researching spalling-influenced parameters. After reviewing plenty of research findings, summarize leading factors that influence fire induced spalling. Study Kodur's test in 2000, calculate spalling rates for finite element analysis. Then tabulate material properties, fire scenarios and test methods. Carry out the finite element tests in ABAQUS and compare results from the analysis, final conclusions are followed.

Chapter 2 presents the background information required to understand the fire-induced spalling problem. The concept of spalling is discussed and the influencing parameters are detailed.

Previous research is presented on experimental testing on concrete beams in fire (Kodur V. K., 2000). The finite element analyses performed in this research are based on several parameters and results from these experimental tests. Chapter 3 details the finite element analyses performed in this research, including geometry, material properties, loading, boundary conditions, and analysis procedures. Chapter 4 presents results in terms of fire induced temperature distribution and Chapter 5 presents conclusions and recommendations for future work.

1.3 Summary of findings

Spalling is the key factor influences temperature distributions when structural members exposed to fire.

High heating rate leads to high possibility of spalling.

High strength concrete, due to its low permeability, experiences higher spalling levels.

1.4 Notation

Symbols	Description	Units
w/c	Ratio of water and cement	
e_f	Fuel load energy density (per unite floor area)	MJ/m ²
F_v	Ventilation factor	m ^{-1/2}
b	Thermal inertia	Ws ^{0.5} /m ² K
k	Thermal conductivity	W/m-K
ρ	Density	kg/m ³
c_p	Specific heat	J/kg-K
f'_c	Characteristic compressive strength of concrete	MPa
a	Specimen width of beam B5	mm
b	Specimen height of beam B5	mm
L	Specimen length of beam B5	mm
d_s	Spalling width in beam B5	mm
b_s	Spalling height in beam B5	mm
L_s	Spalling length in models	mm
L_{s_test}	Spalling length in tests	mm
e_{abs}	Absolute error of the spalling length in models and the spalling length in tests	
d'_s	Spalling width in beam B6	mm
b'_s	Spalling height in beam B6	mm
L'_s	Spalling length in beam B6	mm

a'	Specimen width of beam B6	mm
b'	Specimen height of beam B6	mm
L'	Specimen length of beam B6	mm

2 Background

2.1 Introduction

This chapter presents the background information relevant to the research. In this chapter, the definition of spalling in engineering, the mechanism of spalling, the parameters influencing spalling, and the relative research are introduced.

2.2 Spalling phenomenon

2.2.1 Definition of spalling

Spalling of concrete is defined as the breaking of layers (pieces) of concrete from the surface of structural elements when it is exposed to high and rapidly rising temperatures such as those experienced in fires (Kodur V. K., 2000). Spalling of the surface layer leads to an increase in the temperature of the inner layer of concrete, in other words, increasing the rate of transmission of heat into concrete and developing more severe spalling. High-strength concrete is widely used due to its light weight, lower permeability, higher strength and economy. However accompanied with these advantages, fire induced explosive spalling occurs when the high strength concrete exposed to fire.

2.2.2 Parameters influencing spalling

The mechanism of spalling can be simply described as follows: concrete is heated to a certain temperature, causing a tendency of the water in the concrete to evaporate, which is prevented by concrete and results in the development of pore pressure. As the pressure increases, small pieces

of concrete are expelled from the concrete section. Advanced research provides the fundamental mechanisms that influence spalling: (1) pore pressure and (2) thermal stress. The parameters influencing the fire performance of high strength concrete (HSC), spalling, and fire resistance are: (1) moisture content; (2) heating rate; (3) specimen dimension and shape; (4) aggregate type; (5) concrete density; and (6) compressive strength.

Moisture content normally decreases with age as concrete hydrates. In younger normal strength concrete, moisture contents are usually in the range 3.5 to 5.5% by weight (Malhotra, 1984). Meyer-Ottens (1972) found that, regardless of the stresses imposed or heating rates applied, concrete members with moisture contents less than 3.3% (by weight) did not spall because of lower pore pressures. Many researchers started to work on this area to find out how the w/c (ratio of water and cement) influences explosive spalling. Generally, spalling can occur if the moisture content of the concrete is more than 2% by weight (5% by volume) (Meyer-Ottens C. , Behavior of Concrete Structural Members in Fire Conditions, 1974) and (Meyer-Ottens C. , The Behavior of Concrete Structural Elements in Fires. Spalling of Normal Concrete Elements Under Fire Stress: Causes and Preventive Measures, 1977).

The tendency of spalling is much higher when the HSC specimens are exposed to a faster heating rate. Comparing experiments carried out by Diederichs, Jumppanen and Pentala (1988) shows that when heating high strength (50 to 110 MPa) quartzite aggregates cylindrical concrete specimens (80 mm diameter, and 40 mm length) at 20°C/min, no spalling took place. When heating at 32°C/min only slight spalling occurred. When heating ultra-high strength (190 to 240 Mpa) concretes (moisture 2.3-3.0% by weight) prisms (40 x 40 x 160 mm) in ISO 834:1987 fire,

Jumpannen found the concrete exploded after 7 minutes and continued exploding until 8 minutes of testing when the specimen was completely destroyed. Therefore, heating rate has a major influence on the occurrence of explosive spalling. Increasing the heating rate must lead to increasing of the probability and severity of explosive spalling.

A review of literature shows that the risk of explosive spalling increases with the specimen dimension and shape. Connelly (1995) confirmed the conclusions of Mayer-Ottens (1972) that thicker concrete specimens are less likely to experience explosive spalling in fire. Explosive spalling is unlikely to happen in very thin sections. Experimental evidence also suggests that explosions are less likely in thick members, greater than about 200-300 mm (Copier, 1979). Explosive spalling is, therefore, most likely to occur in 'medium' size sections. Spalling is also more likely in sections with 'rapidly' changing cross-section. Corners, particularly acute-angled ones, have a marked spalling tendency because of higher thermal stresses and the higher rate of heat influx, providing evidence of greater stability of cylinders than cubes (Schneider, 1988).

The type of aggregate used in concrete influences spalling. It is generally recommended to use artificial lightweight aggregates to prevent spalling in low moisture environments (Connolly, 1995). However, if the concrete is likely to be in a high moisture environment, the use of lightweight aggregates could not only promote spalling but also more violent one. The common types of aggregate mixed into concrete are carbonate aggregate and siliceous aggregate. Tests results implicate higher spalling in siliceous aggregate. A survey suggests that only artificial lightweight aggregates, including crushed brick, were found to be free from this risk (1985).

Fire tests of comparing normal density concrete (made with normal weight aggregate) and lightweight concrete (made with lightweight aggregate) have shown that the extent of spalling is higher in the lightweight aggregate group (Hertz, 1984).

One of the most important conclusions of the work by Meyer-Ottens (1972) was that an increase in compressive stress, either by reduction in section size or an increase in loading, encourages explosive spalling. The initial compressive stress in the explored layer of concrete before heating does not by itself promote spalling. However applied loads and restraint increase the susceptibility of concrete members to spalling.

In general, given suitable environmental conditions, and considering loading and high heating rate in the concrete, all concrete can display the capacity for spalling. Medium size sections are more susceptible to spalling than thicker and thinner section. High strength concrete are more susceptible to spalling than normal strength concrete. A review of test results indicate that explosive spalling often takes place within the first 40 minutes of heating if spalling occurs. Explosive spalling also requires moisture content larger than 3% by weight, and the most important parameter for spalling is a high heating rate.

2.3 Previous research

2.3.1 Kodur

Kodur describes different parameters influencing spalling. The test included four beams of rectangular cross section, 406 mm high by 254 mm wide and 3960 mm in length. Silica fume

was added to the concrete to achieve higher strength, and the average compressive cylinder strength of the HSC was 93.9 MPa at 28 days and 106 MPa on the day of testing. The fire resistance tests were carried out by placing the concrete beams in the furnace and exposing them to a desired fire exposure. All beams were tested under two point loads each of which is placed at 1.4 m from the end supports. The extent and nature of spalling was recorded by making visual observations through the windows of the furnace during the fire test and also by conducting volumetric measurements of the beam after tests. Details of parameters and test results would be discussed in 3.4, 3.5 and 3.6.

Test method is also a key factor influencing spalling (Meyer-Ottens C. , 1972). Take a concrete column for example, if the column is heated on three-side, nearly no spalling occurs. However, if the column is heated only on one side, severe spalling can be easily observed. Researchers believe that three-side heating would allow for moisture to escape, avoiding generation of large pore pressure. For one-side heating, hardly escaping of moisture leads to explosive spalling. And also how to set the boundary conditions, since axially restrained would increase the probability of spalling.

Two different spalling rates were observed during the experimental tests. The first spalling rate (spalling rate I) is taken from the HSC Beam B5, while the second spalling rate (spalling rate II) is taken from the HSC Beam B6.

The critical properties of strength, compressive strength, fire profile, and support conditions are shown in Table 2-1 (Dwaikat, M. B.; Kodur, V. K. R., 2009).

Table 2-1 shows that different support conditions and loading ratios cause different extents of spalling. The finite element analyses in this research assume that all parameters that influence spalling are considered and varies on the rate of spalling and beam depth.

Figure 2-1 shows that specimens after fire tests. There is extensive spalling in HSC beam B5. Part (b) shows the spalling pattern on the cross-section. The finite element analyses consider only high strength concrete, thus HSC beam B5 is under consideration.

Figure 2-2 and 2-3 show the variation of normalized spalled volume with time for Beam B5 and B6, respectively. Spalled volumes can be converted to spalled depths by simulation, which are showed in Figure 2-4 and 2-5. The simulation process would be discussed in Chapter 3.

Known from test results that spalling continues for 39 min, and to a depth is 25 mm, thus, the average spalling rate is 0.64 mm/min from the test. Spalling rate I is gotten from the test result of beam B5 in Figure 2-2, in which the spalling period is approximately divided into three parts.

Phase 1: 11 min – 24 min, depth: 18 mm

Phase 2: 24 min – 37 min, depth: 4 mm

Phase 3: 37 min – 50 min, depth: 3 mm

And the spalling steps are tabulated in Table 2-2 (a).

Spalling rate II is taken from the test result from beam B6 which showed in Figure 2-3. Spalling happens at 3 min into the fire and ends at 30 min. The spalling process is made of two phases:

Phase 1: 5 min – 18 min, depth: 20 mm

Phase 2: 18 min – 25 min, depth: 5 mm

The spalling steps are tabulated in Table 2-2 (b).

The analyses consider straight line segments for each phase, i.e. consider constant spalling rates for each phase.

2.3.2 Others

Besides Kodur's research, research results from G. Sanjayan and L. J. Stocks (1993) are also the reference of these analyses. G. Sanjayan and L. J. Stocks carried out two groups of test specimens: one was normal strength concrete beam-slab specimen and the other was high strength silica fume concrete beam-slab. The test results showed spalling hardly occurred in the normal strength concrete specimen group, in contrast, almost all the specimens in the high strength silica fume concrete group generated spalling. Their research focused on the reinforced high strength concrete beam-slab, and discussed about the depth of the concrete cover influencing spalling. The results told that spalling occurred in 200 mm flange with 75 mm depth concrete cover and for the 150 mm flange with 25 mm concrete cover, no spalling happened. They concluded spalling only occurred to the elements with larger concrete cover (75 mm for example). Another phenomenon was the spalling only occurred in the slabs which were only one face fire-exposed, while no spalling occurred in the webs which were three faces fire-exposed. The conclusion based on this phenomenon was three face fire-exposed specimens are much safer than one face exposure because the distance of escaping for moisture was much shorter in three faces fire-exposed case.

From G. Sanjayan and L. J. Stocks (1993), three criteria conditions to ensure the occurrence of concrete spalling are: (1) high strength concrete, (2) larger concrete covers and (3) one face fire exposure.

2.4 Fire scenarios

Fire profile is an important parameter for explosive spalling, because it is related to the spalling rate. In the analyses, the slab is exposed to three types of fires -- ASTM-E119 standard fire (Fire I), and two compartment fires, one assuming concrete walls (Fire II) and one assuming gypsum (Fire III), all of which have high heating rates in the early stages and last for 2 hours. For the Fire II and Fire III, fires start to decay around 0.5 to 1 hour of fire exposure, cooling to room temperature (20°C) and remaining at the room temperature for the rest of time period.

2.4.1 Fire I

Most countries around the world rely on full-size fire-resistance tests to assess the fire performance of building materials and structural elements. The time-temperature curve used in fire-resistance tests is called the 'standard fire'. The most widely used test specifications are ASTM-E119 and ISO-834. The ASTM-E119 curve, which is shown in Figure 2-6, is defined by a number of discrete points, which are shown in Table 2-3. An equation approximating the ASTM-E119 is given by Lie:

$$T = 750 \cdot \left[1 - e^{-3.79553 \cdot \sqrt{t_h}} \right] + 170.41 \cdot \sqrt{t_h} + T_0 \quad (2-1)$$

Where t_h is the time (in hours).

2.4.2 Compartment fires

Both of the two compartment fires are designed from real room fires. Fire II, the concrete fire, is the fire in a room constructed from concrete. Fire III, the gypsum fire, is the fire in a room constructed from gypsum slabs.

2.4.2.1 Compartment description

2.4.2.2 Fire II

The concrete room is 4 m x 6 m in area, 3 m high, with one window 3 m wide and 2 m high.

Fuel load energy density (per unit floor area): $e_f = 2000 \text{ MJ/m}^2$

Ventilation factor: $F_v = 0.079 \text{ m}^{-1/2}$

Figure 2-6 shows the Fire II, compared with Fire I, the ASTM-E119 Standard Fire, Fire II has a decay period. The graph gives a maximum temperature of about 900°C after 43 minutes, dropping to the room temperature after 2 hours. The decay rate $(dT/dt)_{ref}$ equals to 562.5°C according to Eurocode.

2.4.2.3 Fire III

The gypsum room is 4 m x 6 m in area, 3 m high, with one window 3 m wide and 2 m high.

Fuel load energy density (per unit floor area): $e_f = 2000 \text{ MJ/m}^2$

Ventilation factor: $F_v = 0.079 \text{ m}^{-1/2}$

Figure 2-7 shows the Fire III. The Fire III has the highest maximum temperature around 1230 °C at 0.7 hours of fire exposure, dropping to room temperature at a rate of

$$dT/dt = (dT/dt)_{ref} \cdot \sqrt{(Fv/0.04)/\sqrt{(b/1900)}} \quad (2-2)$$

Where, dT/dt = decay rate

$(dT/dt)_{ref}$ = reference decay rate, 625 °C/hour

F_v = ventilation factor

b = thermal inertia of gypsum

thus, the decay rate in Fire III is 1773 °C/hour .

2.4.3 Comparison of fire scenarios

Figure 2-8 compares the three different fire scenarios. Fire III has the highest peak temperature of the three fires. Temperature in Fire I increase from the beginning to the end of the fire, while both Fire III and Fire II are composed with a decay phase. Fire III starts to decay earlier and decreases at a faster rate. In the early stage, Fire I and Fire II follow similar paths, while Fire III has a more rapid heating rate.

2.5 Thermal properties of the concrete used in analyses

High strength concrete used to make the slabs is of a same type: conductivity, density (Eurocode2, 1992) and specific heat (Kodur & Sultan, 2003) are the same and showed below:

The thermal conductivity k (W/m-K) decreases with an increase in temperature. With silica fume added into the concrete mix, the thermal conductivity may be calculated according to Equation (2-3).

For $20^{\circ}\text{C} < T < 1000^{\circ}\text{C}$

$$k = 2.00 - 0.0011 \cdot T \quad (2-3)$$

Table 2-4 shows the thermal conductivity of the concrete used in analyses.

The density ρ (kg/m³) may be considered as independent of the concrete temperature and can be determined to 2300 kg/m³.

The specific heat c_p (J/kg-K) of concrete is generally expressed in terms of thermal capacity which is a product of density and specific heat as showed in Equation (2-4).

For $0^{\circ}\text{C} \ll T \ll 200^{\circ}\text{C}$

$$\rho c_p = (0.005T + 1.70) \times 10^6$$

For $200^{\circ}\text{C} < T \ll 400^{\circ}\text{C}$

$$\rho c_p = 2.70 \times 10^6$$

For $400^{\circ}\text{C} < T \ll 500^{\circ}\text{C}$

$$\rho c_p = (0.013T - 2.50) \times 10^6$$

For $500^{\circ}\text{C} < T \ll 600^{\circ}\text{C}$

$$\rho c_p = (-0.013T + 10.50) \times 10^6$$

For $600^{\circ}\text{C} < T \ll 1000^{\circ}\text{C}$

$$\rho c_p = 2.70 \times 10^6 \quad (2-4)$$

Table 2-5 shows the specific heat of the concrete used in analyses.

2.6 Yield Strength of Reinforced Steel Bars

Eurocode 2 provides mechanical performance of high strength concrete and reinforced high strength concrete structures in fire. The thermal performance of reinforcement in slabs is based on the tensile capacity. The reduction of the characteristic strength of a reinforcing steel as a function of the temperature (T) is allowed for by the coefficient $k_s(T)$ for which:

$$f_{sk}(T) = k_s(T) \cdot f_{yk}(20^\circ\text{C}) \quad (2-5)$$

In the absence of more accurate information, the following $k_s(T)$ values should be used for reinforcement.

For $20^\circ\text{C} \ll T \ll 350^\circ\text{C}$

$$k_s(T) = 1.0$$

For $350^\circ\text{C} < T \ll 700^\circ\text{C}$

$$k_s(T) = (6500 - 9T)/3500$$

For $700^\circ\text{C} < T \ll 1200^\circ\text{C}$

$$k_s(T) = (1200 - T)/5000 \quad (2-6)$$

Coefficient $k_s(T)$ can be treated as the normalized strength of the steel. Figure 2-10 explains how dramatic the decrease of reinforcement strength when a fire happens.

Table 2-1 Properties and Results for Tested RC Beams

Property	Beam B5	Beam B6
Strength	HSC	HSC
f'_c (MPa)	93.3	93.3
Fire Exposure	LF	LF
Support condition	Simply supported	Axially restrained
Loading ratio	0.65	0.55
Extent of spalling(%)	7.0	8.7

Table 2-2 Spalling Rates from Tests

Spalling rate I		Spalling rate II	
Time (min)	Depth(mm)	Time (min)	Depth(mm)
11-24	15	5-18	15
24-37	3	18-25	5
37-50	2		

Table 2-3 Fire I, Fire II, and Fire III

Fire I		Fire II		Fire III	
Time(s)	Temperature(°C)	Time(s)	Temperature(°C)	Time(s)	Temperature(°C)
0	20	0	20	0	20
300	538	300	560	300	944
600	704	600	700	600	1048
1800	843	1200	789	1800	1216
3600	927	1800	841	2000	1232
7200	1010	2400	887	2400	1145
14400	1093	2610	895	3000	945
28800	1260	3000	827	3600	744
		3600	709	5700	41
		6000	234	6000	20
		7200	0	7200	20

Table 2-4 Thermal conductivity of the concrete used in analyses

Temperature(°C)	Conductivity k (W/Mk)
0	2.00
100	1.89
200	1.78
400	1.56
500	1.45
600	1.34
1000	0.9
1200	0.9

Table 2-5 Specific heat of the concrete used in analyses

Temperature(°C)	Specific Heat c_p (J/kgK)
0	739
100	957
200	1174
400	1174
500	1739
600	1174
1000	1174
1200	1174

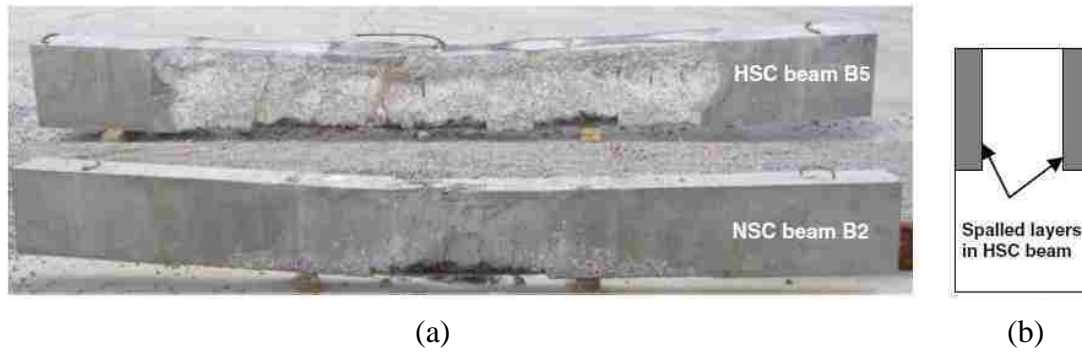


Figure 2-1 Experimental spalling results: (a) Spalling in NSC beam B2 and HSC beam B5; and (b) cross section showing spalling in HSC beam.

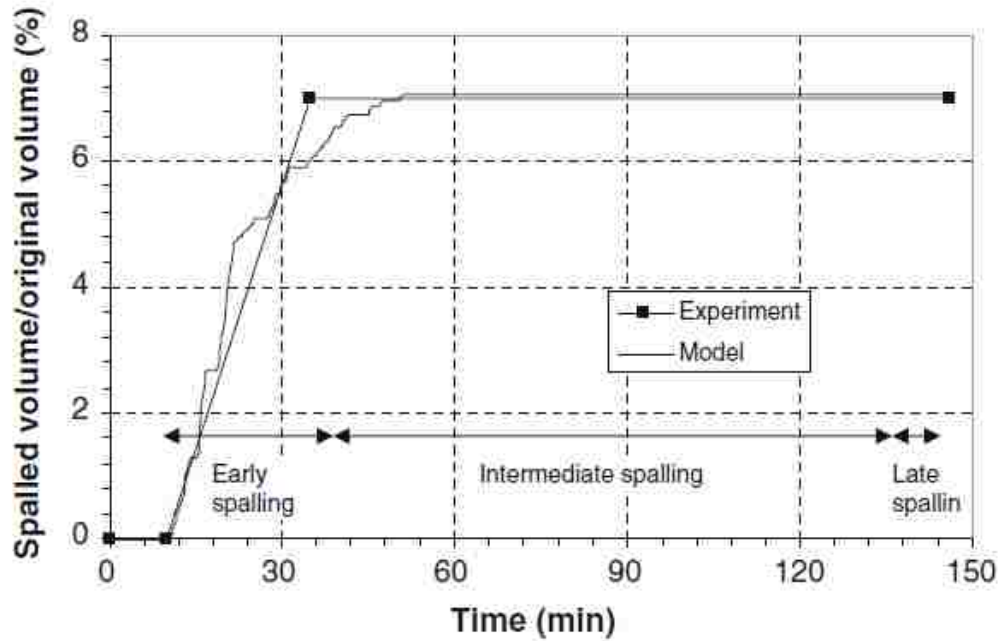


Figure 2-2 Experimental result of the normalized spalling volume of Beam B5

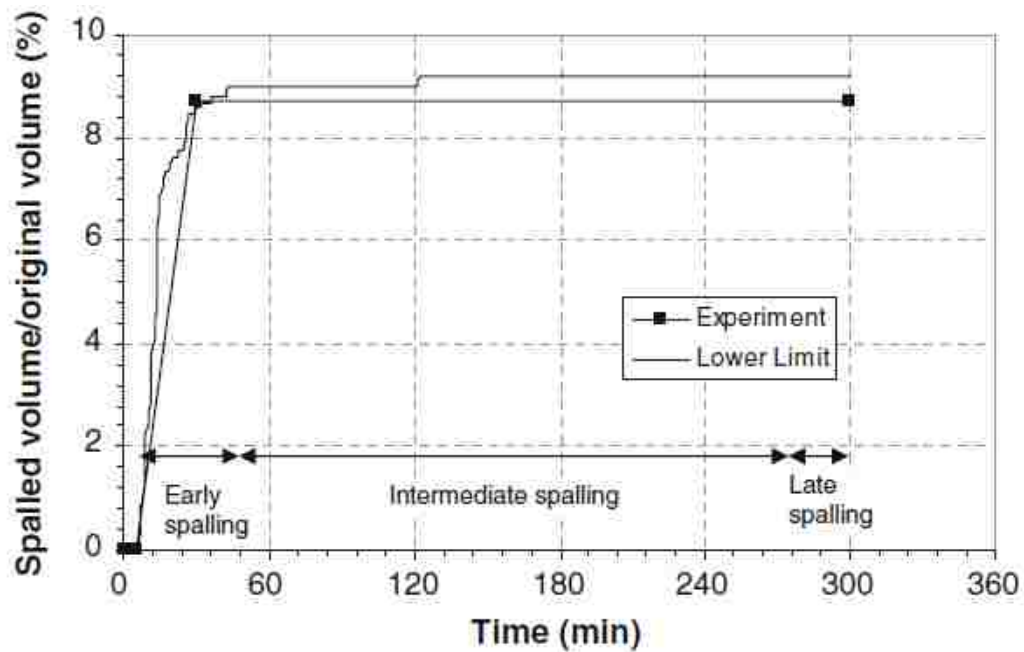


Figure 2-3 Experimental result of normalized spalling volume of Beam B6

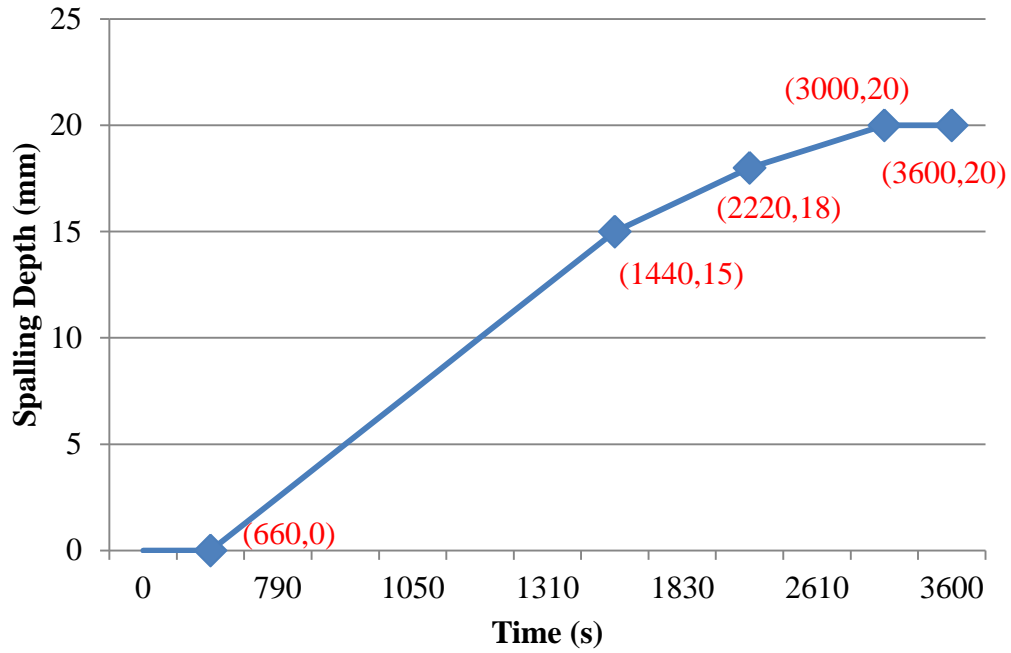


Figure 2-4 Development of spalling depth I with time

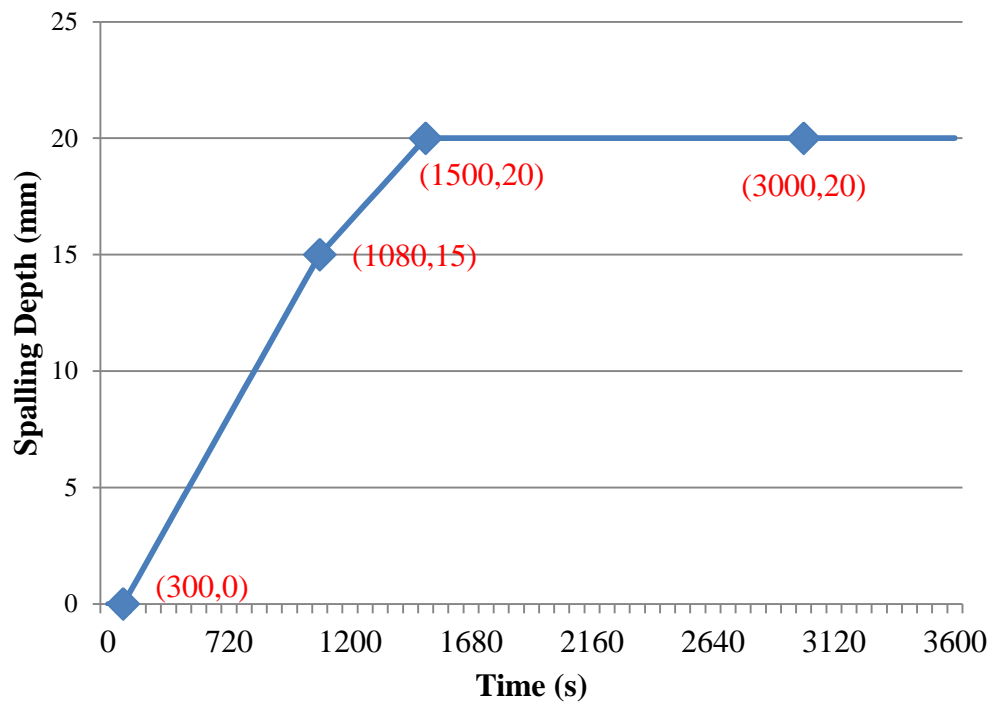


Figure 2-5 Development of spalling depth II with time

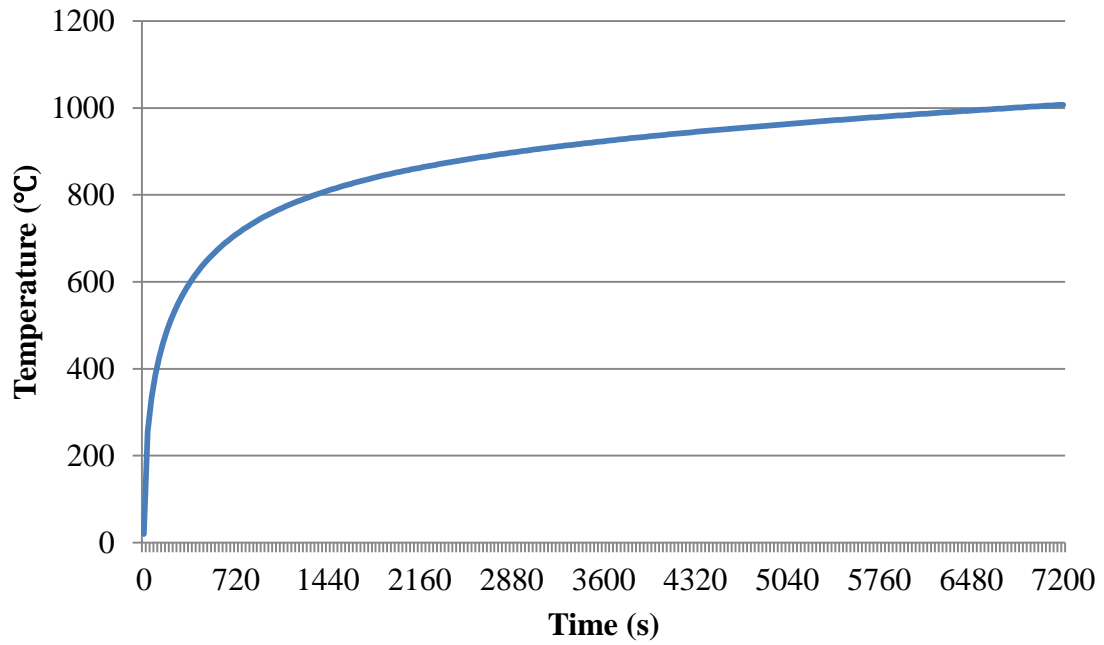


Figure 2-6 Fire I—ASTM-E119 standard fire

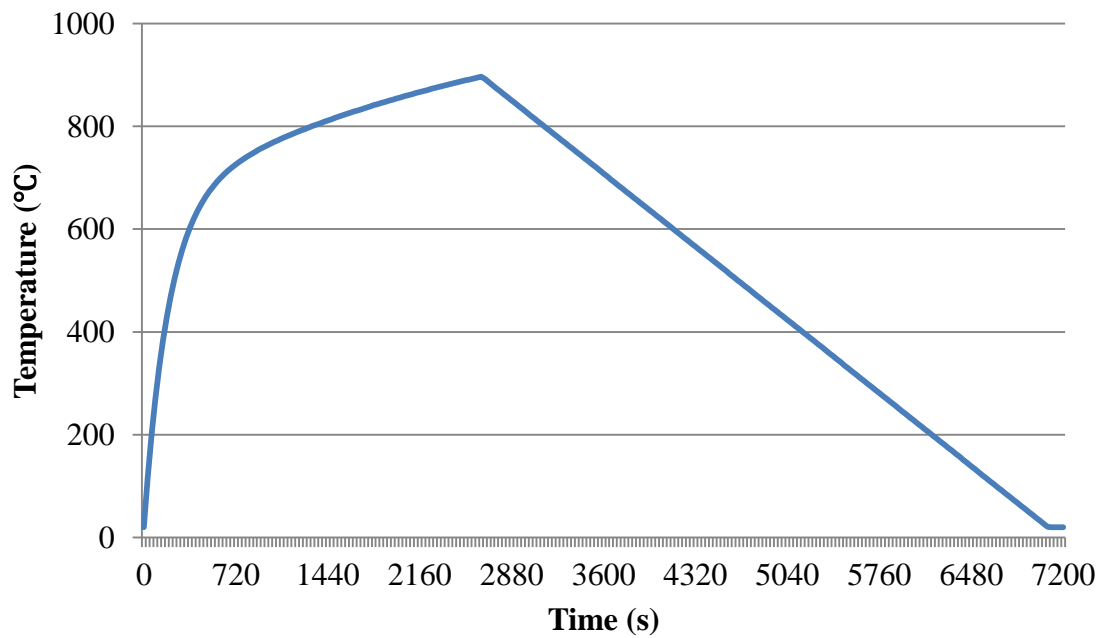


Figure 2-7 Fire II—Concrete fire

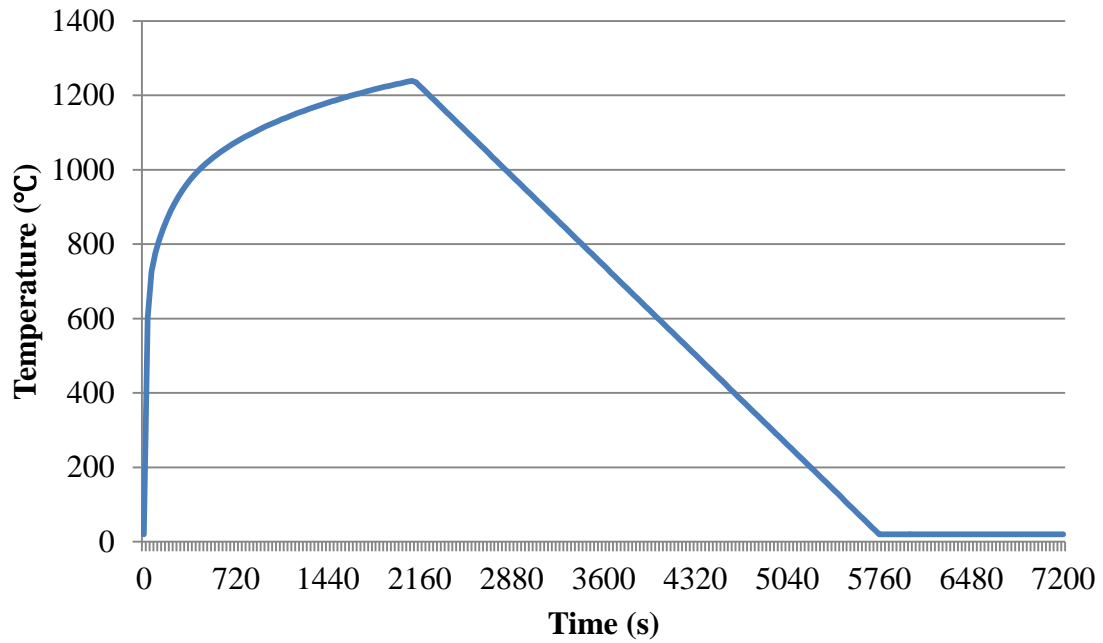


Figure 2-8 Fire III—Gypsum fire

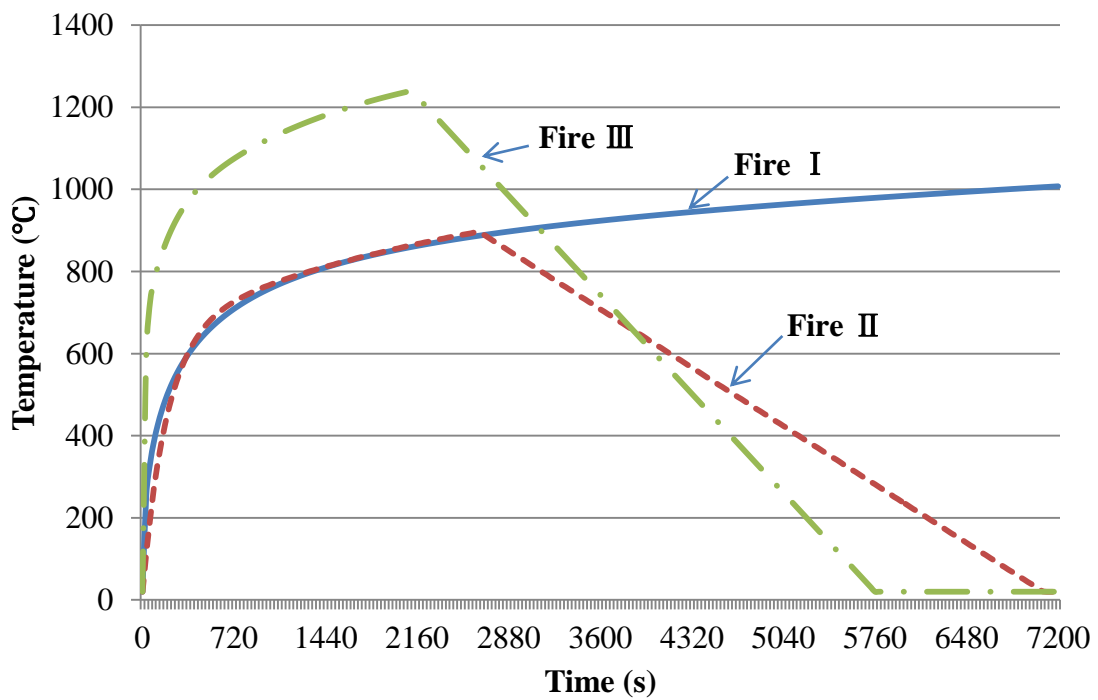


Figure 2-9 Fire I, Fire II and Fire III

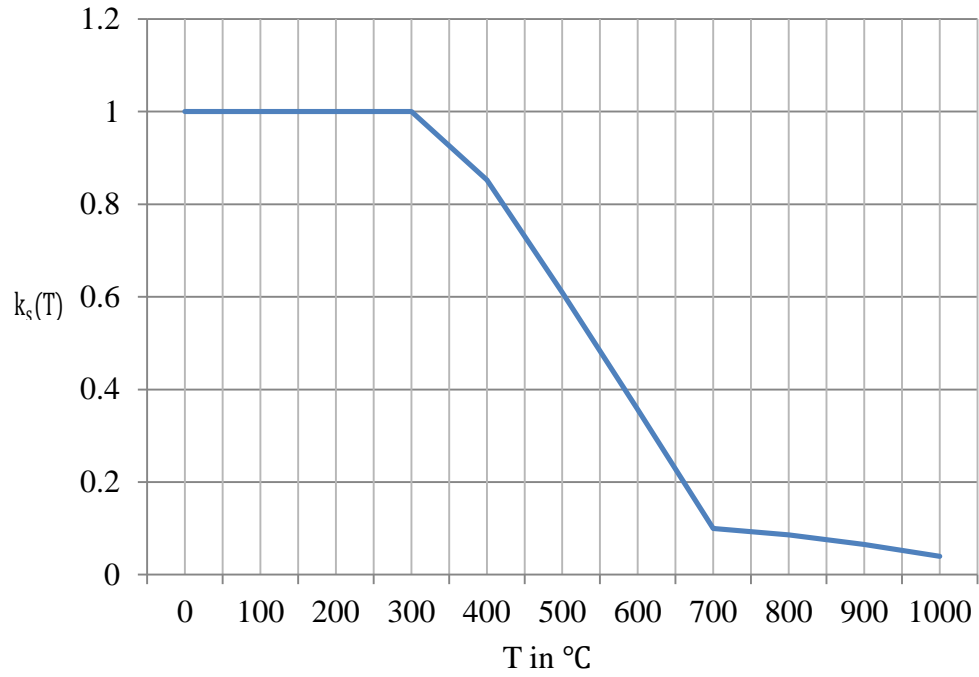


Figure 2-10 Strength of reinforcement decreases with temperature

3 Finite element analysis procedure

3.1 Introduction

Finite element analysis is widely used in engineering to simulate performances of structures under a variety loading conditions. This report presents analyses of specimens exposed to fire conditions. The analyses mainly focus on the influence of heating rate, specimen dimensions, and spalling rates, on the temperature distribution of the concrete sections.

In the finite element analyses, slab specimens are tested. The analyses simulates a fire occurring in a room of a building, and are idealized by exposing only the bottom surface of the slab to fire. The boundary conditions of the slab are adiabatic on the perpendicular sides (left and right sides of the model) and the initial condition is an uniform distribution of temperature of 20°C. Convection and radiation are the boundary conditions on the top and bottom surfaces. The analyses assume all the critical conditions are present to guarantee the occurrence of explosive spalling. Once spalling occurs, specified thicknesses of concrete layers are spalled off in the slab and elements are removed in the finite element model. Different spalling scenarios are compared with the control “no spall” scenario to examine the influence of the spalling rate on the performance of HSC.

3.2 Geometry

The geometry of the models is based on Kodur’s experimental tests (2000), beams are 254 x 406 x 3960 mm (width x height x length). The analyses are based on the results for Beam B5;

spalling depth is 25 mm into beam's width, and occurs over the beam's height. The spalling cross section is shown in Figure 2-1(b). Experimental tests show that spalling occurs at 11 minutes and stops at 50 minutes into the fire, and the spalling volume is 7.0 percentage of the original volume.

The length of spalling, L_s can be calculated.

$$\frac{d_s b_s L_s}{abL} = \frac{(25 \times 2) \times 406 \times L_s}{254 \times 406 \times 3960} = \frac{7.0}{100} \quad (3-1)$$

Where: d_s = spalling width in beam B5

b_s = spalling height in beam B5

L_s = spalling length in beam B5

a = specimen width of beam B5

b = specimen height of beam B5

L = specimen length of beam B5

Thus, $L_s = 1408$ mm.

This spalling length can be treated as severe extent along beam length.

Figure 2-1(a) shows the extent of spalling in Beam B5. The severe spalling length is approximately 3/5 of the entire spalling length. And the entire spalling length is about 3/5 of the whole beam length. The severe extent spalling length along beam length (L_{s_test}) is,

$$L_{s_test} = L \cdot 0.6 \cdot 0.6 = 1426 \quad (3-2)$$

Where, L_{s_test} = severe spalling length measured from the test

The absolute error of the spalling length in models and the spalling length in tests is,

$$e_{abs} = \frac{|L_s - L_{s_test}|}{L_s} = \frac{|1408 - 1426|}{1408} = \frac{1.28}{100} \quad (3-3)$$

Where: e_{abs} = absolute error of the spalling length in models and the spalling length in tests

L_s = spalling length in models

L_{s_test} = spalling length in tests

Since e_{abs} equals to 1.28%, which is smaller than 5%, L_s is approaching L_{s_test} .

For beam B6, the spalling width is the same as that in beam B5, meanwhile, the spalling volume reduces to 1.5%.

$$\frac{d'_s b'_s L'_s}{a' b' L'} = \frac{(25 \times 2) \times 406 \times L'_s}{254 \times 406 \times 3960} = \frac{1.5}{100} \quad (3-4)$$

Where: d'_s = spalling width in beam B6

b'_s = spalling height in beam B6

L'_s = spalling length in beam B6

a' = specimen width of beam B6

b' = specimen height of beam B6

L' = specimen length of beam B6

Thus, $L'_s = 302$ mm, which is almost the same value as measured from specimen in the test.

The author concludes that spalling is isotropic through height and length. The analyses performed in this research include two 2D models, the dimension are 100 x 300 mm and 100 x 100 mm. The depth (into the page) is assumed as 100 mm for both models.

3.3 Simulation of spalling rates

Linear approximation is used in the finite element analyses to approximate the actual spalling rates during the experimental tests (Kodur V. K., 2000). Increasing the intervals used in approximation increases the accuracy of the simulation, however, reducing the intervals, which means reducing the quantity of elements of the models, decreases the calculating time for ABAQUS. The total spalling depths in models are divided into several phases as showed in Table 2-2 (a) and (b). Both the two spalling rate cases have a 15 mm spalling depth at their first spalling phases (Phase-1). The element size in Phase-1 is 5 x 5 mm for both of the two spalling rate cases, thus the first 15mm spalling depth is divided into 3 parts, 5mm each as showed in Figure 3-3 and Figure 3-4. In spalling rate I case, the second spalling depths is 3 mm and the third spalling depth is 2 mm. Therefore, the element size in Phase-2 is 5 x 3 mm and 5 x 2 mm in Phase-3. In spalling rate II case, there is 5 mm depth left for Phase-2 in spalling rate II case, thus, the element size for Phase-2 is 5 x 5 mm.

Figure 3-3 illustrates the mathematical approximation of spalling rate I. Phase-1 is the process that the first 15 mm spalling depth taking 780 seconds (1440 minus 660 seconds) to finish. Spalling rate is assumed constant in this phase, therefore, each 5 mm spalling depth needs 260 seconds. The three phases are marked as Phase-1(a), Phase-1(b) and Phase-1(c). In order to carry out the approximation, each step jumps at the middle of each 260 seconds. Mark the start time of Phase-1(a) 0, then count 130 seconds before the step jumps. The actual first spalling time should plus the period before Phases-1(a), thus, add 660 seconds to this spalling period of 130 seconds, which would be 790 seconds of fire exposure when the first step of spalling occurs in the mathematical approximation. Same process for Phase-1(b): mark the beginning time of the second 5 mm spalling depth 0, then counting 130 seconds occurs another step jump. So does Phase-1(c). Phase-2, with the starting time at 1440 seconds from the beginning of fire exposure and lasting for 780 seconds, is divided into two steps equally, when at the middle point a jump occurs. Same applies to Phase-3 in which the last 2 mm depth spalls from the model. The original spalling depths developing with time is show in dashed line in Figure 3-3, meanwhile, the solid line shows the mathematical approximation of this process.

Figure 3-4 shows the mathematical approximation of spalling rate in spalling rate II case: three steps for the first 15 mm spalling depth and one step for the last 5 mm spalling depth. The first three steps take 260 seconds each and 420 seconds for the last step.

Table 3-1 and Table 3-2 summarize the spalling steps of the two spalling rate cases talked above (spalling rate I and spalling rate II) and tabulate the spalling depths in each spalling

phases for both of the spalling rate cases. Table 3-1 shows spalling depth I and Table 3-2 shows spalling depth II.

3.4 Text matrix

Set the moisture content, concrete density, concrete strength and test method constant, the finite element analyses were carried out aiming to find out the influence of dimensions, types of fires and spalling rates. The analysis scenarios are showed in Table 3-3.

3.5 Boundary conditions

The boundary conditions refer to convection and radiation where the heat flow exists. The ability of convection is expressed by heat transfer coefficient h while radiation is defined using emissivity ε . The boundary conditions are different from fire side (bottom side), top side (no fire exposure) and other sides (no fire flow). The heat transfer coefficient and emissivity of each side is showed in Table 3-4.

3.6 Loads

In these analyses, the slabs were one surface exposed to fires as illustrated in Figure 3-5 and (a) for the 100 x 100 mm model (Model 100), meanwhile, (b) for the Model 300 (Model 300).

Relating the models to the real slabs in buildings, set the fires heat from the bottom surface of the slabs and the bottom surface of the models.

3.7 Analysis methods

For the spalling cases, models run from the beginning to the time of the first spalling happened, then paused for spalling off one 5 mm thick layer of elements from the fire-exposed side of the model. A new layer was exposed to fire. Continued running the new dimensioned model, paused at the moment that another 5 mm layer of elements spalling off. Same procedures were carried out for the following spalling steps. Up until the fire ends stopped the model. Exposed nodal temperature of each running steps, merged them together to get a whole development of nodal temperature for 2 hours.

Meanwhile, only one running step is needed for the no spalling cases. Run the models for 2 hours and exposed the data of nodal temperature for the entire period.

The rectangular shaped models can be located in ABAQUS CAE by the coordinates of four corner points. Table 3-5 shows the coordinates for locating 100 x and Figure 3-6 are the illustrations of Model 100. Model 300 is expressed by Table 3-5 and Figure 3-7.

Table 3-1 Spalling depth I

Step	Time (s)	Depth (mm)	Accumulative depth (mm)
No Spalling	0-790	0	0
Phase-1(a)	790-1050	5	5
Phase-1(b)	1050-1310	5	10
Phase-1(c)	1310-1830	5	15
Phase-2	1830-2610	3	18
Phase-3	2610-7200	3	18

Table 3-2 Spalling depth II

Step	Time (s)	Depth (mm)	Accumulative depth (mm)
No Spalling	0-430	0	0
Phase-1(a)	430-690	5	5
Phase-1(b)	690-950	5	10
Phase-1(c)	950-1290	5	15
Phase-2	1290-7200	5	20

Table 3-3 Analysis Scenarios

Model size	Fire		
	I	II	III
Model 100	Spalling rate I Spalling rate II No spalling	Spalling rate I Spalling rate II No spalling	Spalling rate I Spalling rate II No spalling
Model 300	Spalling rate I Spalling rate II No spalling	Spalling rate I Spalling rate II No spalling	Spalling rate I Spalling rate II No spalling

Table 3-4 Boundary conditions--convection and radiation

	Heat transfer coefficient h (W/M ² K)	Emissivity ε
Fire side	25	0.8
Top side	4	0.4
Sides	Adiabatic, no heat flow	Adiabatic, no heat flow

Table 3-5 Coordinates of corner points of Model 100 and Model 300

Node number	Coordinate for Model 100	Coordinate for Model 300
A	(-50,0,0)	(-50,0,0)
B	(50,0,0)	(50,0,0)
C	(50,0,100)	(50,0,300)
D	(-50,0,100)	(-50,0,300)

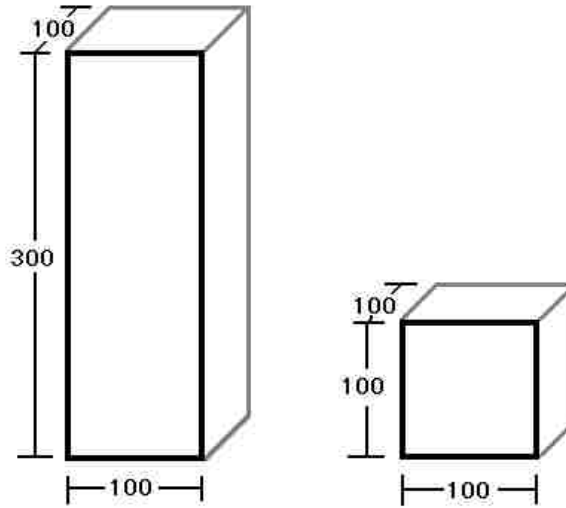


Figure 3-1 3D Specimens taken from experiments

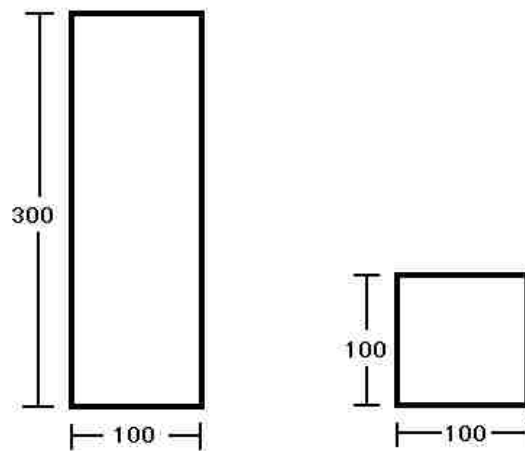


Figure 3-2 Idealized 2-D Models for FEA

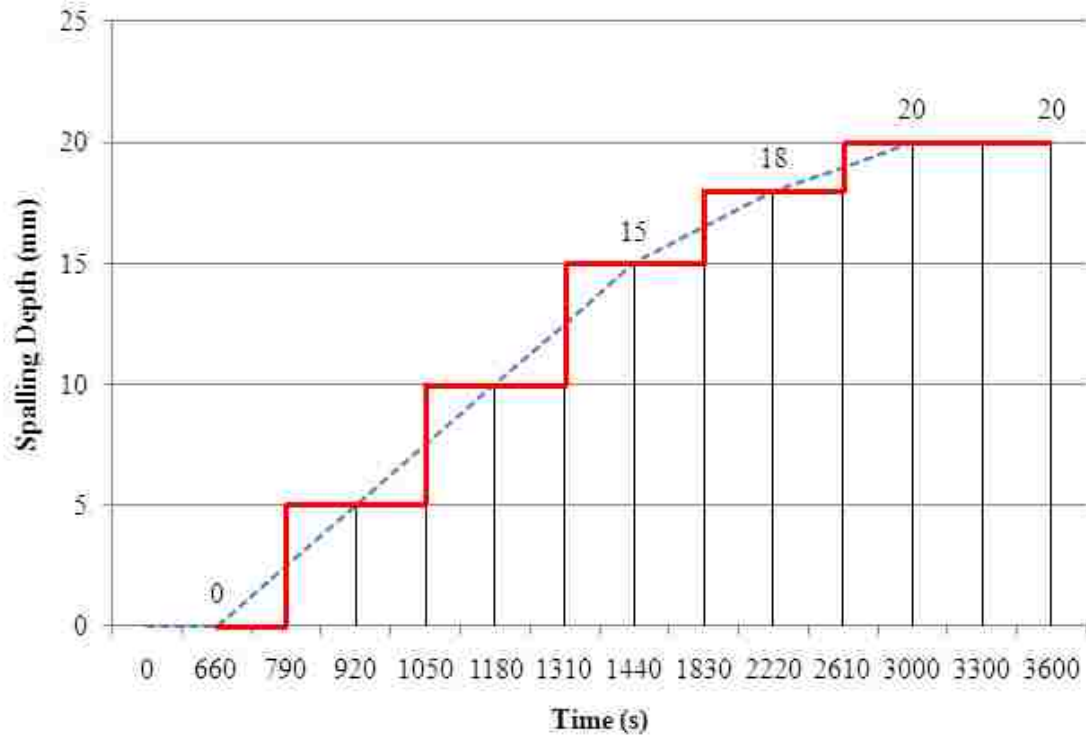


Figure 3-3 Stepped spalling depth I for Analysis

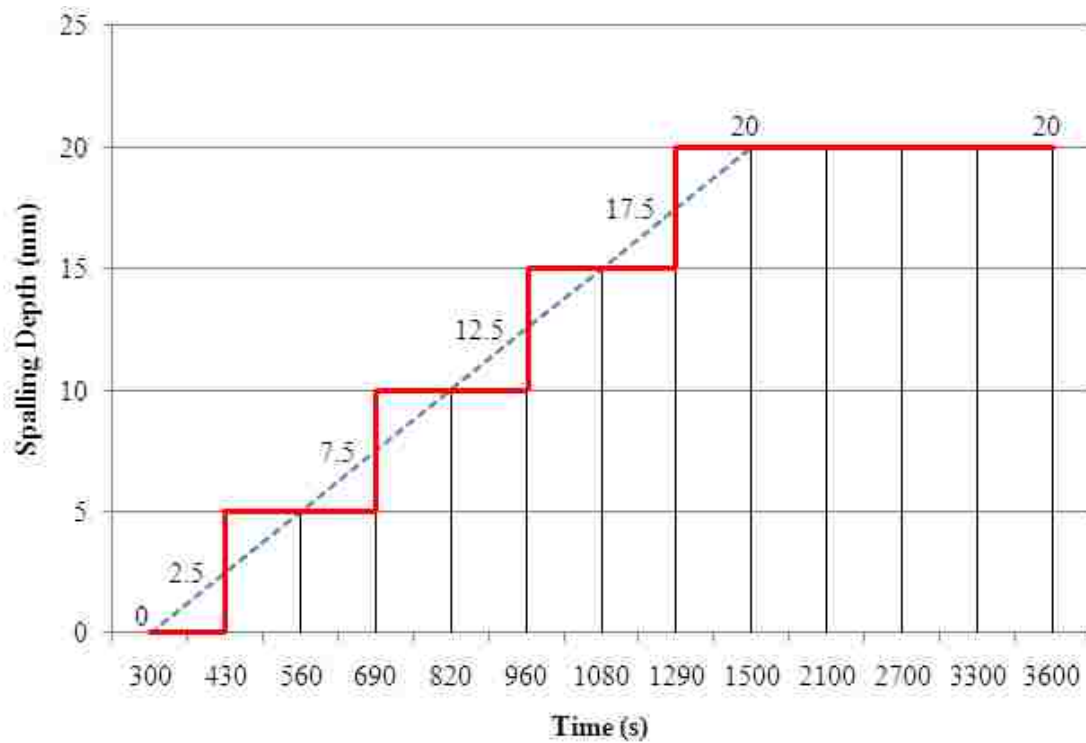
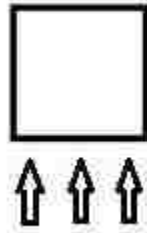


Figure 3-4 Stepped spalling depth II for Analysis

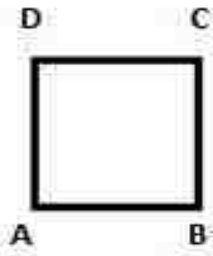


(a) Model 100 exposed to fire



(b) Model 300 exposed to fire

Figure 3-5 Illustration of fire happens to the models



(a) Model 100



(b) Model 300

Figure 3-6 Model 100 and Model 300

4 Analysis Results-Temperatures

4.1 Introduction

According to the conclusion from Copier (1979), the actual amount of reinforcement is less important than the moisture content in influencing explosive spalling. The reinforced high strength concrete slab models are also built in ABAQUS. Comparing temperature distribution of the reinforced group and the pure concrete group, the difference can hardly be measured. Besides, the aim of this paper focuses on spalling which is the character of concrete other than steel bars. Thus the finite element analyses of pure high strength concrete slabs are discussed here.

A path, composed vertically through each model and made of six points or five points (depends on the number of spalling steps), records the nodal temperatures of these five or six points along the path and tabulate them as the analysis results for each model. The composing points of a path are taken from each fire-exposed surface when spalling occurred. More spalling steps generate more fire-exposed surfaces and therefore more points along the path. In Model 100 with spalling rate I, spalling period is divided into 5 steps, as a result, 5 new surfaces would be exposed to fires. Node 1 locates at the bottom surface (value in y direction: 0.0) which would spall off in the first spalling step. As the first 5mm spalling off, a previous inner layer becomes a new bottom surface exposed to fire, where point 2 is taken from (value in y direction: 5.0). So do the next 3 points (values are 10.0, 15.0, 18.0, and 20.0 respectively), all lie on a new bottom surface after a spalling step occurs.

Finite element analyses are organized in three main groups. The first group requires specimens exposing to fire I. In the second group, specimens would be exposed to fire II, and specimens in

the third group will face fire III. There are two sizes of specimens in each group, Model 100 and M300. Take the first group for example, Model 100 would perform a spalling process with spalling rate I firstly and export nodal temperature distribution. Another model will carry out a Model 100 specimen with spalling rate II exposed to fire I and get the nodal temperature distribution as the result. The following analysis is a Model 100 specimen go through the fire period for the whole two hours without spalling happens. Three finite element models for Model 100 in the first group, and another three models for Model 300 performed spalling process with spalling rate I, spalling rate II and no spalling happens. There are six finite element models perform different spalling rate cases in one group totally. Same finite element analyses happen to the second group and the third group.

4.2 Nodal temperature

Figure 4-1 shows the scale used to plot the temperature distributions. With this scale as reference, nodal temperature distributions in each model are showed directly and clearly.

4.2.1 Specimens exposed to fire I

4.2.1.1 Model 100 develops spalling rate I

As implicated in Figure 3-3, for spalling rate I case, the spalling depths is divided into 6 parts considering element size (5 x 5mm), consequently, the heat transfer procedure is stepped by the occurrence of spalling. Model 100 runs for the first 790 seconds when the first 5mm depth layer spalls off, continue running the 100mm x 95mm model for the next 260 seconds, accumulated to be 1050 seconds, then another 5mm layer for another 260 seconds, then the next 3mm and 2mm.

There are 6 points (Table 4-1) for spalling rate 1, starts from the very bottom of the model to the layer which would be the fire-facing surface by all the five spalling steps. 20 mm above point 1 which is the total spalling depth lies point 6.

Temperature distribution of each step for Model 100 is showed in Table 4-2. At the beginning of the heating process, the temperature decreases from the bottom surface into the model. As the fire continues for 790 seconds, when the surface temperature is up to 620 °C, a 5 mm thickness layer spalls off from the bottom surface, the temperature moves inwards into the model. As the fifth steps that 2 mm thickness layer is removed from the model, spalling ends.

The nodal temperatures of symbolic points are shown in Figure 4-2 (a) and (b). The different in these two figures in Figure 4-2 is (b) specifying the first 1800 seconds period in which spalling often happens.

4.2.1.2 Model 100 develops spalling rate II

For spalling rate II, there are five steps in spalling process, and five points on the five spalling layers exposed correspondingly. The coordinates of theses five points are showed in Table 4-1 (the second column). Spalling occurs earlier and lasts shorter than spalling rate I case. Specimens went through heavier spalling periods which are showed in Table 4-3 of the development of nodal temperature distributions. Nodal temperature distributions of five symbolic points are showed in Figure 4-3 (a) and (b).

4.2.1.3 Model 100 develops no spalling

A path with six points is made to specimens as a comparison with the spalling cases. Coordinates of these six symbolic points are also showed in Table 4-1 (the third column). For this specific, no spalling condition, only the moment at which the temperature of each points reach their peak values are showed in Table 4-4. Temperature distributions are showed in Figure 4-4.

4.2.1.4 Model 300 develops spalling rate I

Same procedures are carried out expect changing Model 100 to Model 300. Six symbolic points (Table 4-1) are the same as in Model 100. The heating process of Model 300 is tabulated in Table 4-5 and the development of nodal temperatures with time is showed in Figure 4-5 (a) and (b).

4.2.1.5 Model 300 develops spalling rate II

There are five spalling steps in spalling rate II and the path is made of five points for each spalling process as showed in Table 4-1 (the second column). The heat transfer procedure is showed in Table 4-6 for all the five spalling steps and the development of nodal temperature distributions are showed in Figure 4-6 (a) and (b).

4.2.1.6 Model 300 develops no spalling

For this no spalling case, coordinates of six symbolic points are also showed in Table 4-1 (the third column). Table 4-7 shows the peak value moment of nodal temperature distributions for all the nodes in this model. The nodal temperature distributions of these six symbolic points are exported as the analysis results as showed in Figure 4-7.

4.2.2 Specimens exposed to fire II

In this section, specimens would perform fire resisting against Fire II.

4.2.2.1 Model 100 develops spalling rate I

Same spalling procedure took place in this specimen as the specimen tested in Chapter 4.2.1.1. Six spalling steps happened and coordinates of six symbolic points are the same as showed in Table 4-1. The only difference is the specimen exposed to a higher heating rate, and the corresponding nodal temperature distributions would be higher than that discussed in Chapter 4.2.1.1. Heat transfer procedure of this specimen is showed in Table 4-8 and the development of nodal temperature distributions are showed in Figure 4-8 (a) and (b).

4.2.2.2 Model 100 develops spalling rate II

Coordinate of five symbolic points are showed in Table 4-1 and the spalling procedure are tabulated in Table 4-9. Analysis results, the nodal temperature distributions are showed in Figure 4-9 (a) and (b).

4.2.2.3 Model 100 develops no spalling

For this no spalling case, coordinates of six symbolic points are also showed in Table 4-1 (the third column). Table 4-10 shows the peak value moment of nodal temperature distributions for all the nodes in this model. The nodal temperature distributions of these six symbolic points are exported as the analysis results as showed in Figure 4-10.

4.2.2.4 Model 300 develops spalling rate I

Same procedures are carried out expect changing Model 100 to Model 300. Six symbolic points (Table 4-1) are the same as in Model 100. The heating process of Model 300 is tabulated in Table 4-11 and the development of nodal temperatures with time is showed in Figure 4-11 (a) and (b).

4.2.2.5 Model 300 develops spalling rate II

Coordinate of five symbolic points are showed in Table 4-1 and the spalling procedure are tabulated in Table 4-12. Analysis results, the nodal temperature distributions are showed in Figure 4-12 (a) and (b).

4.2.2.6 Model 300 develops no spalling

For this no spalling case, coordinates of six symbolic points are also showed in Table 4-1 (the third column). Table 4-13 shows the peak value moment of nodal temperature distributions for all the nodes in this model. The nodal temperature distributions of these six symbolic points are exported as the analysis results as showed in Figure 4-13.

4.2.3 Specimens exposed to fire III

In this section, specimens would perform fire resisting against Fire II.

4.2.3.1 Model 100 develops spalling rate I

Same spalling procedure took place in this specimen as the specimen tested in Chapter 4.2.1.1 and Chapter 4.2.2.1. Six spalling steps happened and coordinates of six symbolic points are the same as showed in Table 4-1. The only difference is the specimen exposed to the highest heating rate among these three, and the corresponding nodal temperature distributions would be higher than that the other discussed before. Heat transfer procedure of this specimen is showed in Table 4-14 and the development of nodal temperature distributions are showed in Figure 4-14 (a) and (b).

4.2.3.2 Model 100 develops spalling rate II

Coordinate of five symbolic points are showed in Table 4-1 and the spalling procedure are tabulated in Table 4-15. Analysis results, the nodal temperature distributions are showed in Figure 4-15 (a) and (b).

4.2.3.3 Model 100 develops no spalling

For this no spalling case, coordinates of six symbolic points are also showed in Table 4-1 (the third column). Table 4-16 shows the peak value moment of nodal temperature distributions for all the nodes in this model. The nodal temperature distributions of these six symbolic points are exported as the analysis results as showed in Figure 4-16.

4.2.3.4 Model 300 develops spalling rate I

Same procedures are carried out expect changing Model 100 to Model 300. Six symbolic points (Table 4-1) are the same as in Model 100. The heating process of Model 300 is tabulated in Table 4-17 and the development of nodal temperatures with time is showed in Figure 4-17 (a) and (b).

4.2.3.5 Model 300 develops spalling rate II

Coordinate of five symbolic points are showed in Table 4-1 and the spalling procedure are tabulated in Table 4-18. Analysis results, the nodal temperature distributions are showed in Figure 4-18 (a) and (b).

4.2.3.6 Model 300 develops no spalling

For this no spalling case, coordinates of six symbolic points are also showed in Table 4-1 (the third column). Table 4-19 shows the peak value moment of nodal temperature distributions for

all the nodes in this model. The nodal temperature distributions of these six symbolic points are exported as the analysis results as showed in Figure 4-19.

4.3 Summary of results

4.3.1 Nodal temperature comparison of the spalling case and no spalling case

In this section, nodal temperature distributions of spalling cases and no spalling cases with the same fire and spalling rate conditions are compared in same figures, providing a direct way to tell how spalling influences the performances of high strength concrete in fires. Nodal temperature distributions of six symbolic points were exported as analysis results for spalling rate I case as well as five points' temperature distributions were presented for spalling rate II case. In order to regular comparisons, only five points are showed in the comparison figures for each case. Coordinate for these five symbolic points are showed in Table 4-1 (the second column).

Comparisons of the maximum nodal temperature distributions for each case and the moments when nodal temperature reaches maximum would also be present. Table 4-20 shows the comparison of five symbolic points' maximum nodal temperature under different spalling rate cases exposed to fire I and the moments when nodal temperature reached maximum are showed in Table 4-21. With same spalling rate and same fire exposed to, nodal temperatures of five symbolic points are nearly the same for Model 100 and Model 300, thus Table 4-20 shows Model 100 only. Table 4-22 and Table 4-24 show the comparison of five symbolic points' maximum nodal temperature under different spalling rate cases exposed to fire II and fire III.

The moments when nodal temperature reached maximum are showed in Table 4-23 for specimens exposed to fire II and Table 4-25 for specimens exposed to fire III.

4.3.1.1 Model 100 exposed to fire I

In this section, three 100 mm x 100 mm specimens experienced spalling rate I, spalling rate II and without spalling occurrence. Figure 4-20 (a) shows the development of temperature distributions of Node 1 (of the five symbolic points along the path) going through three different spalling cases when exposed to fire I. Figure 4-20 (b) is the comparison of nodal temperature distributions for Node 2 in each of the spalling rate cases. Figure 4-20 (c) – (e) show the comparisons of the Node 3, Node 4 and Node 5 respectively.

4.3.1.2 Model 100 exposed to fire II

The comparison process is the same as discussed in Chapter 4.3.1.1 expect for specimens in this section would be exposed to fire II. Nodal temperature distributions for five symbolic points are showed in Figure 4-21 (a) – (e).

4.3.1.3 Model 100 exposed to fire III

The comparison process is the same as discussed in Chapter 4.3.1.1 expect for specimens in this section would be exposed to fire III. Nodal temperature distributions for five symbolic points are showed in Figure 4-22 (a) – (e).

4.3.1.4 Model 300 exposed to fire I

In this section, three 100 mm x 300 mm specimens with same five symbolic points as showed in Table 4-1 (the second column) experienced spalling rate I, spalling rate II and without spalling occurrence. Figure 4-23 (a) – (e) show the comparisons of nodal temperature distributions from Node 1 to Node 5 with three spalling rate cases.

4.3.1.5 Model 300 exposed to fire II

The comparison process is the same as discussed in Chapter 4.3.1.4 expect for specimens in this section would be exposed to fire II. Nodal temperature distributions for five symbolic points are showed in Figure 4-24 (a) – (e).

4.3.1.6 Model 300 exposed to fire III

The comparison process is the same as discussed in Chapter 4.3.1.4 expect for specimens in this section would be exposed to fire III. Nodal temperature distributions for five symbolic points are showed in Figure 4-25 (a) – (e).

4.3.2 Reduction of reinforcement strength

This research is based on pure high strength concrete slabs, in this section, reinforced steel bars would be introduced into analyses.

From the tests by Kodur (2000) discussed above, the yield strength of reinforcement steel bars is 420 MPa. Eurocode 2 provides coefficient $k_s(T)$ to express the reduction of yield strength of reinforcing steel, the value of which can be calculated using Equation 2-6. According to the conclusion by Sanjayan and Stocks (1993), Model 100 would occur spalling with a 25 mm depth concrete cover while Model 300 with a 75 mm depth concrete cover may spall. A node located (0.0, 25.0, 0.0) of Model 100 and a node located (0.0, 75.0, 0.0) for Model 300 would be recorded nodal temperatures. These nodes are supposed to replace the concrete by reinforcing steel bars and the nodal temperatures are used to show how the yield strength decreases when exposed to fires.

For each analysis case, only the peak values for these nodes are showed in Table 4-26 to 4-28. The yield strength of reinforcing steel ($f_{sk}(T)$) is the yield strength at 20 °C ($f_{yk}(20^\circ\text{C}) = 420$ MPa), multiplied by the reducing coefficient $k_s(T)$.

Case A1: Model 100 with 25 mm concrete cover exposed to fire I performed Spalling rate I

Peak temperature for the steel bars: 856 °C

$$k_s(T) = 0.0688$$

$$f_{sk}(T) = 0.0688 \times 420 = 29 \text{ MPa}$$

Case A2: Model 100 with 25 mm concrete cover exposed to fire I performed Spalling rate II

Peak temperature for the steel bars: 855 °C

$$k_s(T) = 0.069$$

$$f_{sk}(T) = 0.069 \times 420 = 29 \text{ MPa}$$

Case A3: Model 100 with 25 mm concrete cover exposed to fire I performed No Spalling

Peak temperature for the steel bars: 624 °C

$$k_s(T) = 0.295$$

$$f_{sk}(T) = 0.295 \times 420 = 124 \text{ MPa}$$

Case A4: Model 300 with 75 mm concrete cover exposed to fire I performed Spalling rate I

Peak temperature for the steel bars: 684 °C

$$k_s(T) = 0.141$$

$$f_{sk}(T) = 0.141 \times 420 = 59 \text{ MPa}$$

Case A5: Model 300 with 75 mm concrete cover exposed to fire I performed Spalling rate II

Peak temperature for the steel bars: 682 °C

$$k_s(T) = 0.146$$

$$f_{sk}(T) = 0.146 \times 420 = 61 \text{ MPa}$$

Case A6: Model 300 with 75 mm concrete cover exposed to fire I performed No Spalling

Peak temperature for the steel bars: 622 °C

$$k_s(T) = 0.301$$

$$f_{sk}(T) = 0.301 \times 420 = 126 \text{ MPa}$$

Case B1: Model 100 with 25 mm concrete cover exposed to fire II performed Spalling rate I

Peak temperature for the steel bars: 743 °C

$$k_s(T) = 0.091$$

$$f_{sk}(T) = 0.091 \times 420 = 38 \text{ MPa}$$

Case B2: Model 100 with 25 mm concrete cover exposed to fire II performed Spalling rate II

Peak temperature for the steel bars: 733 °C

$$k_s(T) = 0.093$$

$$f_{sk}(T) = 0.093 \times 420 = 39 \text{ MPa}$$

Case B3: Model 100 with 25 mm concrete cover exposed to fire II performed No Spalling

Peak temperature for the steel bars: 545 °C

$$k_s(T) = 0.499$$

$$f_{sk}(T) = 0.499 \times 420 = 209 \text{ MPa}$$

Case B4: Model 300 with 75 mm concrete cover exposed to fire II performed Spalling rate I

Peak temperature for the steel bars: 598 °C

$$k_s(T) = 0.362$$

$$f_{sk}(T) = 0.362 \times 420 = 152 \text{ MPa}$$

Case B5: Model 300 with 75 mm concrete cover exposed to fire II performed Spalling rate II

Peak temperature for the steel bars: 596 °C

$$k_s(T) = 0.378$$

$$f_{sk}(T) = 0.378 \times 420 = 159 \text{ MPa}$$

Case B6: Model 300 with 75 mm concrete cover exposed to fire II performed No Spalling

Peak temperature for the steel bars: 544 °C

$$k_s(T) = 0.501$$

$$f_{sk}(T) = 0.501 \times 420 = 211 \text{ MPa}$$

Case C1: Model 100 with 25 mm concrete cover exposed to fire III performed Spalling rate I

Peak temperature for the steel bars: 1041 °C

$$k_s(T) = 0.032$$

$$f_{sk}(T) = 0.032 \times 420 = 13 \text{ MPa}$$

Case C2: Model 100 with 25 mm concrete cover exposed to fire III performed Spalling rate II

Peak temperature for the steel bars: 1080 °C

$$k_s(T) = 0.024$$

$$f_{sk}(T) = 0.024 \times 420 = 10 \text{ MPa}$$

Case C3: Model 100 with 25 mm concrete cover exposed to fire III performed No Spalling

Peak temperature for the steel bars: 776 °C

$$k_s(T) = 0.085$$

$$f_{sk}(T) = 0.085 \times 420 = 36 \text{ MPa}$$

Case C4: Model 300 with 75 mm concrete cover exposed to fire III performed Spalling rate I

Peak temperature for the steel bars: 847 °C

$$k_s(T) = 0.071$$

$$f_{sk}(T) = 0.071 \times 420 = 30 \text{ MPa}$$

Case C5: Model 300 with 75 mm concrete cover exposed to fire III performed Spalling rate II

Peak temperature for the steel bars: 855 °C

$$k_s(T) = 0.069$$

$$f_{sk}(T) = 0.069 \times 420 = 29 \text{ MPa}$$

Case C6: Model 300 with 75 mm concrete cover exposed to fire III performed No Spalling

Peak temperature for the steel bars: 773 °C

$$k_s(T) = 0.086$$

$$f_{sk}(T) = 0.086 \times 420 = 36 \text{ MPa}$$

4.3.3 Observation

This section presents the observation from Figure 4-20 to Figure 4-25 and reduction of reinforcing steel yield strength.

- (1) Figure (a) in each figure gives the first step of fire resistant performance and no spalling happened. For same sized specimens exposed to a same fire, nodes with the same labels displayed the same temperature distribution at same moments. Nodes lied in the surface layers (fire exposed faces) would spall off at the end of the first step for spalling cases and the development of nodal temperature distributions of these nodes stopped.

- (2) Nodal temperature distributions for group with spalling rate II developed smoothly with time before 430 seconds, when spalling depth I started to spall. Figure (b) shows that curve of Node 2 jump up to a higher temperature level. Same temperature jumps happened to (c)-(e). Meanwhile, the group with spalling rate I and no spalling developed smoothly still. Timing is a key factor for developing nodal temperature, spalled and exposed to fire earlier, nodal temperature gained higher. Early period is the most rapid heating zone that heating distributes the most. Figure (b) also shows that nodal temperature of the group with spalling rate II was the highest among three spalling cases every moment after spalling occurred. Heat transfer is more efficient when directly conducting to fires than conducting to the external concrete.
- (3) No matter at which spalling rate specimens performed, nodes in the same layer would come up to a same temperature at the end of fires.
- (4) Figure 2-10 shows the theoretical reduction of reinforcing steel yield strength at elevated temperature. The analysis results show the same dramatic decrease of yield strength. The peak temperature for both Case C1 and Case C2 excess 1000 °C, the yield strength of reinforcing steel bars is almost vanished.
- (5) Reinforcing steel yield strength at elevated temperature in Case A1 and Case A2 are nearly the same. While yield strength reduced less in Case A3 compared with Case A1 and Case A2.

- (6) Compare the steel yield strength from Case A1, Case B1 and Case C1, same specimen with same spalling performance exposed to different fires. The nodal temperature is highest in Case C1 and the yield strength decreases largest in Case C1.

4.3.4 Conclusion

- (1) For each certain node in no spalling cases, take Node 6 in Figure 4-4 for example, curve of nodal temperature distribution with time follows exactly the same general shape but lesser temperatures of the fire which the model is exposed to, fire I in this example.
- (2) For the spalling cases, such as point 2 of Model 100 exposed to fire I (Figure 4-2) for example. The first 5mm layer (spalling depth I) spalling off led the second layer where point 2 locates exposed to fire. Development of nodal temperature went smoothly for the first 790s and jumped to a higher level of temperature to continue. As implicates in Figure 4-2, development of nodal temperature of Node 1 ended at 790s, meanwhile jumps happened to Node 2-Node 6, “jump” reflects removal of concrete layers and direct exposure to fire at the surface.
- (3) Look into one figure of no spalling cases such as Figure 4-4, compare the peak temperature of the surface layer (Node 1) and the layer locates 20 mm above (Node 6) specifically. The temperature of Node 6 was about 90 percent of that of Node 1 at a same moment. Same happened to all the other no spalling cases. In another word, along the

paths which are made to collect and export nodal temperatures, peak nodal temperature decreases around 10 percent from start points to the end points. Generally temperatures decrease over the height of the slab.

(4) For fire I group, the first spalling occurred to the group with spalling rate I when surface temperature of specimens were around 620°C. While when surface temperature reached 500 °C spalling happened to the group with spalling rate II.

(5) Spalling occurred at the early stage of fires where heating rates are the highest for all types of fires.

(6) Temperature of fire I increase with time from beginning to the end, nodal temperature increase correspondingly. Compare the temperature performances of Node 5 in Table 4-20. Node 5 located at the layer which didn't spall off in any spalling rate cases and kept been heated for 7200 seconds. Maximum temperature occurred at 7200 seconds for these spalling rate cases, but maximum values decrease from spalling rate I to spalling rate II then to no spalling case. Maximum temperature of spalling rate I case is 38 percent larger than that of no spalling case as well as maximum temperature of spalling rate II is around 38 percent larger than that of no spalling case. Therefore, spalling greatly influences temperature distribution.

(7) From the observation (5), spalling rate is not an important factor influences the performance of reinforcing steel bars. The critical factor is whether spalling occurs. Cases

with spalling occurring gained higher temperature thus reduced the yield strength of the steel bars.

- (8) As observation (6) points, the types of fire which specimens exposed to promote differences in the performance of steel bars at elevated temperature. Fire III has the highest peak temperature among the three, therefore, specimens exposed to fire III would occur severe spalling and destroy the steel bars too.

Table 4-1 Nodal coordinates of symbolic points on the path for spalling rate I case, spalling rate II case and no spalling case

Node number	Coordinates for spalling rate I case	Coordinates for spalling rate II case	Coordinates for no spalling case
1	(0.0,0.0,0.0)	(0.0,0.0,0.0)	(0.0,0.0,0.0)
2	(0.0,5.0,0.0)	(0.0,5.0,0.0)	(0.0,5.0,0.0)
3	(0.0,10.0,0.0)	(0.0,10.0,0.0)	(0.0,10.0,0.0)
4	(0.0,15.0,0.0)	(0.0,15.0,0.0)	(0.0,15.0,0.0)
5	(0.0,18.0,0.0)	(0.0,20.0,0.0)	(0.0,18.0,0.0)
6	(0.0,20.0,0.0)		(0.0,20.0,0.0)

Table 4-2 Heat transfer procedure of Model 100 with spalling rate I exposed to fire I

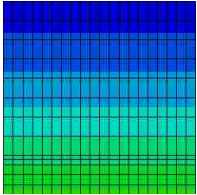
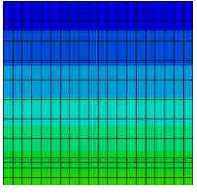
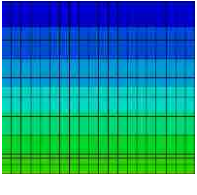
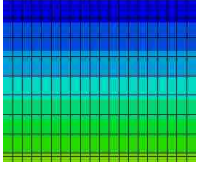
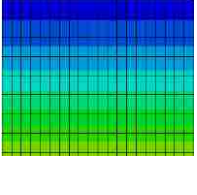
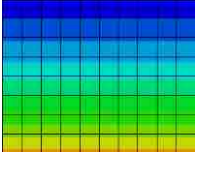
Time (s)	0-790	790-1050	1050-1310
			
Time (s)	1310-1830	1830-2610	2610-7200
			

Table 4-3 Heat transfer procedure of Model 100 with spalling rate II exposed to fire I

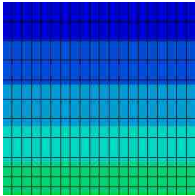
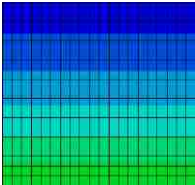
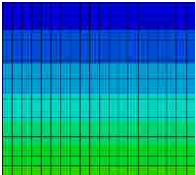
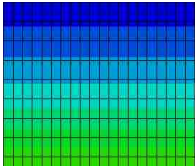
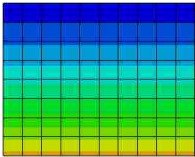
Time (s)	0-430	430-690	690-950
			
Time (s)	950-1290	1290-7200	
			

Table 4-4 Peak values moment of temperature distribution of Model 100 exposed to fire I

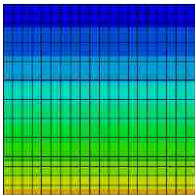
Time (s)	7200
	

Table 4-5 Heat transfer procedure of Model 300 with spalling rate I exposed to fire I

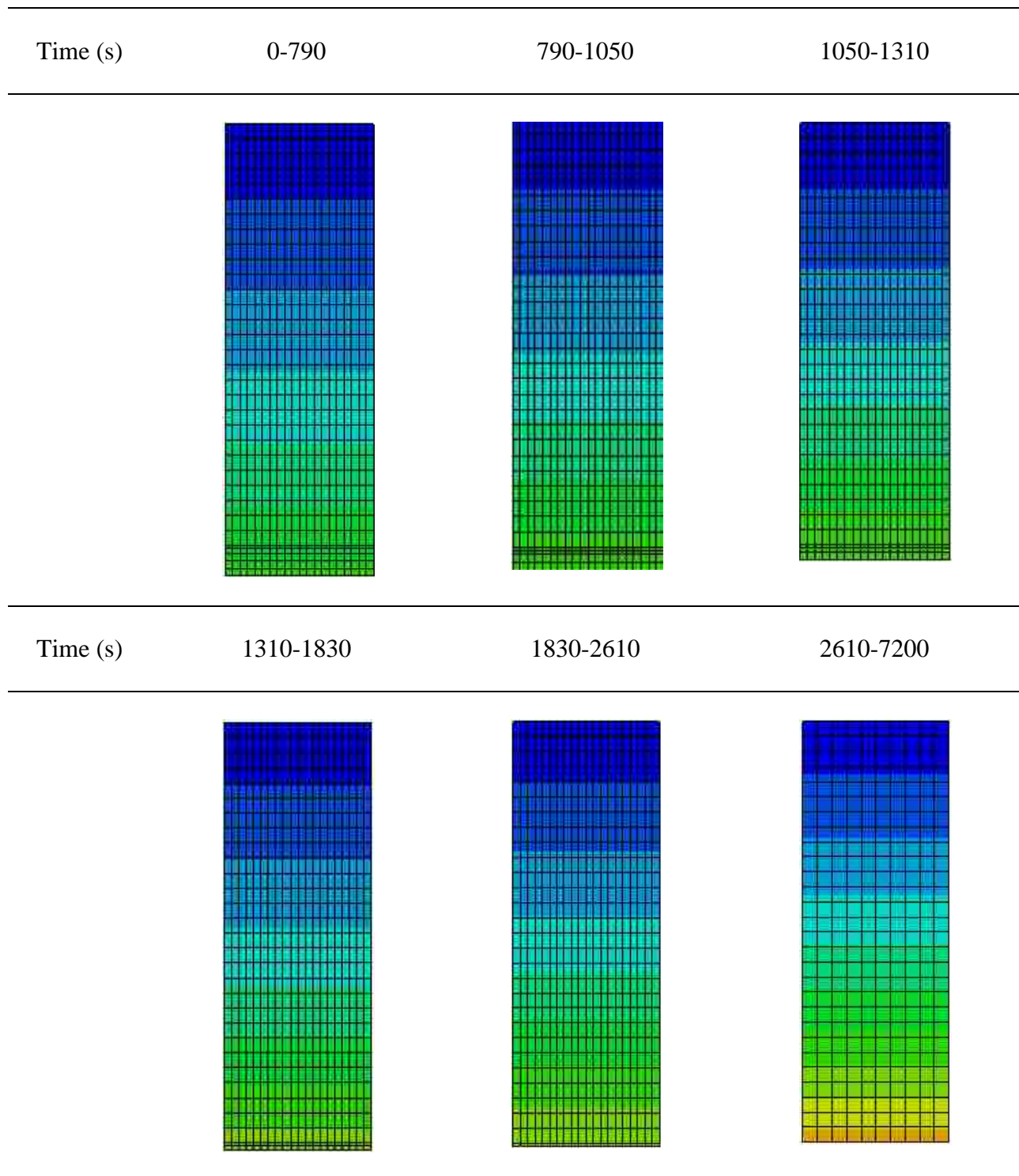


Table 4-6 Heat transfer procedure of Model 300 with spalling rate II exposed to fire I

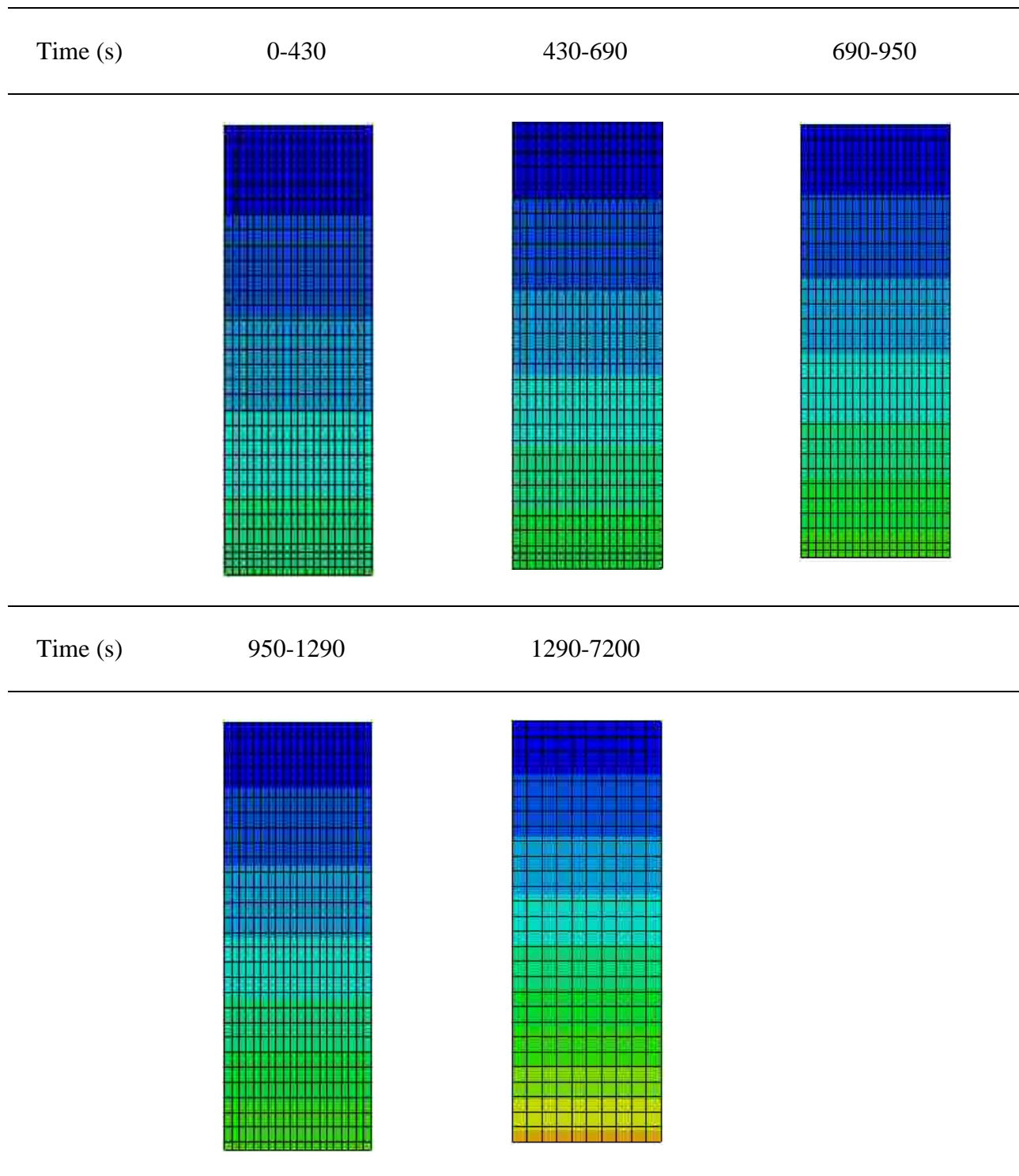


Table 4-7 Peak values moment of temperature distribution of Model 300 exposed to fire I

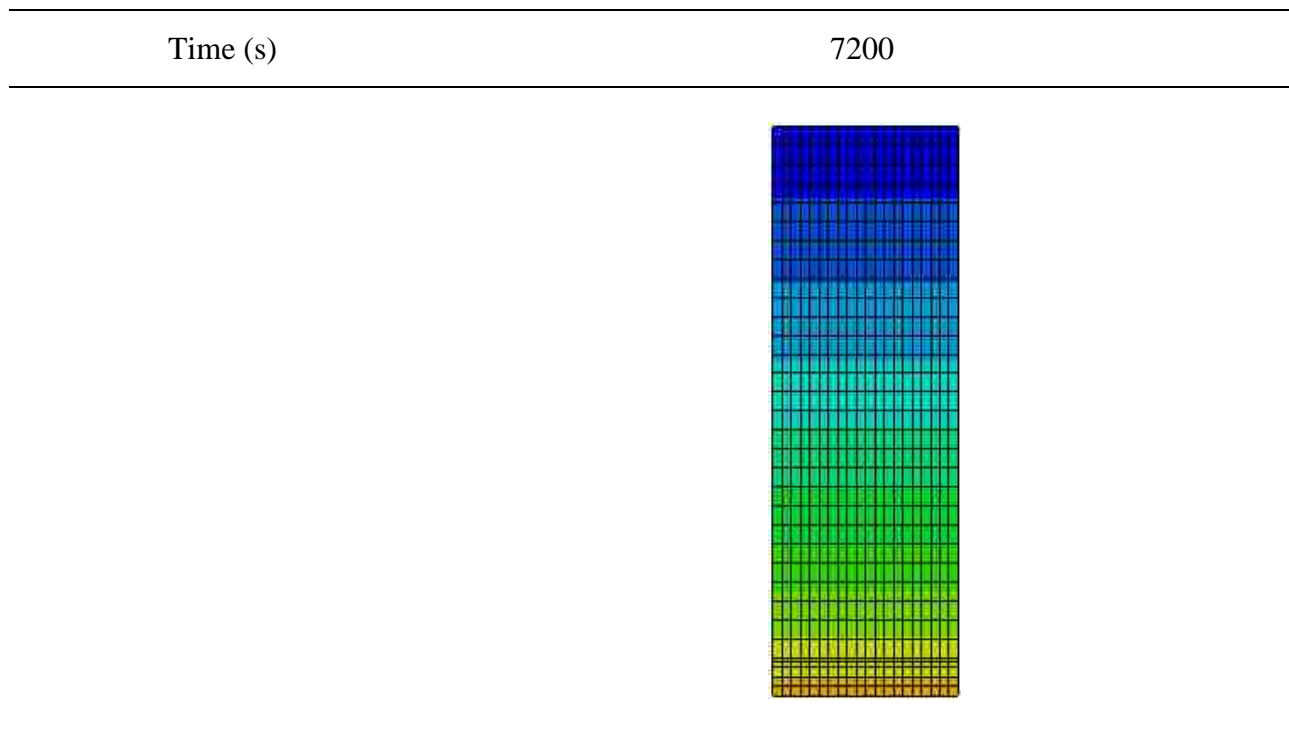


Table 4-8 Heat transfer procedure of Model 100 with spalling rate I exposed to Fire II

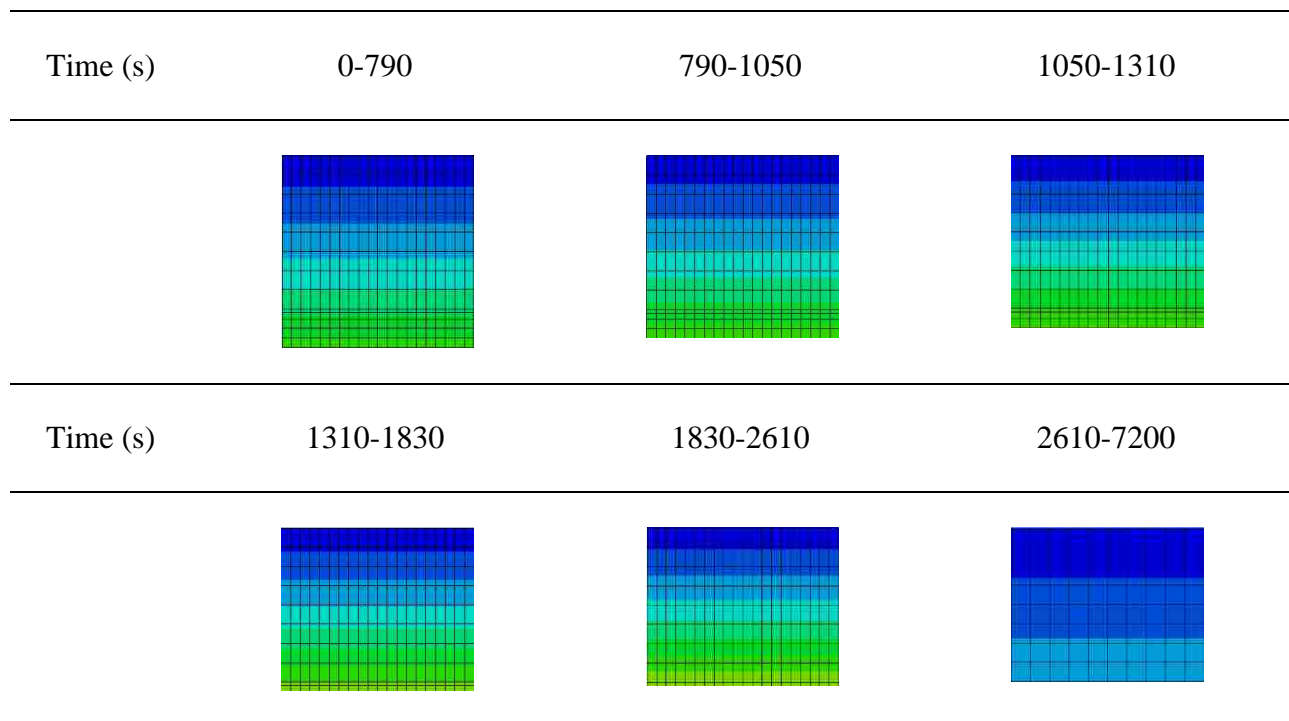


Table 4-9 Heat transfer procedure of Model 100 with spalling rate II exposed to fire II

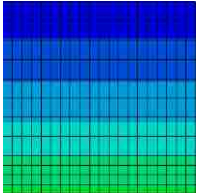
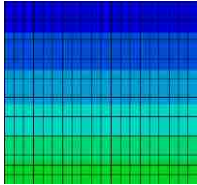
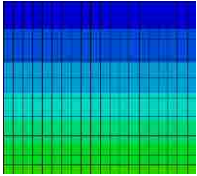
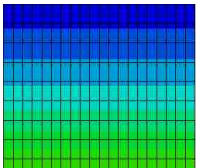
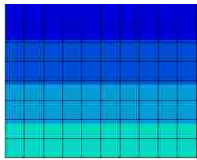
Time (s)	0-430	430-690	690-950
			
Time (s)	950-1290	1290-7200	
			

Table 4-10 Peak values moment of temperature distribution of Model 100 exposed to fire II

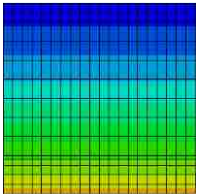
Time (s)	2500
	

Table 4-11 Heat transfer procedure of Model 300 with spalling rate I exposed to fire II

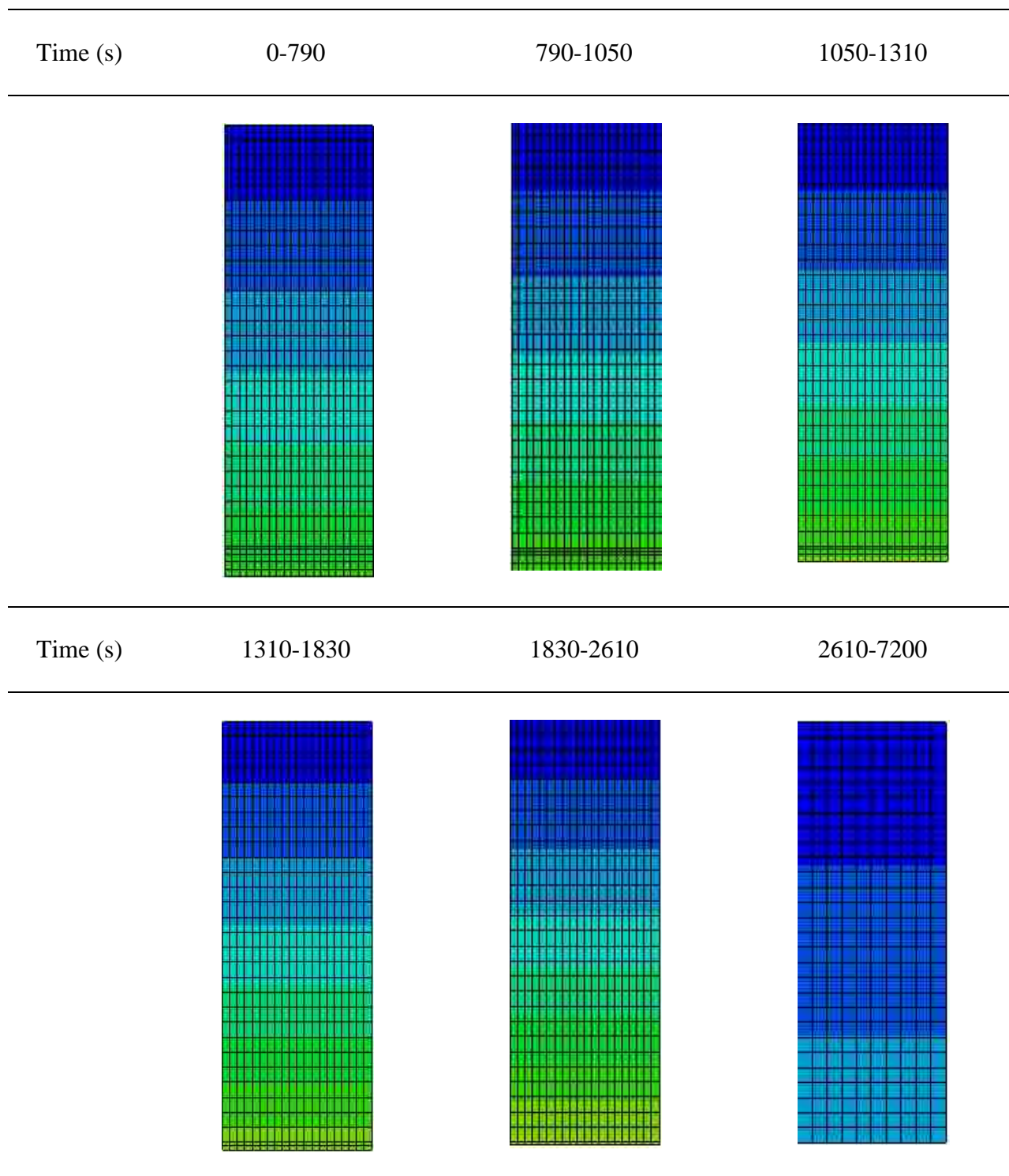


Table 4-12 Heat transfer procedure of Model 300 with spalling rate II exposed to fire II

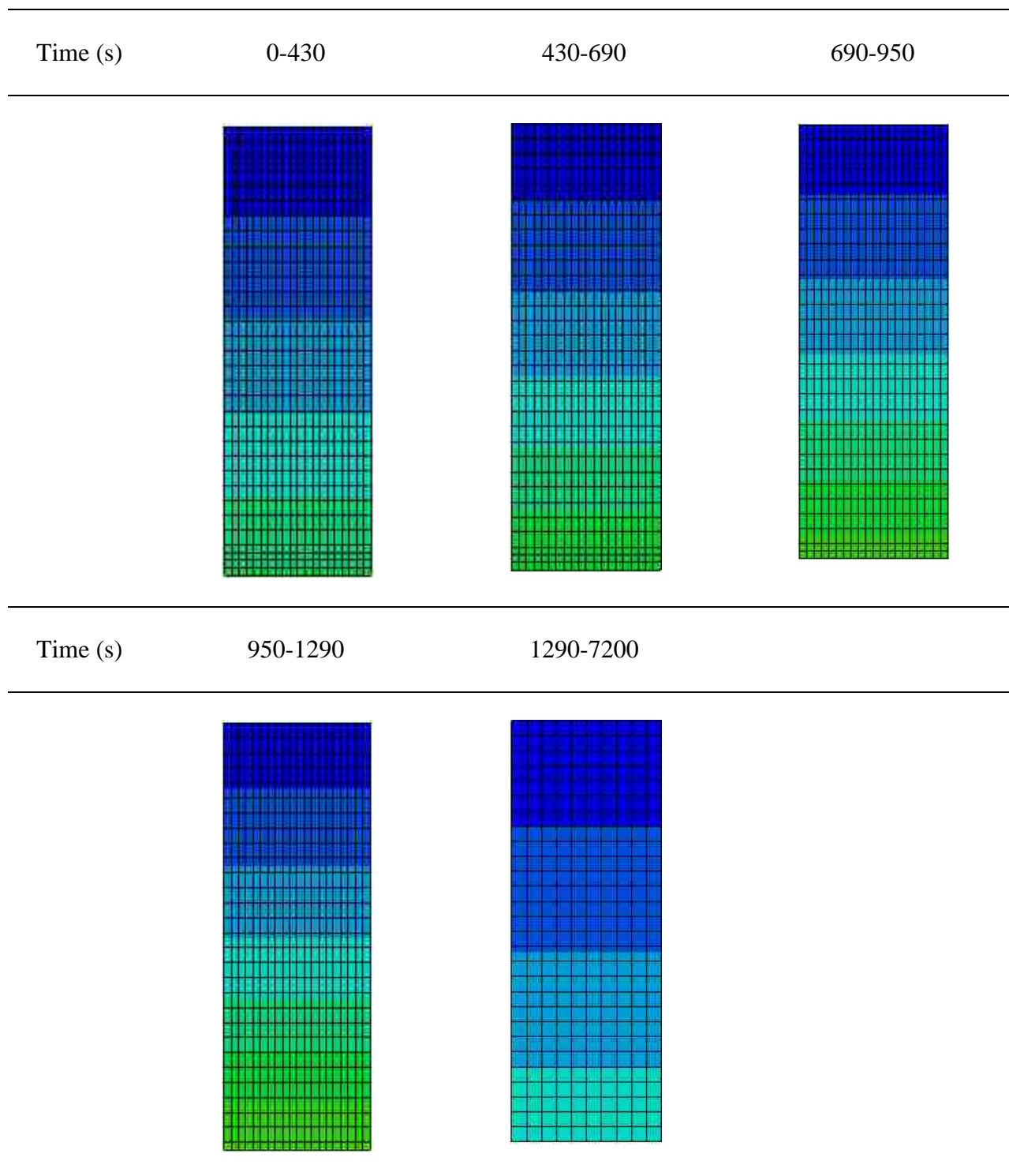


Table 4-13 Peak values moment of temperature distribution of Model 300 exposed to fire II

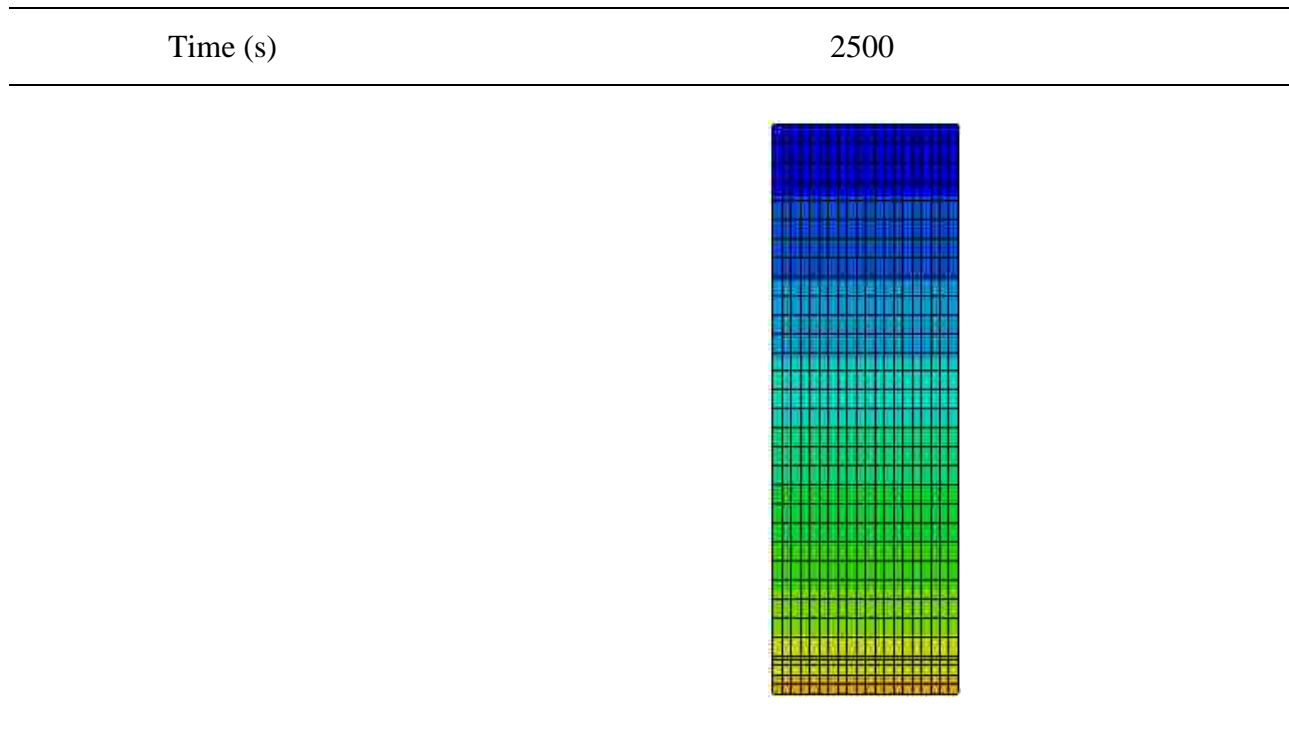


Table 4-14 Heat transfer procedure of Model 100 with spalling rate I exposed to fire III

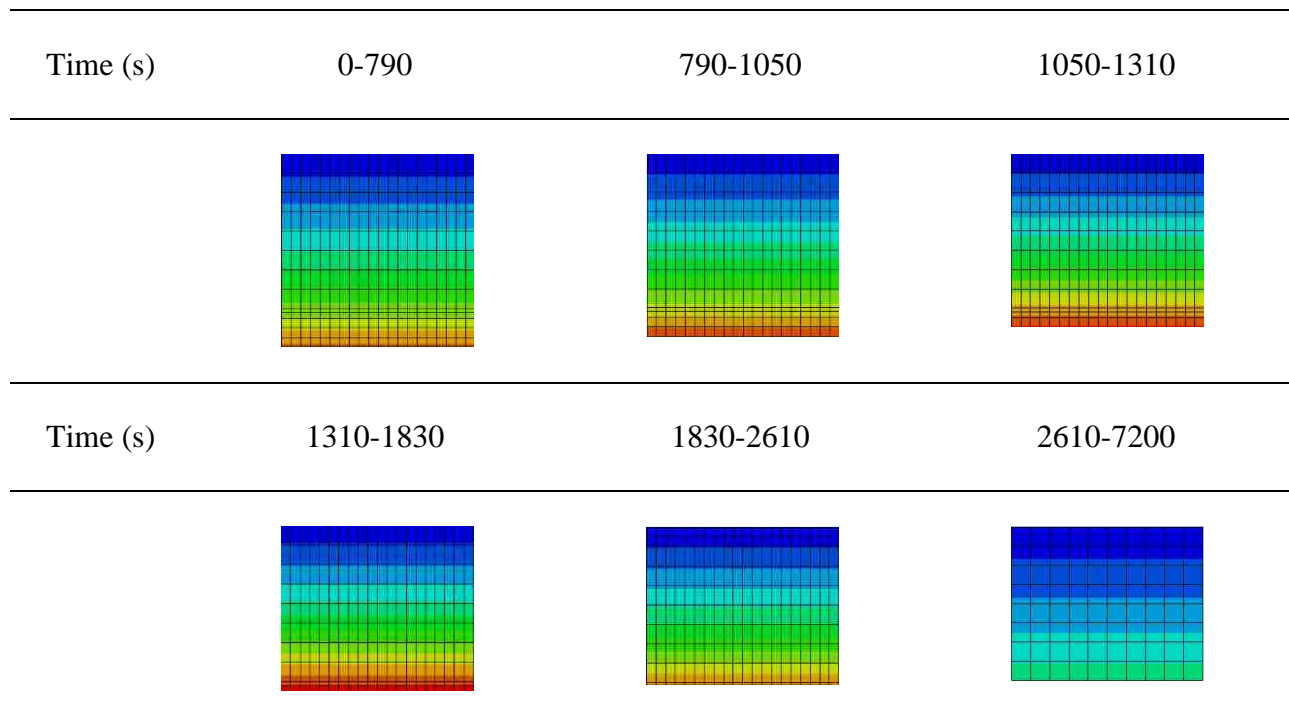


Table 4-15 Heat transfer procedure of Model 100 with spalling rate II exposed to fire III

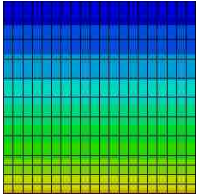
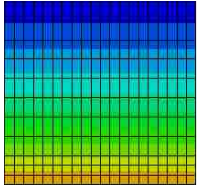
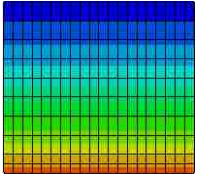
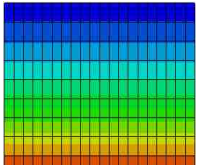
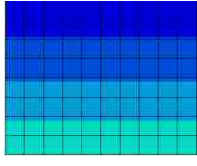
Time (s)	0-430	430-690	690-950
			
Time (s)	950-1290	1290-7200	
			

Table 4-16 Peak values moment of temperature distribution of Model 100 exposed to fire III

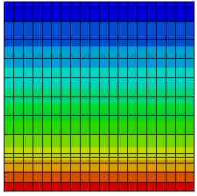
Time (s)	2100
	

Table 4-17 Heat transfer procedure of Model 300 with spalling rate I exposed to fire III

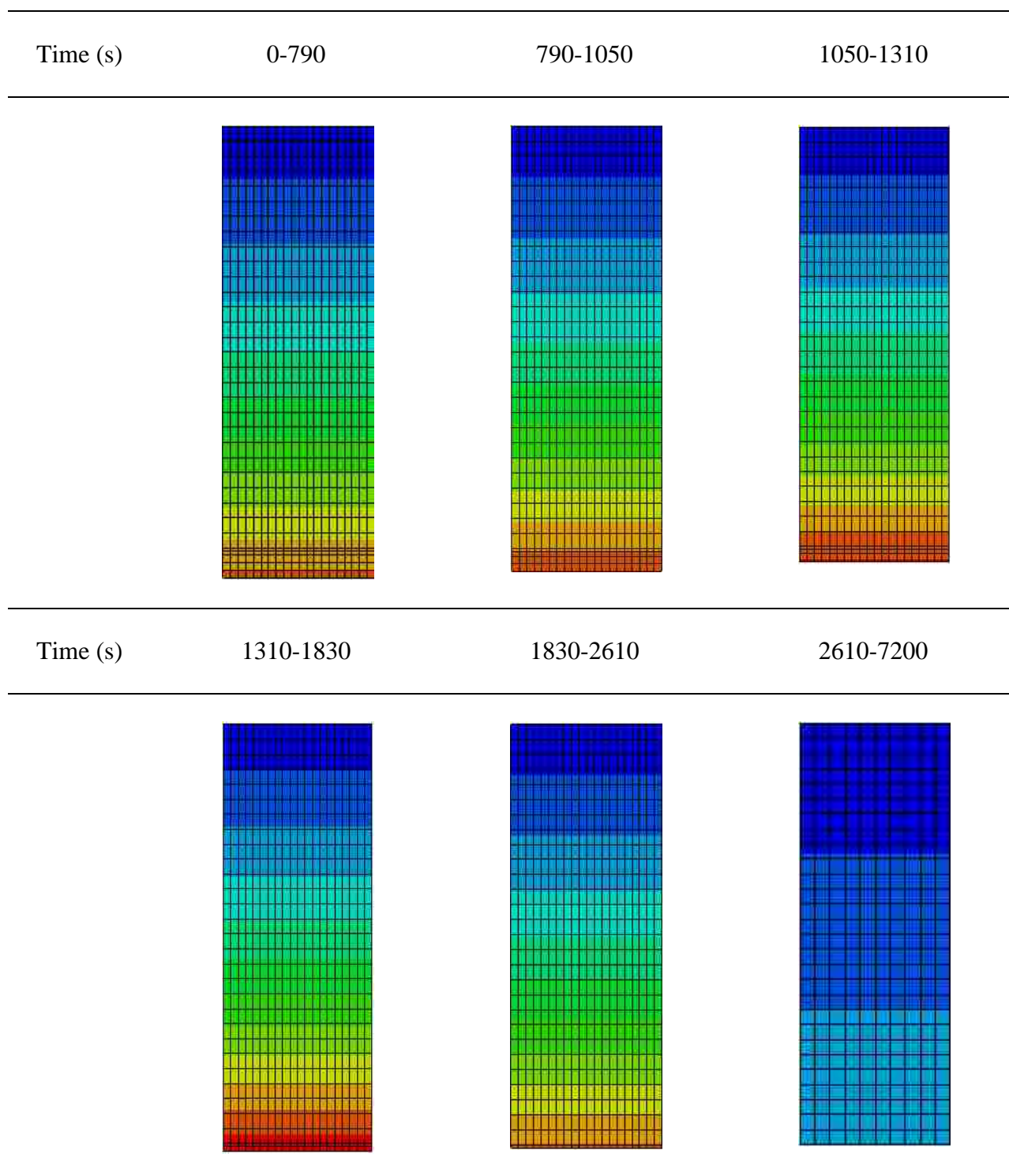


Table 4-18 Heat transfer procedure of Model 300 with spalling rate II exposed to fire III

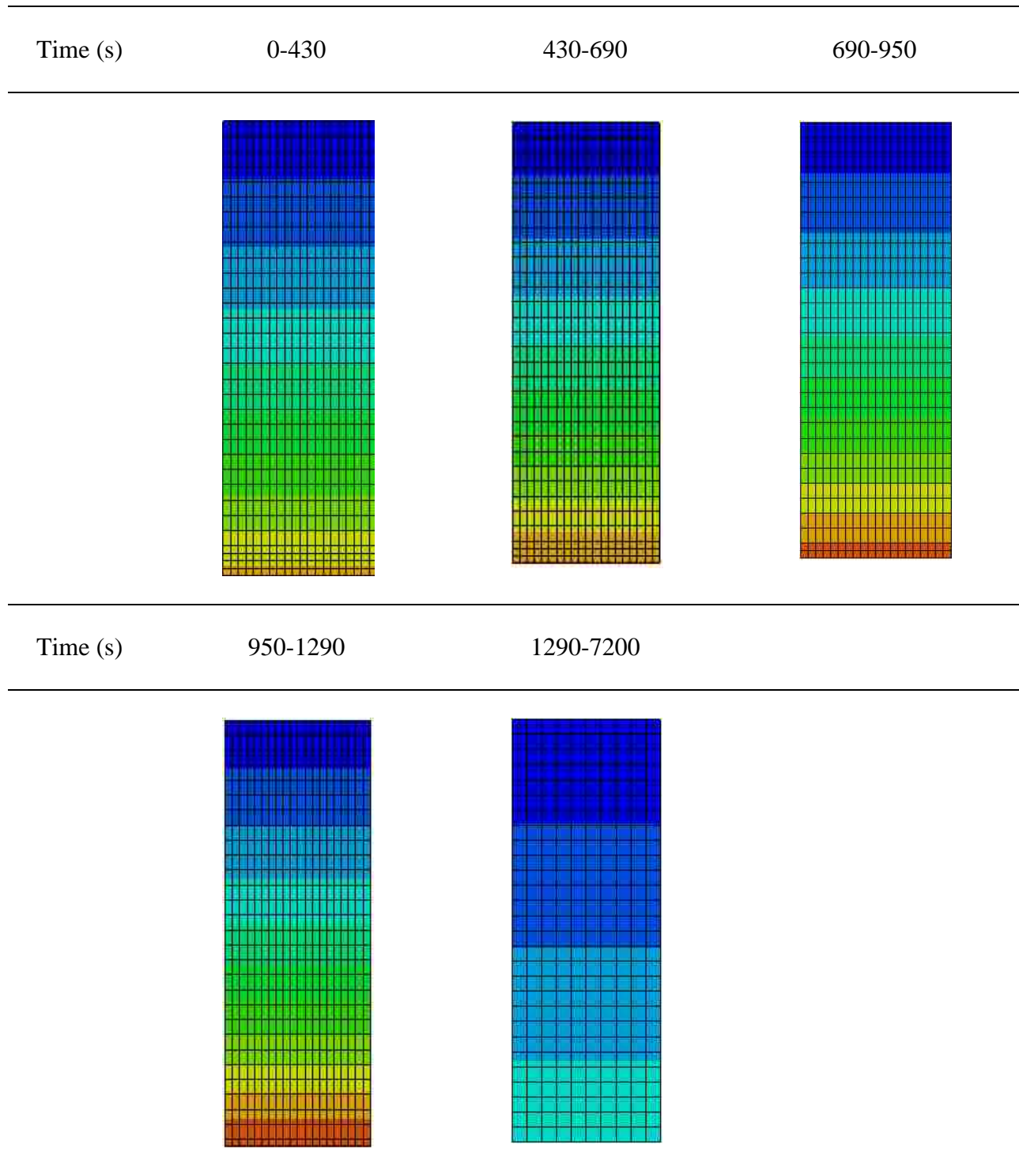


Table 4-19 Peak values moment of temperature distribution of Model 300 exposed to fire III

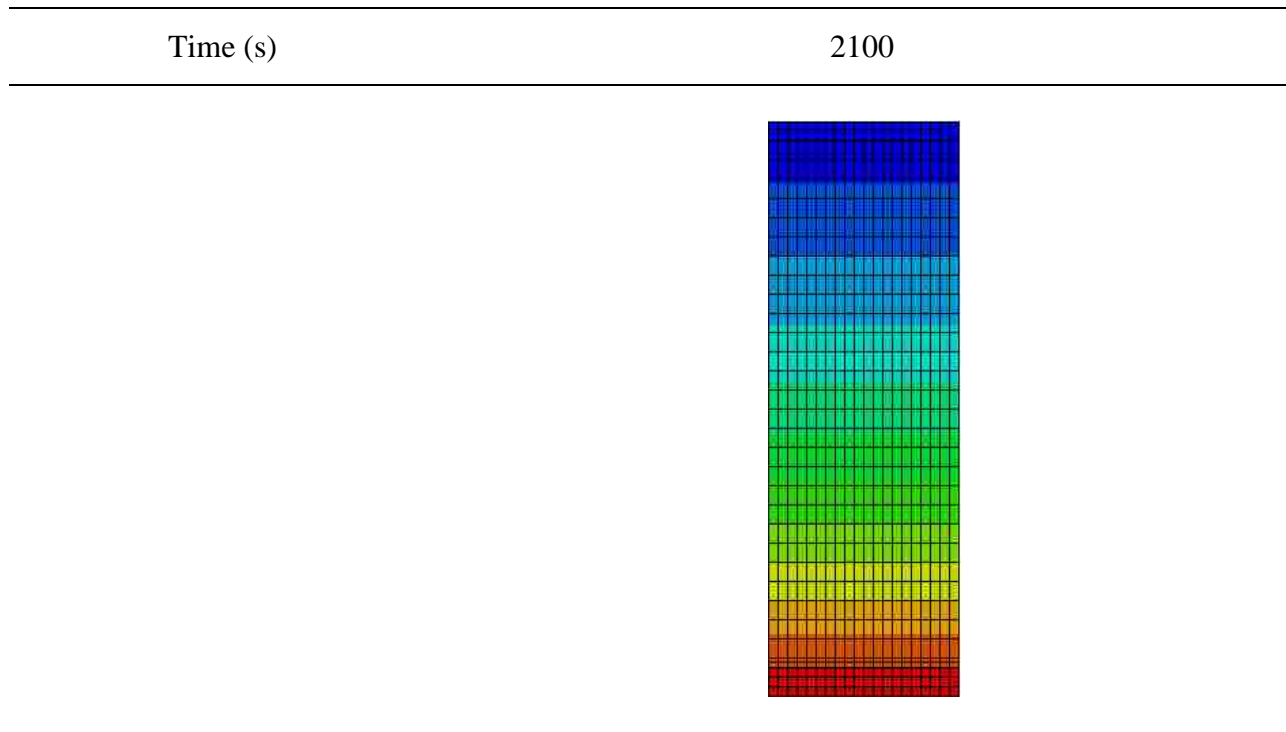


Table 4-20 Comparison of maximum temperature for Model 100 and Model 300 with all spalling rate cases exposed to fire I

Node number	Maximum temperature (°C)		
	Spalling rate I	Spalling rate II	No spalling
1	622	508	940
2	671	580	871
3	707	654	804
4	756	704	740
5	940	937	680

Table 4-21 Moments when nodal temperature researches maximum for Model 100 and Model 300 exposed to fire I

Node number	Time of maximum temperature (s)		
	Spalling rate I	Spalling rate II	No spalling
1	790	430	7200
2	1050	690	7200
3	1310	950	7200
4	1830	1290	7200
5	7200	7200	7200

Table 4-22 Comparison of maximum temperature for Model 100 and Model 300 with all spalling rate cases exposed to fire II

Node number	Maximum temperature (°C)		
	Spalling rate I	Spalling rate II	No spalling
1	639	524	809
2	678	618	751
3	710	666	696
4	759	708	643
5	813	802	592

Table 4-23 Moments when nodal temperature researches maximum for Model 100 and Model 300 exposed to fire II

Node number	Time of maximum temperature (s)		
	Spalling rate I	Spalling rate II	No spalling
1	790	430	2500
2	1050	690	2500
3	1310	950	2500
4	1830	1290	2500
5	2630	2550	2500

Table 4-24 Comparison of maximum temperature for Model 100 and Model 300 with all spalling rate cases exposed to fire III

Node number	Maximum temperature (°C)		
	Spalling rate I	Spalling rate II	No spalling
1	1028	931	1189
2	1074	1007	1101
3	1111	1058	1015
4	1167	1108	931
5	1145	1188	850

Table 4-25 Moments when nodal temperature researches maximum for Model 100 and Model 300 exposed to fire III

Node number	Time of maximum temperature (s)		
	Spalling rate I	Spalling rate II	No spalling
1	790	430	2100
2	1050	690	2100
3	1310	950	2100
4	1830	1290	2100
5	2090	2090	2100

Table 4-26 Peak temperature of the steel bars for Model 100 and Model 300 exposed to fire I and the reinforcing steel yield strength

	Model 100 with 25 mm cover		Model 300 with 75 mm cover	
	Peak temperature (°C)	Yield strength (MPa)	Peak temperature (°C)	Yield strength (MPa)
Spalling rate I	856	29	684	59
Spalling rate II	855	29	682	61
No spalling	624	124	622	126

Table 4-27 Peak temperature of the steel bars for Model 100 and Model 300 exposed to fire II and the reinforcing steel yield strength

	Model 100 with 25 mm cover		Model 300 with 75 mm cover	
	Peak temperature (°C)	Yield strength (MPa)	Peak temperature (°C)	Yield strength (MPa)
Spalling rate I	743	38	598	152
Spalling rate II	733	39	592	159
No spalling	545	209	544	211

Table 4-28 Peak temperature of the steel bars for Model 100 and Model 300 exposed to fire III and the reinforcing steel yield strength

	Model 100 with 25 mm cover		Model 300 with 75 mm cover	
	Peak temperature (°C)	Yield strength (MPa)	Peak temperature (°C)	Yield strength (MPa)
Spalling rate I	1041	13	847	30
Spalling rate II	1080	10	855	29
No spalling	776	36	773	36

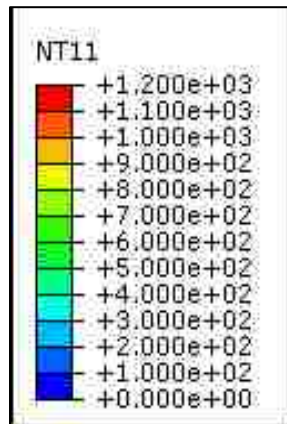
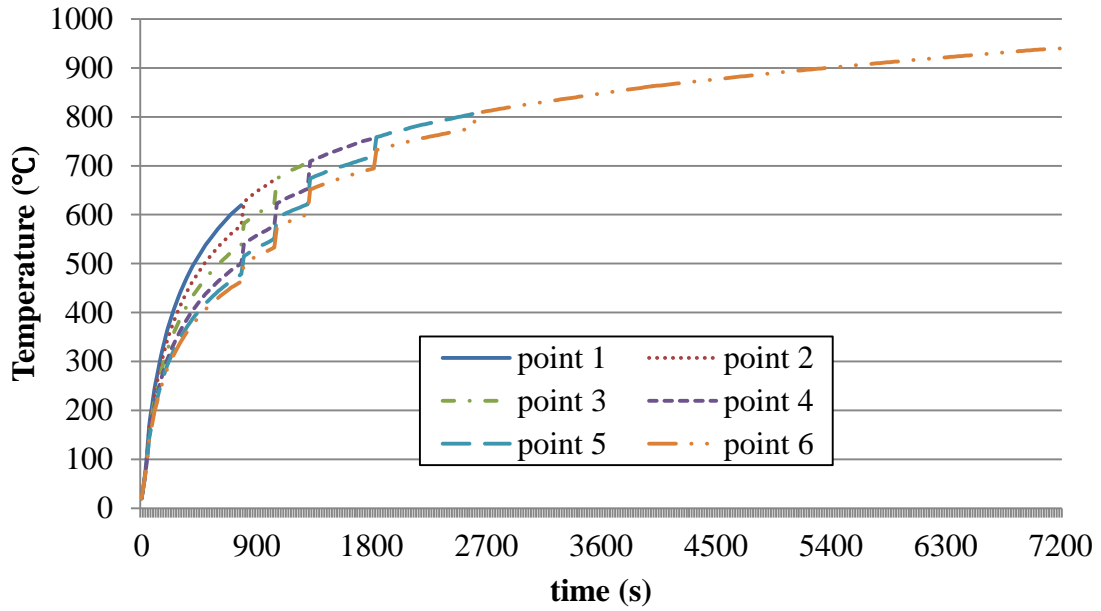
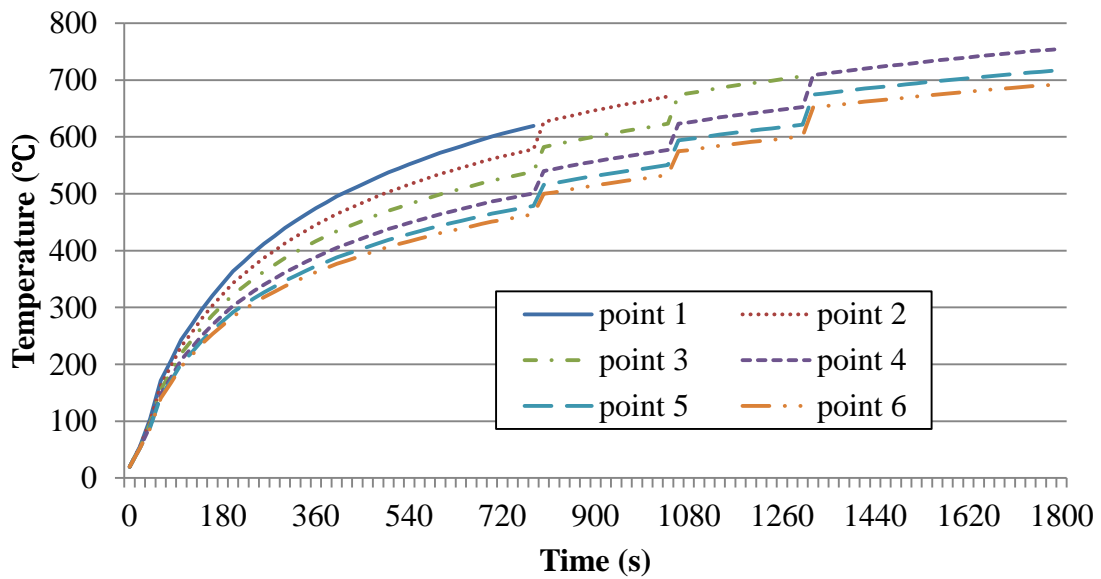


Figure 4-1 Temperature distribution

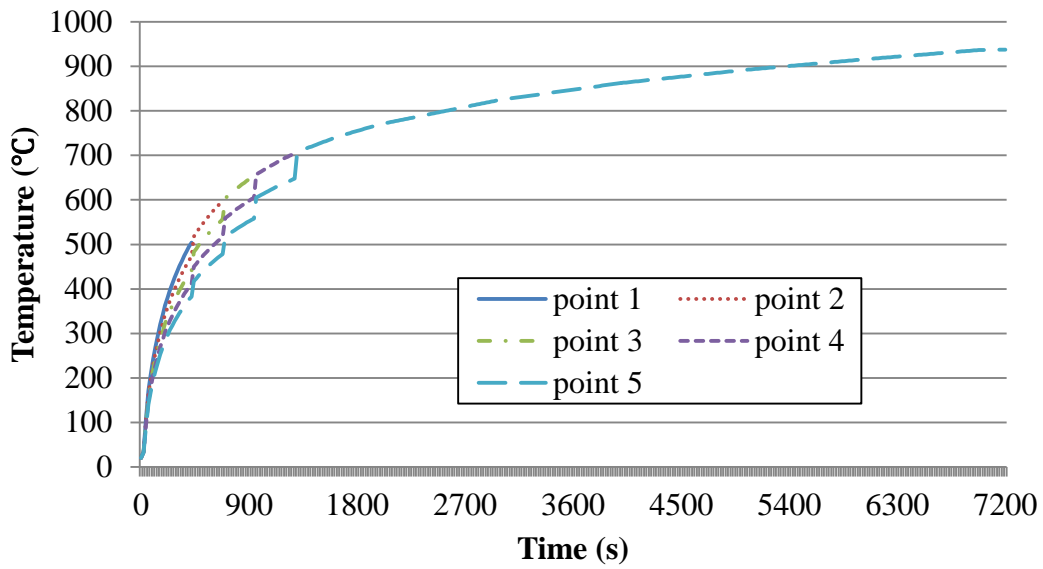


(a) Two hours' development of nodal temperature

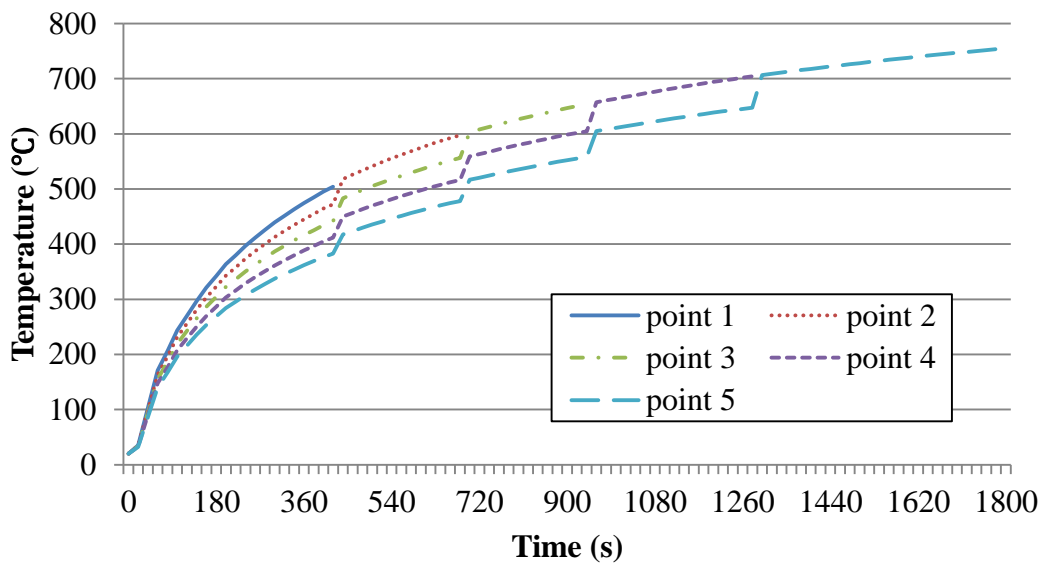


(b) A half hour's development of nodal temperature

Figure 4-2 Nodal Temperature of the symbolic points of Model 100 with spalling rate I exposed to fire I



(a) Two hours' development of nodal temperature



(b) A half hour's development of nodal temperature

Figure 4-3 Nodal Temperature of the symbolic points of Model 100 with spalling rate II exposed to fire I

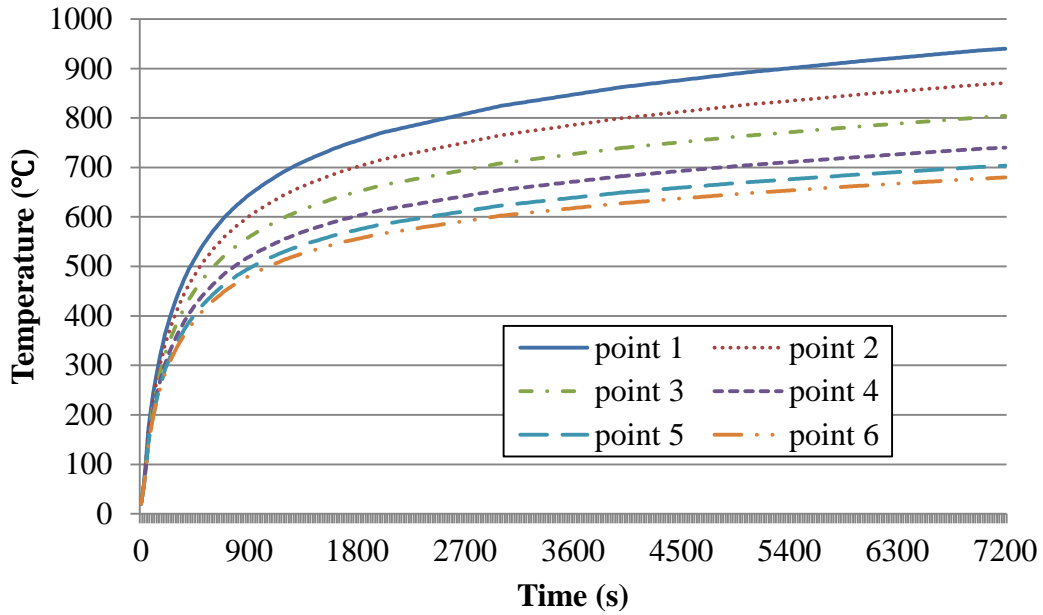
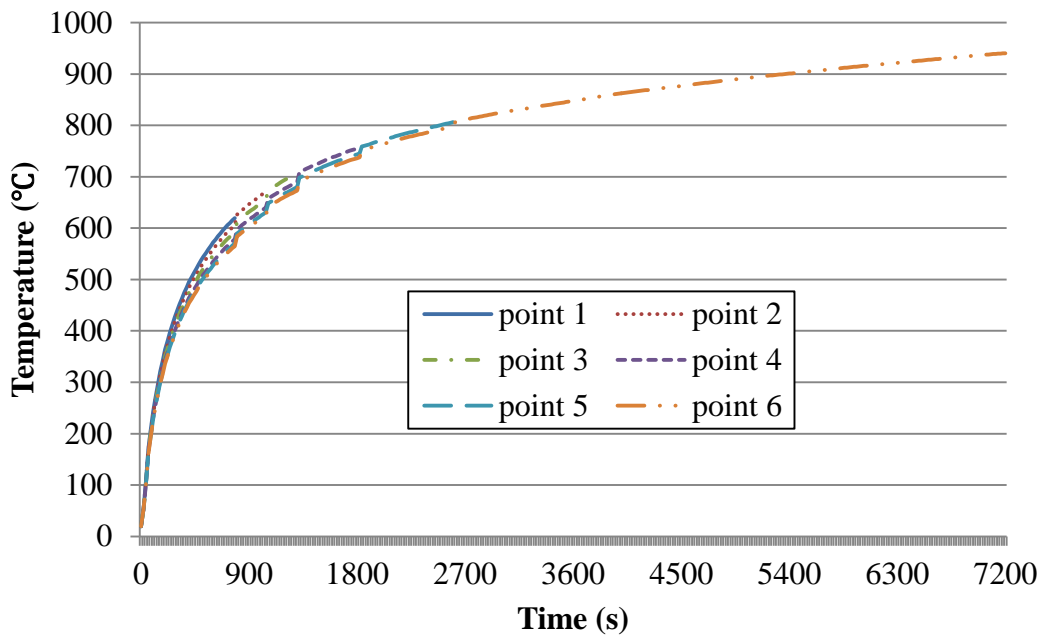
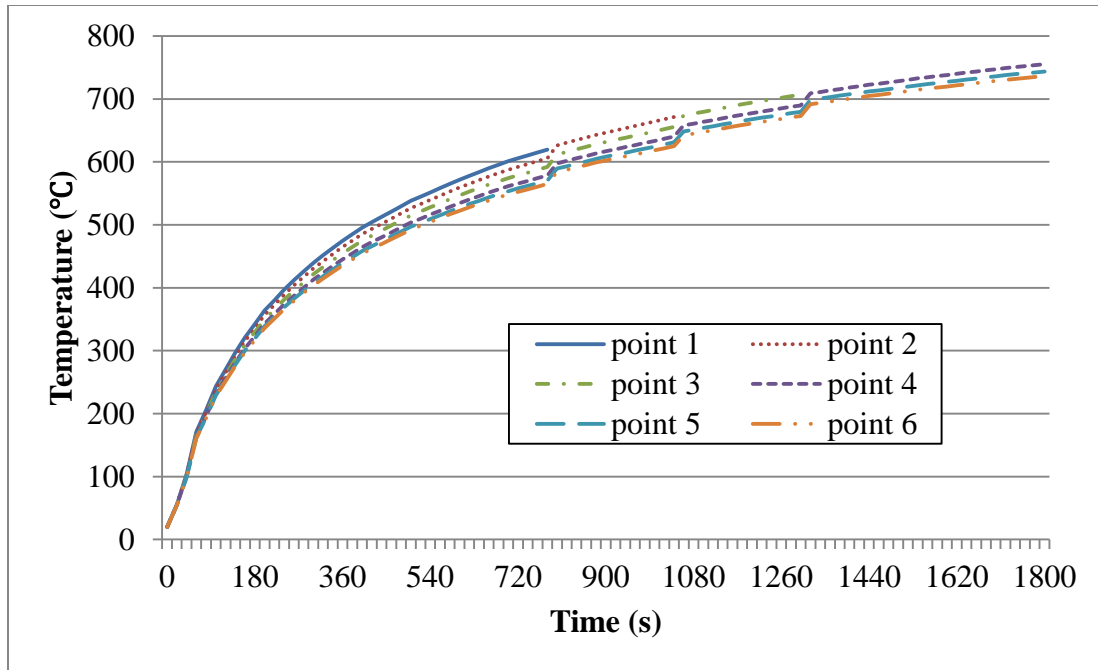


Figure 4-4 Nodal Temperature of the symbolic points of Model 100 with no spalling exposed to fire I

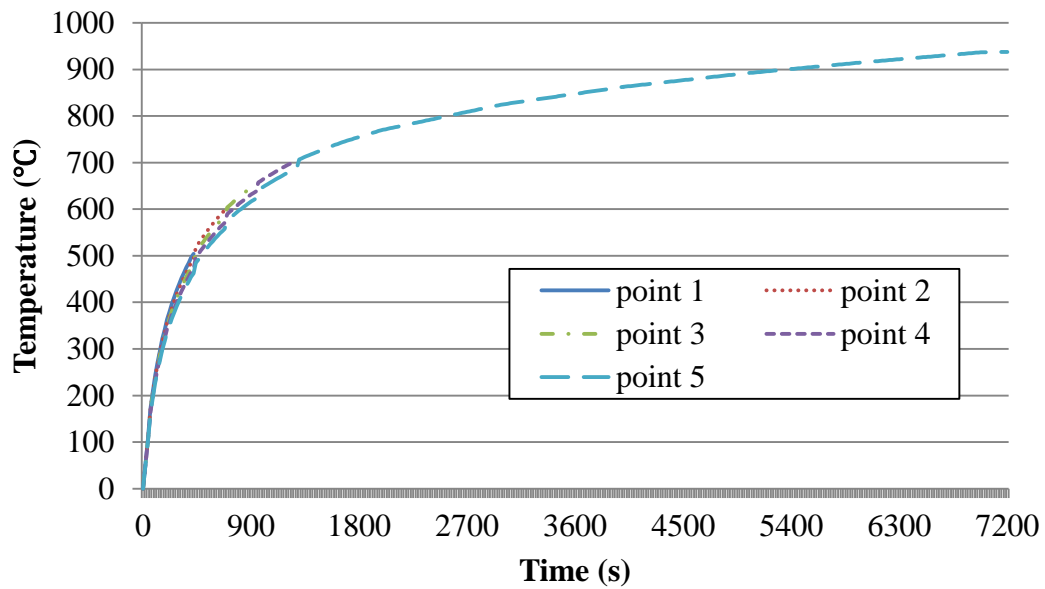


(a) Two hours' development of nodal temperature

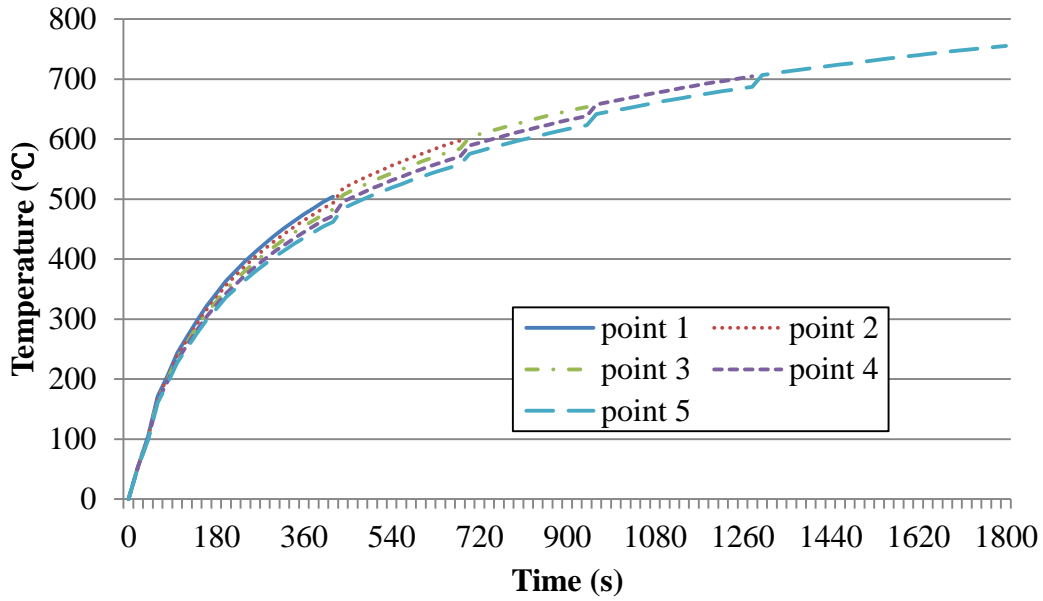


(b) A half hour's development of nodal temperature

Figure 4-5 Nodal Temperature of the symbolic points of Model 300 with spalling rate I exposed to fire I



(a) Two hours' development of nodal temperature



(b) A half hour's development of nodal temperature

Figure 4-6 Nodal Temperature of the symbolic points of Model 300 with spalling rate II exposed to fire I

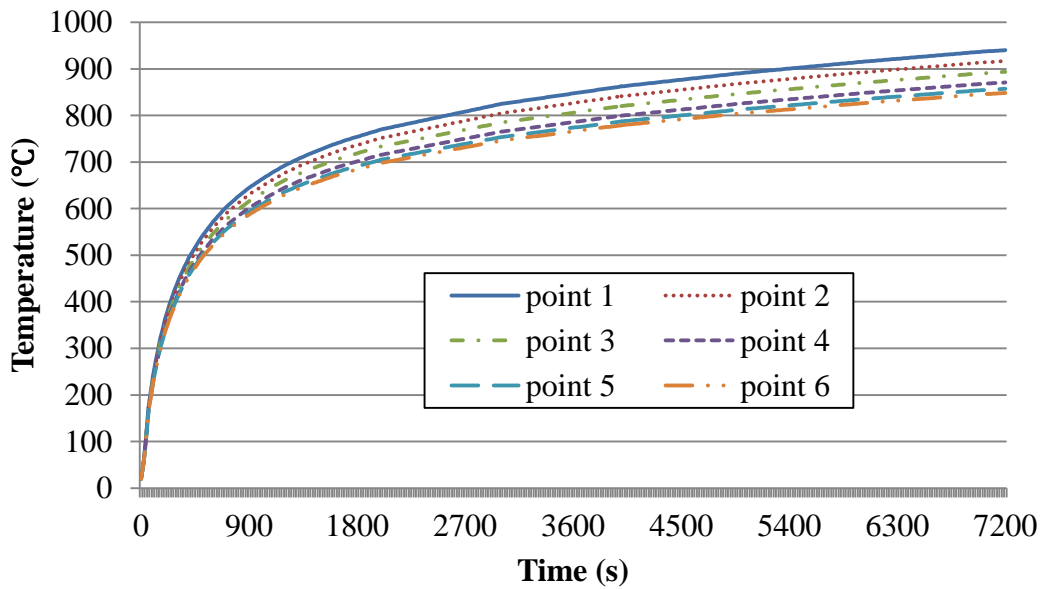
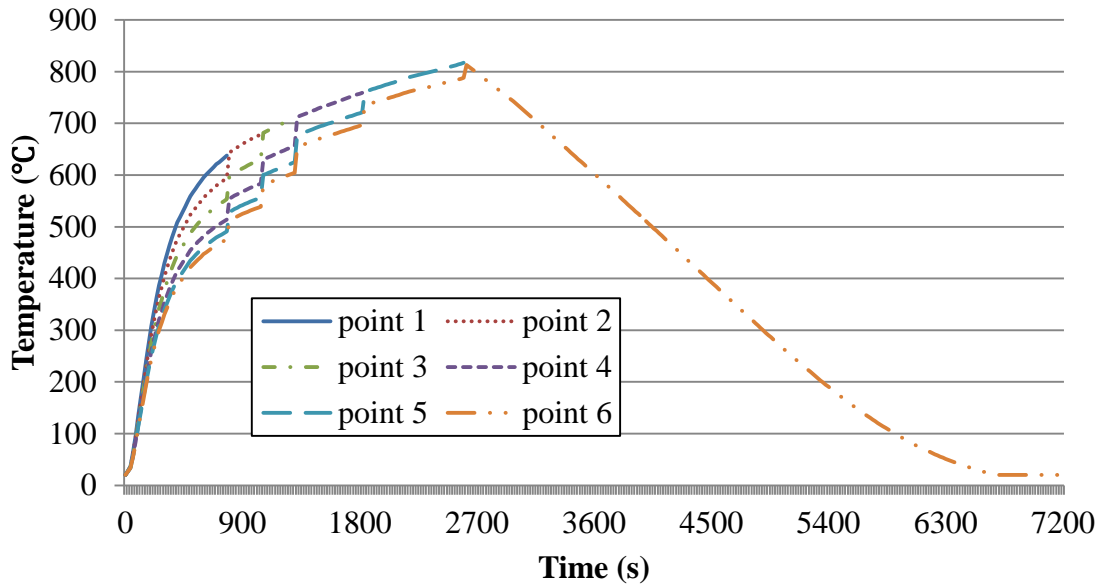
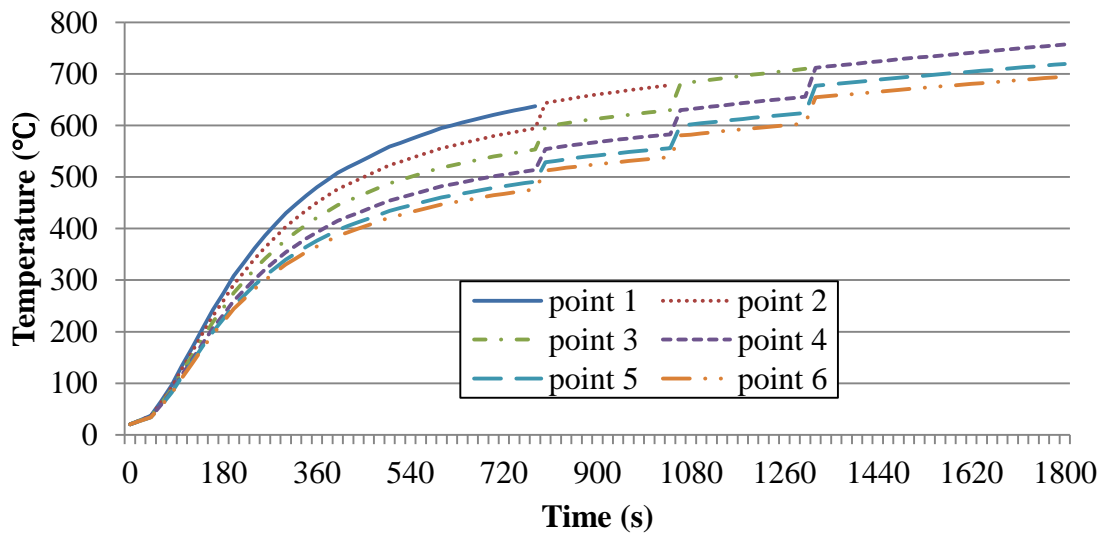


Figure 4-7 Nodal Temperature of the symbolic points of Model 300 with no spalling exposed to fire I

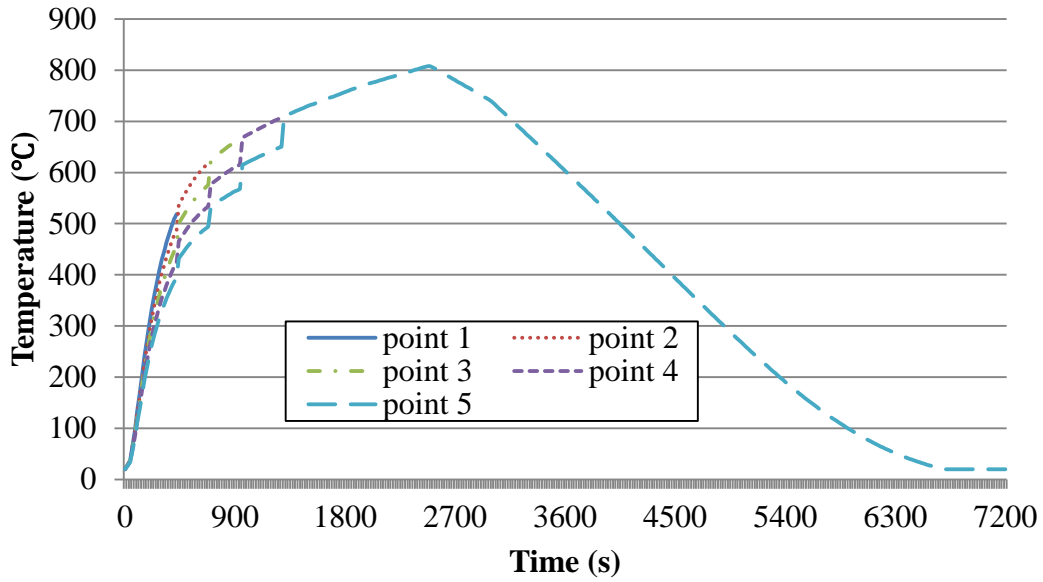


(a) Two hours' development of nodal temperature

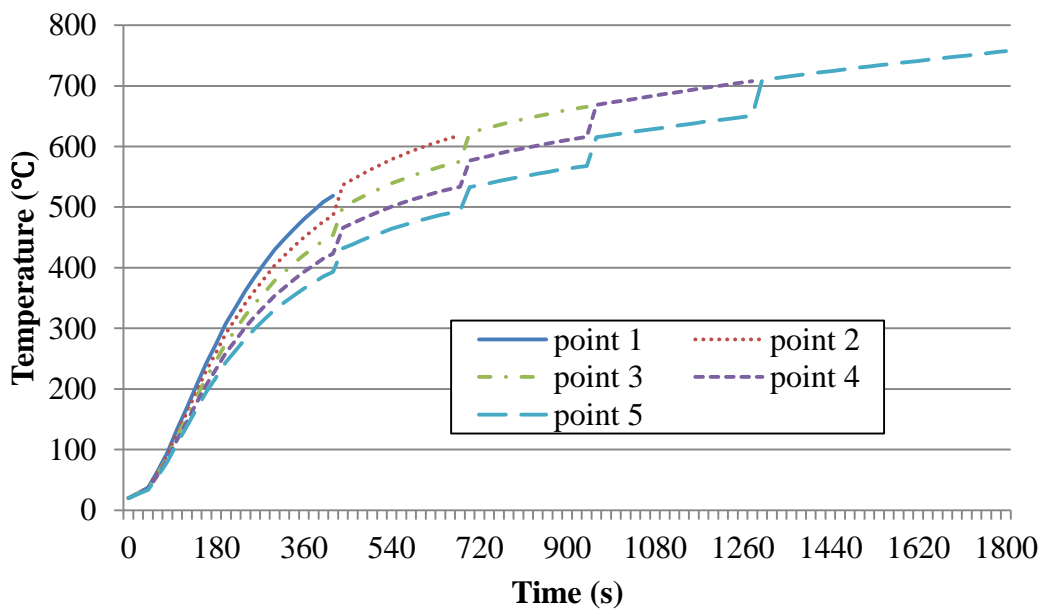


(b) A half hour's development of nodal temperature

Figure 4-8 Nodal Temperature of the symbolic points of Model 100 with spalling rate I exposed to fire II



(a) Two hours' development of nodal temperature



(b) A half hour's development of nodal temperature

Figure 4-9 Nodal Temperature of the symbolic points of Model 100 with spalling rate II exposed to fire II

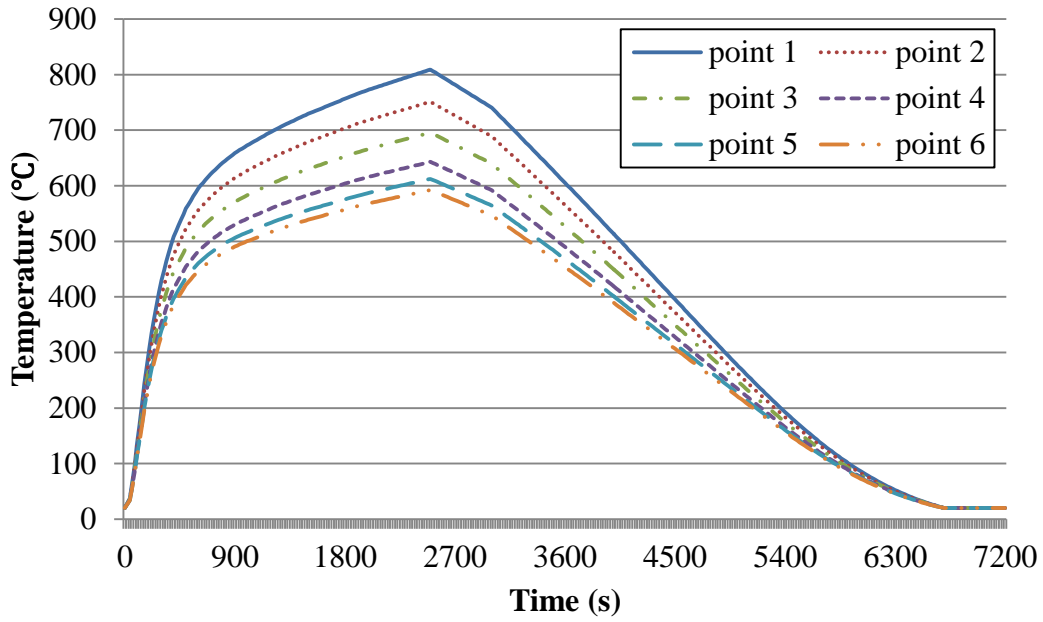
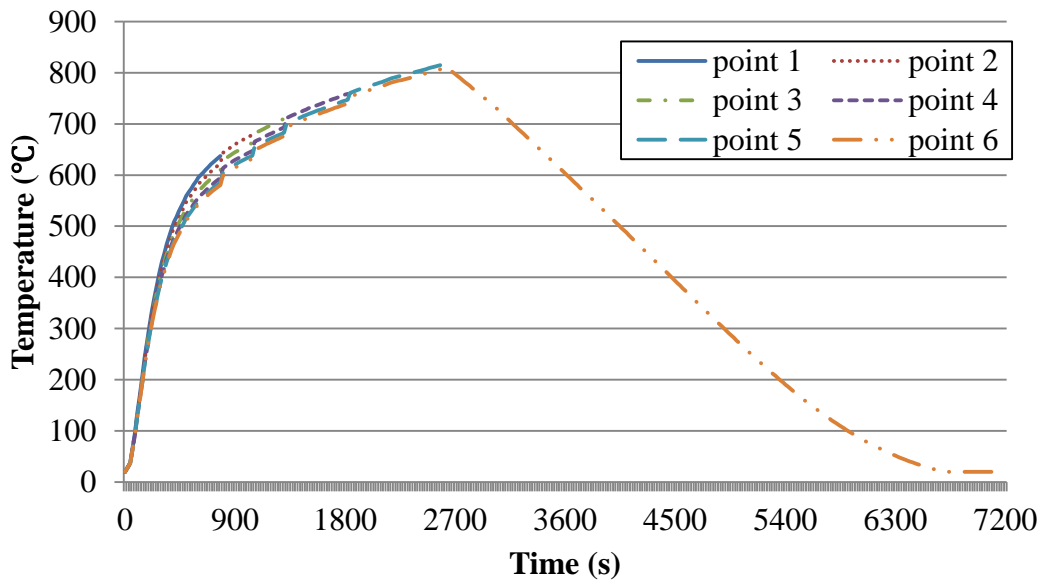
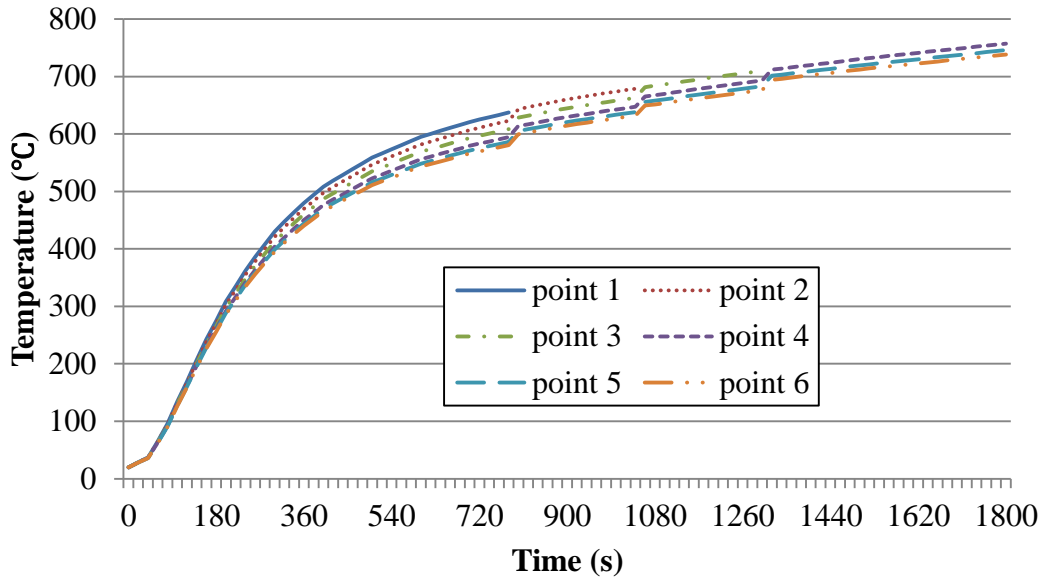


Figure 4-10 Nodal Temperature of the symbolic points of Model 100 with no spalling exposed to fire II

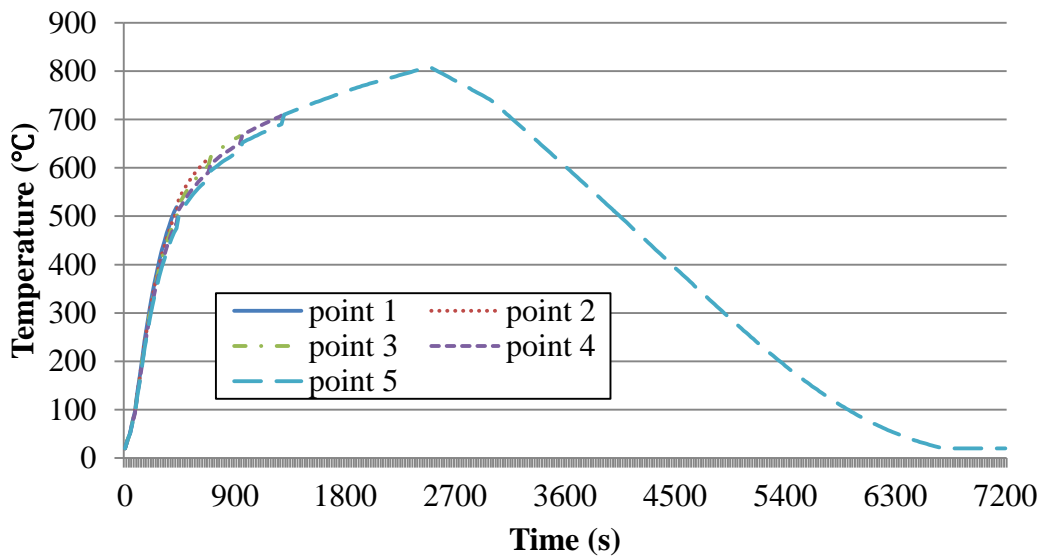


(a) Two hours' development of nodal temperature

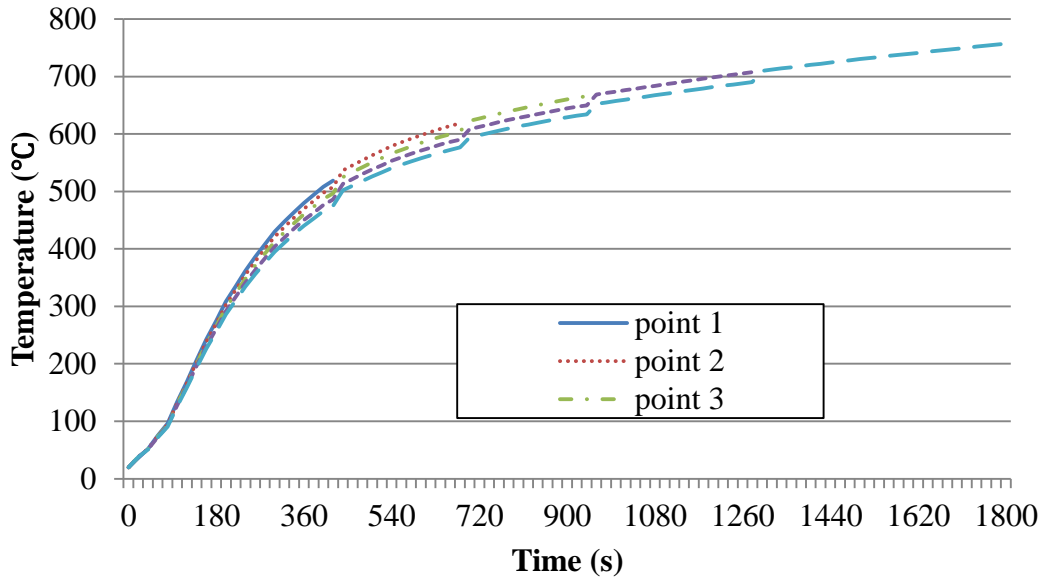


(b) A half hour's development of nodal temperature

Figure 4-11 Nodal Temperature of the symbolic points of Model 300 with spalling rate I exposed to fire II



(a) Two hours' development of nodal temperature



(b) A half hour's development of nodal temperature

Figure 4-12 Nodal Temperature of the symbolic points of Model 300 with spalling rate II exposed to fire II

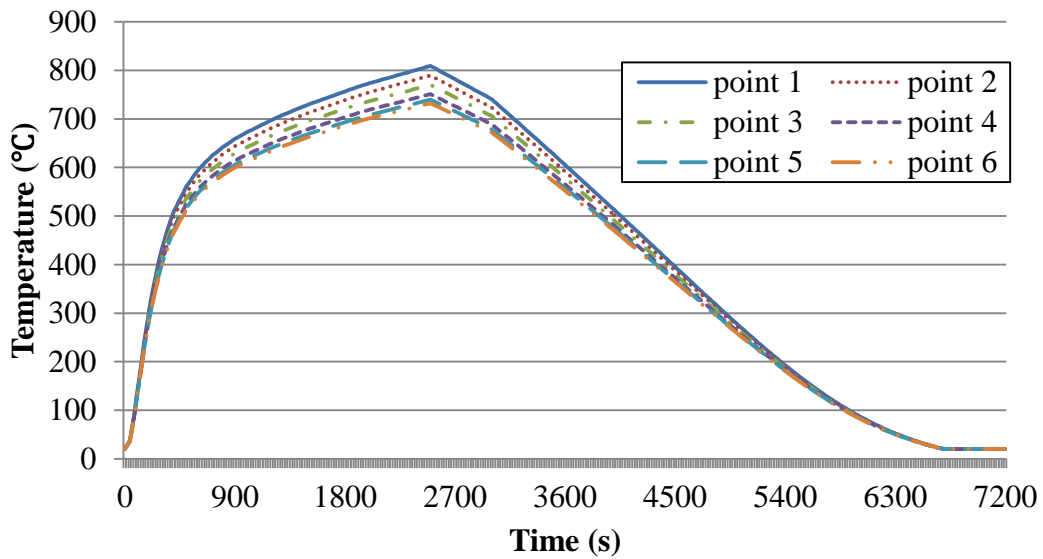
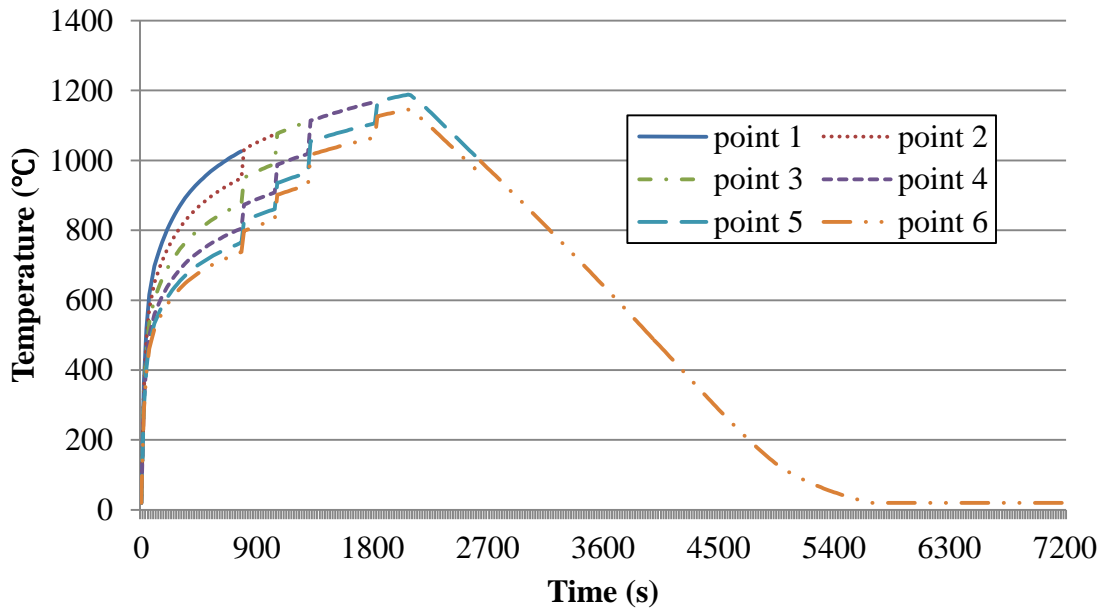
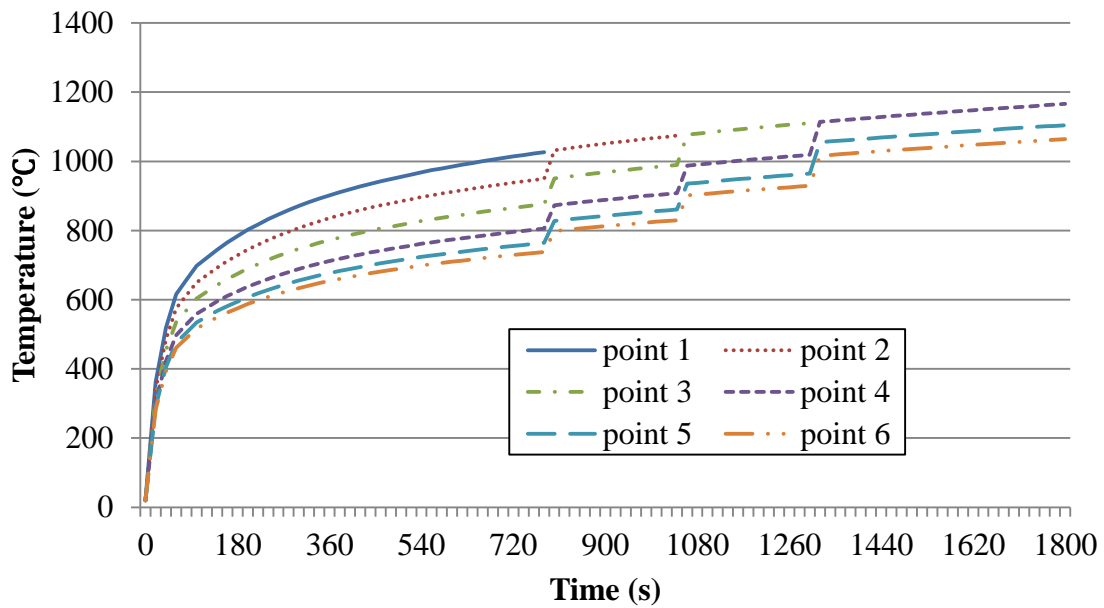


Figure 4-13 Nodal Temperature of the symbolic points of Model 300 with no spalling exposed to fire II

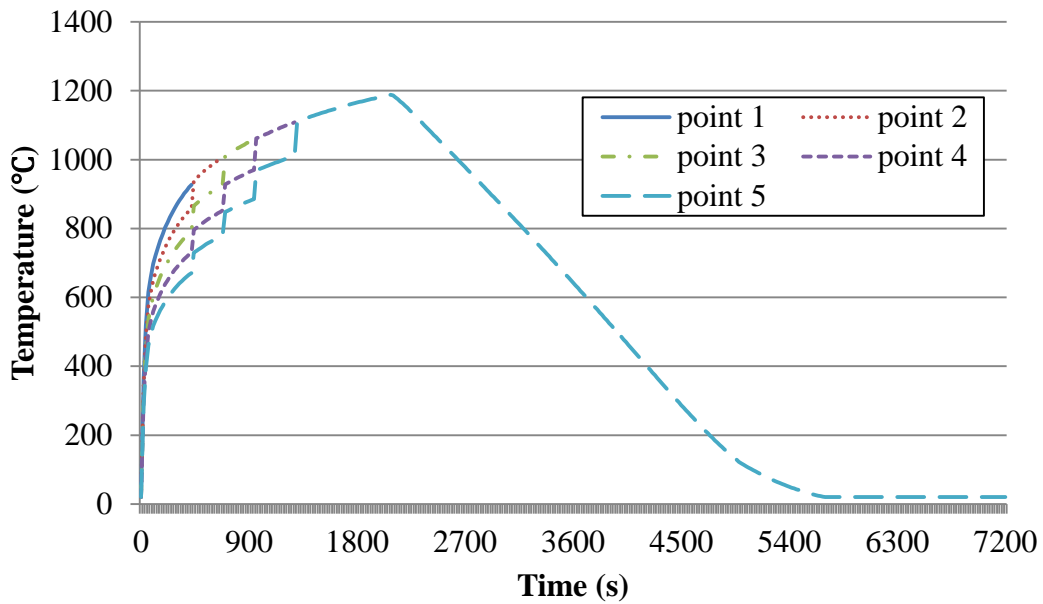


(a) Two hours' development of nodal temperature

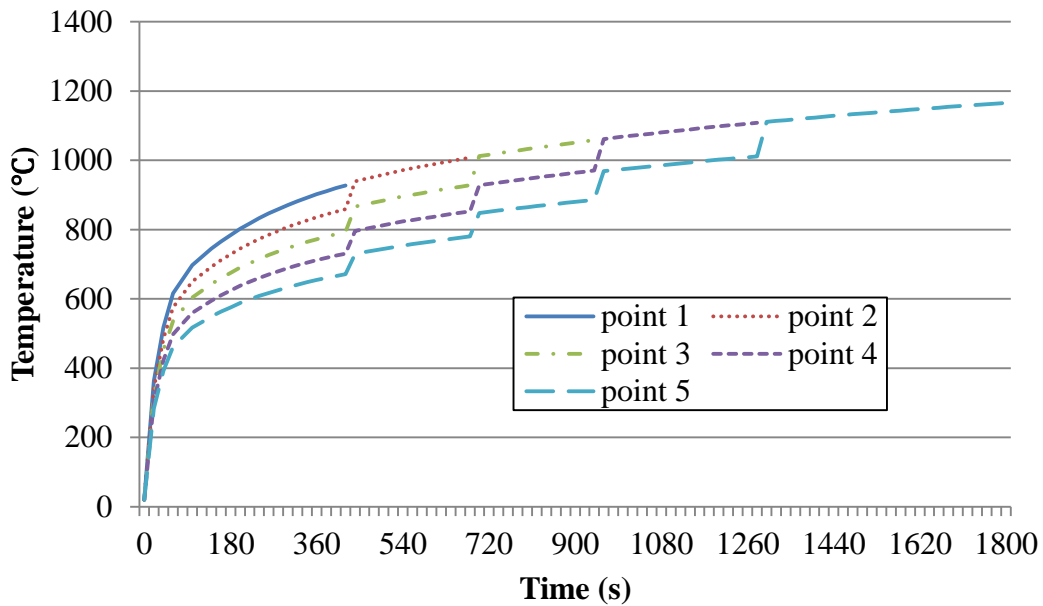


(b) A half hour's development of nodal temperature

Figure 4-14 Nodal Temperature of the symbolic points of Model 100 with spalling rate I exposed to fire III



(a) Two hours' development of nodal temperature



(b) A half hour's development of nodal temperature

Figure 4-15 Nodal Temperature of the symbolic points of Model 100 with spalling rate II exposed to fire III

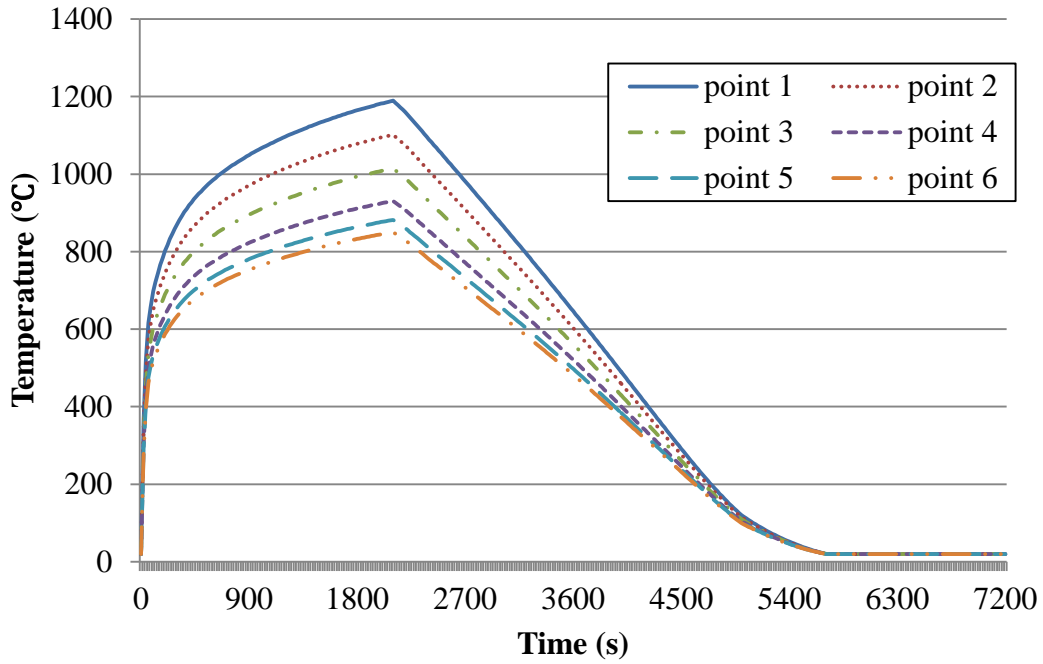
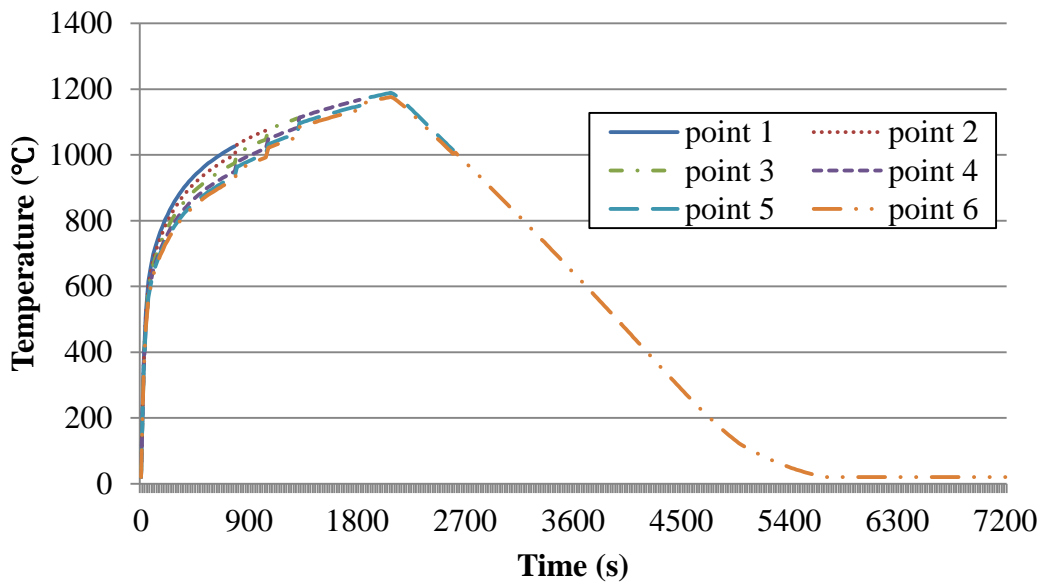
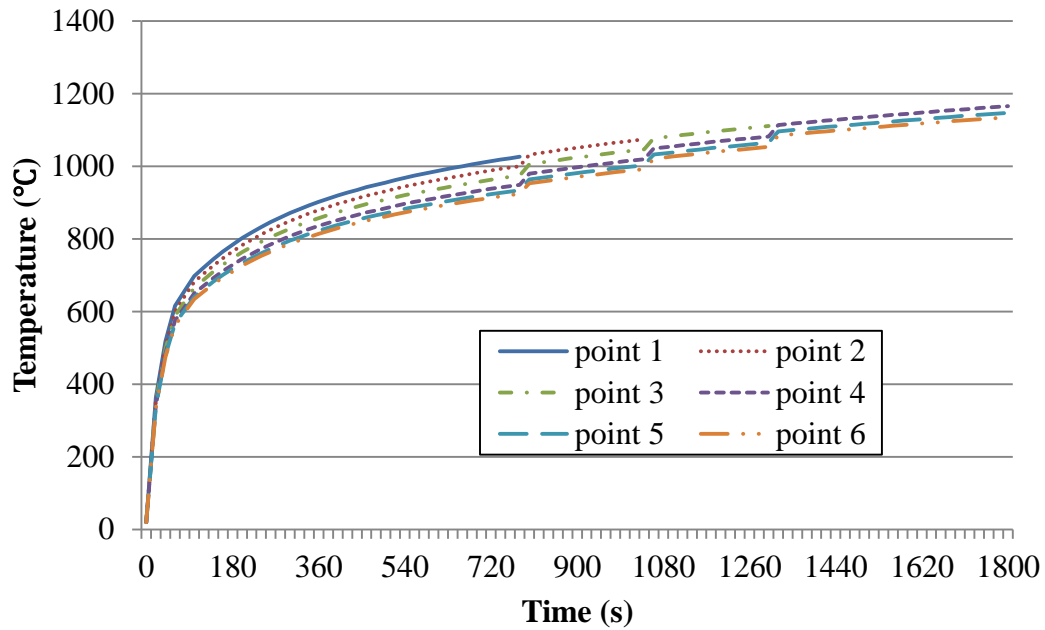


Figure 4-16 Nodal Temperature of the symbolic points of Model 100 with no spalling exposed to fire III

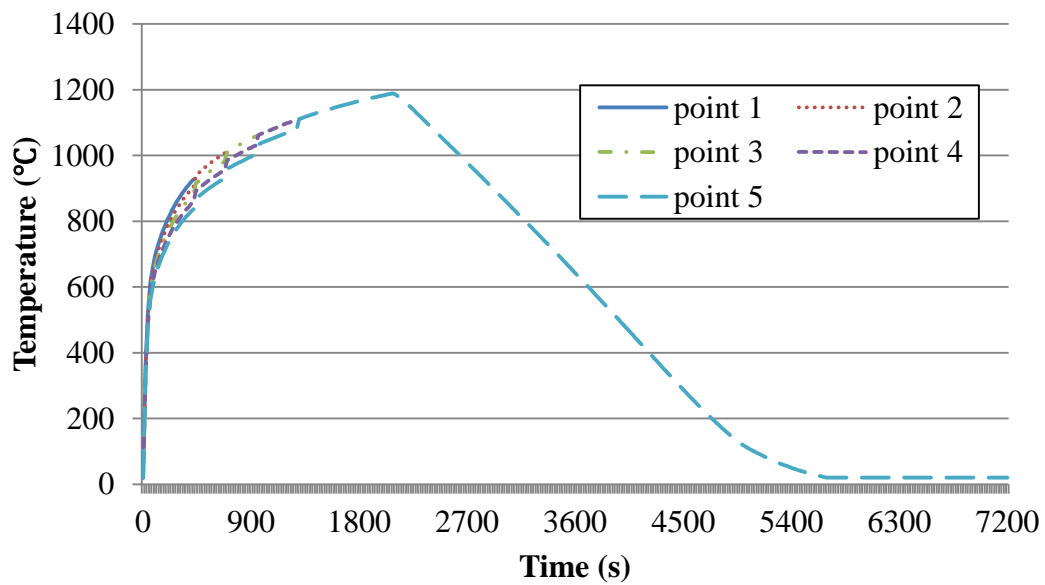


(a) Two hours' development of nodal temperature

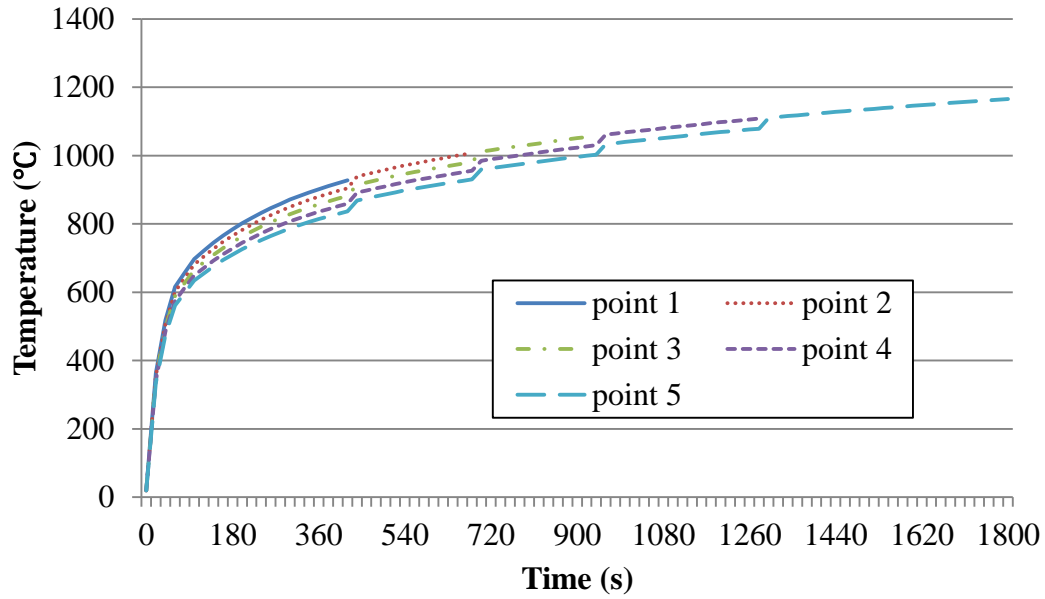


(b) A half hour's development of nodal temperature

Figure 4-17 Nodal Temperature of the symbolic points of Model 300 with spalling rate I exposed to fire III



(a) Two hours' development of nodal temperature



(b) A half hour's development of nodal temperature

Figure 4-18 Nodal Temperature of the symbolic points of Model 300 with spalling rate II exposed to fire III

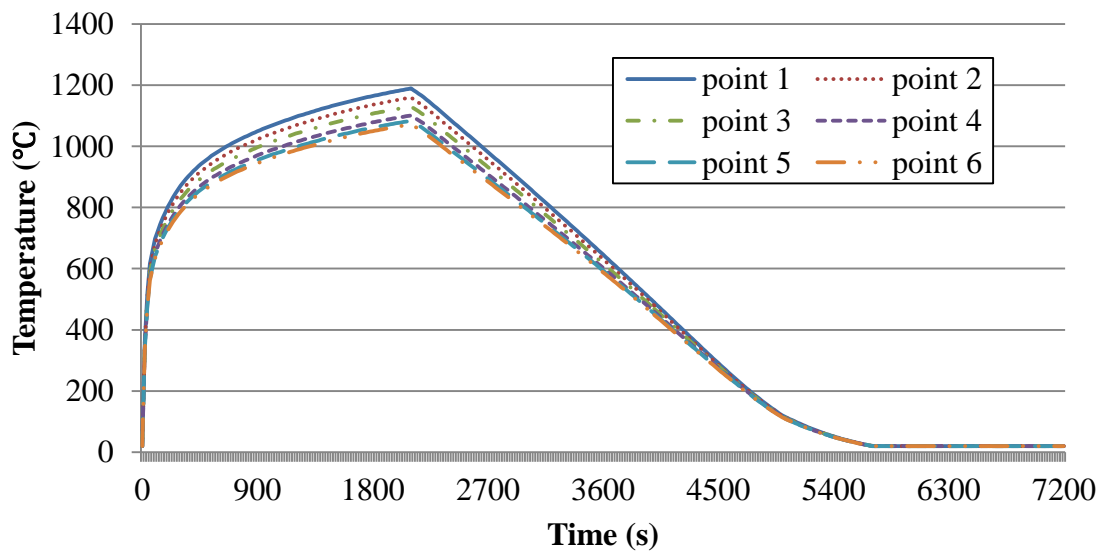
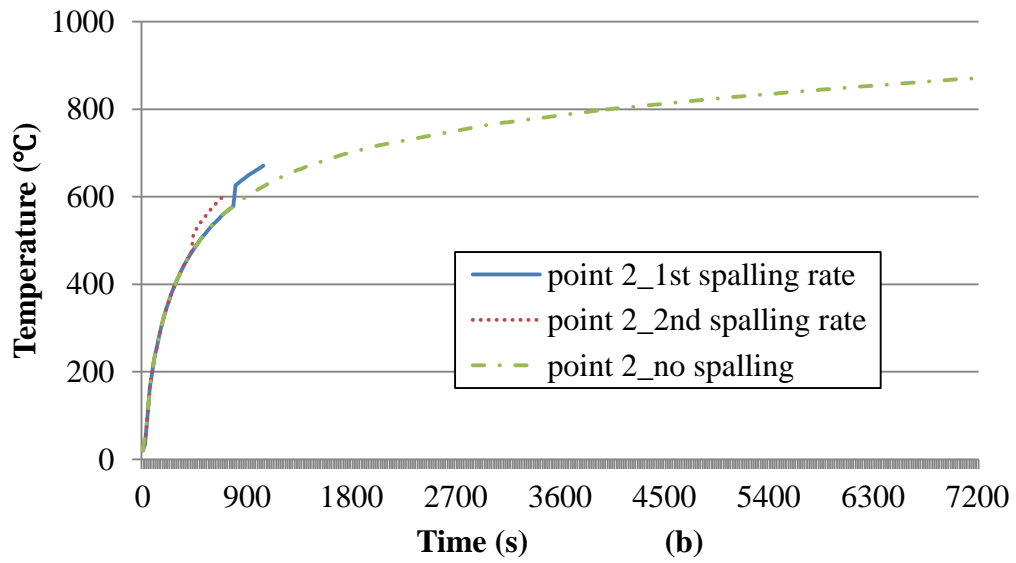
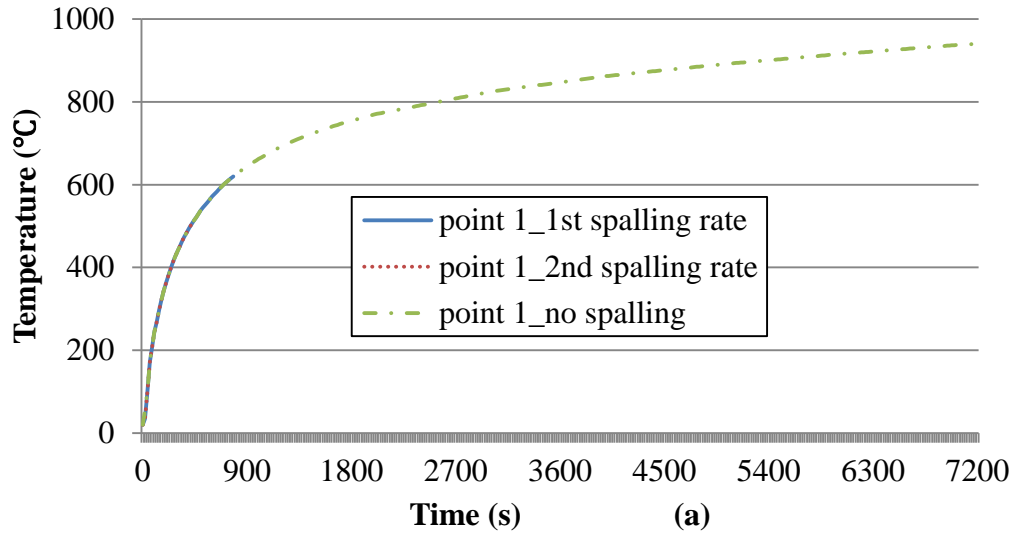
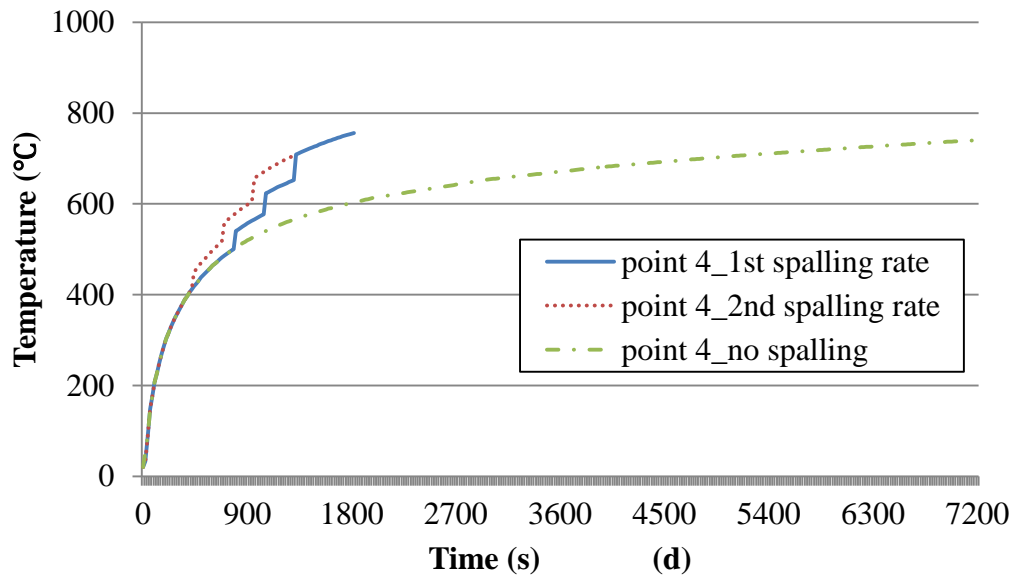
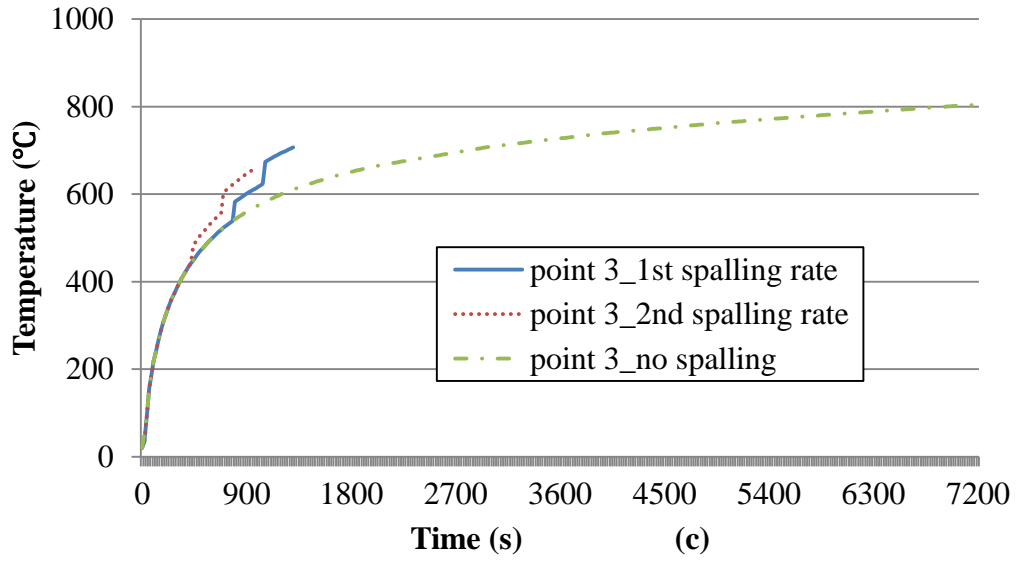


Figure 4-19 Nodal Temperature of the symbolic points of Model 300 with no spalling exposed to fire III





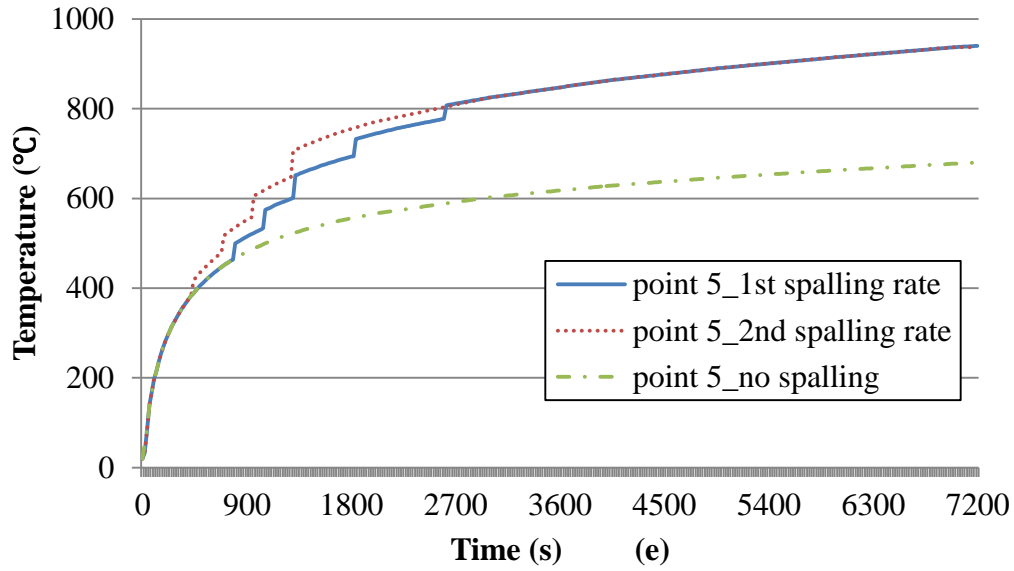
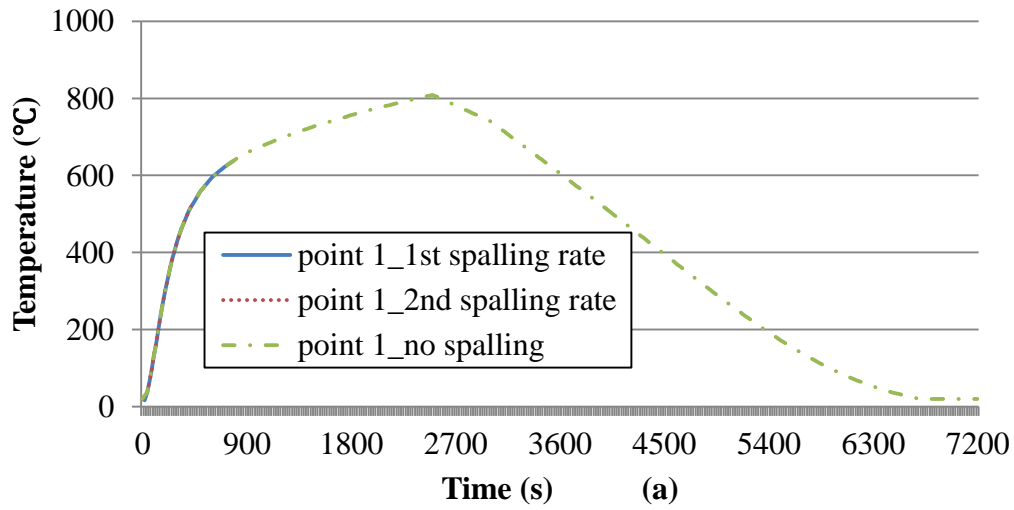
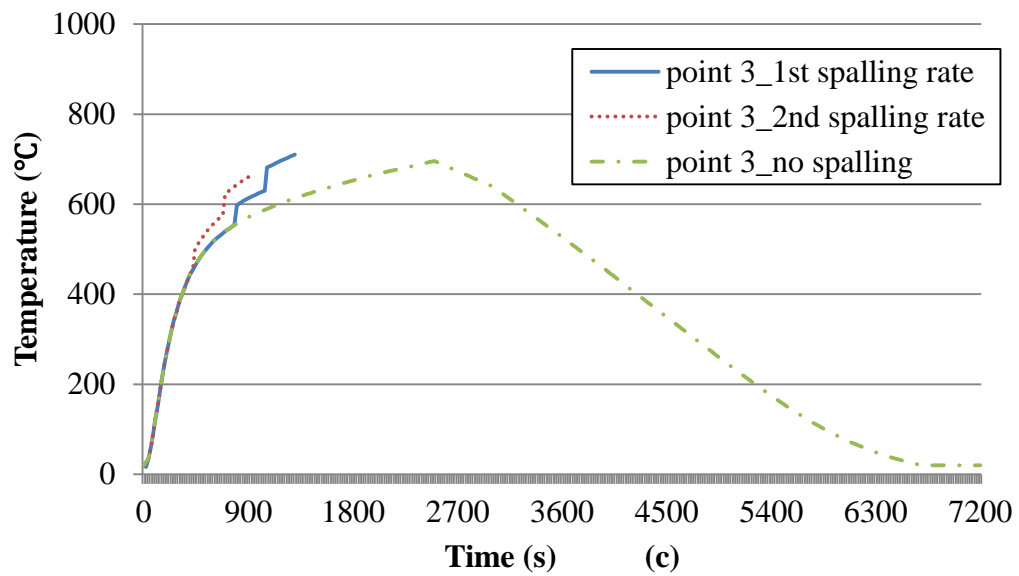
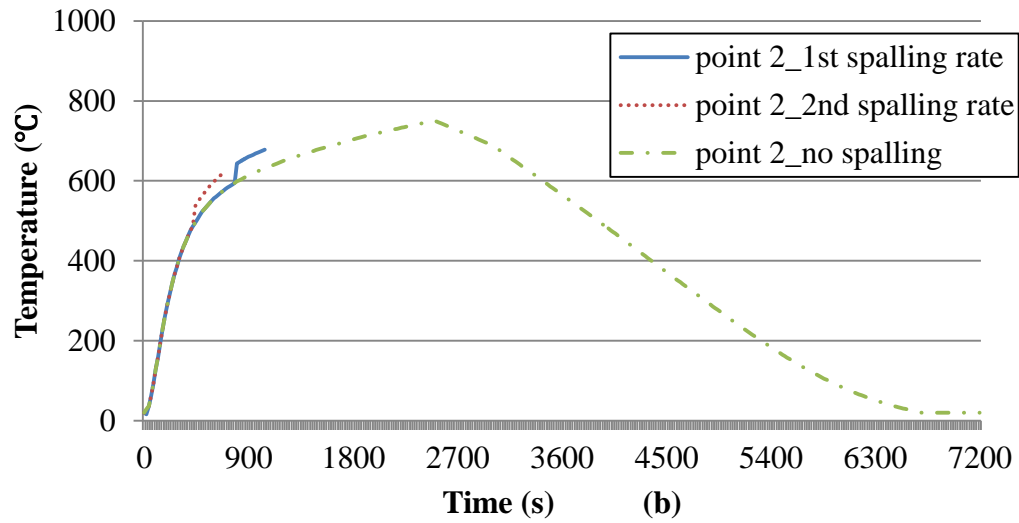


Figure 4-20 Nodal temperature comparison for Model 100 with all spalling rate cases exposed to fire I





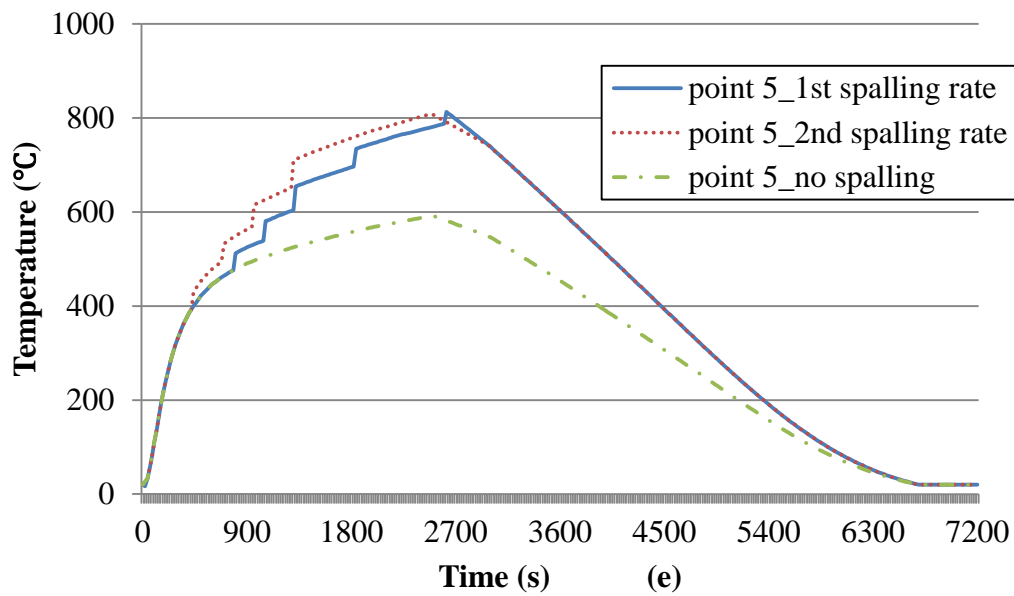
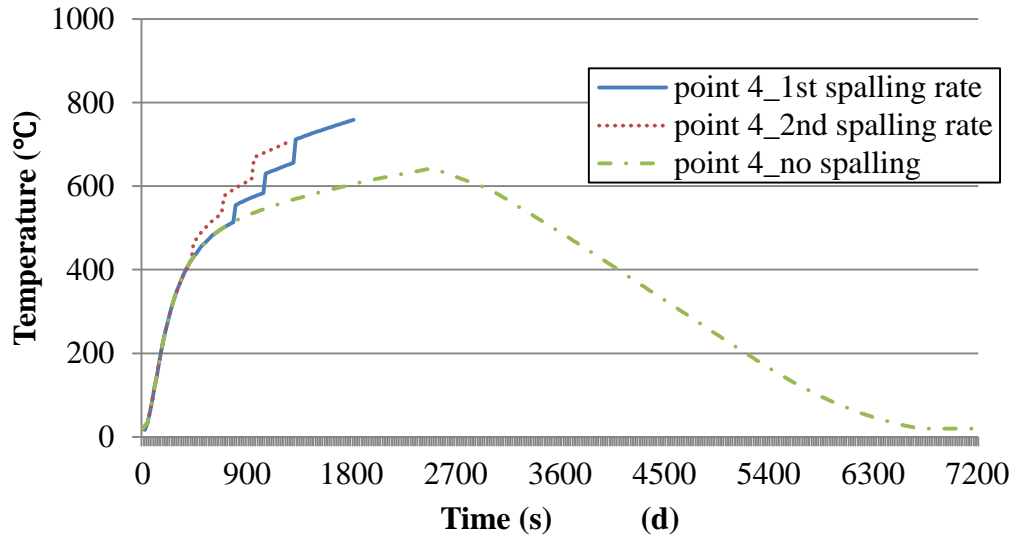
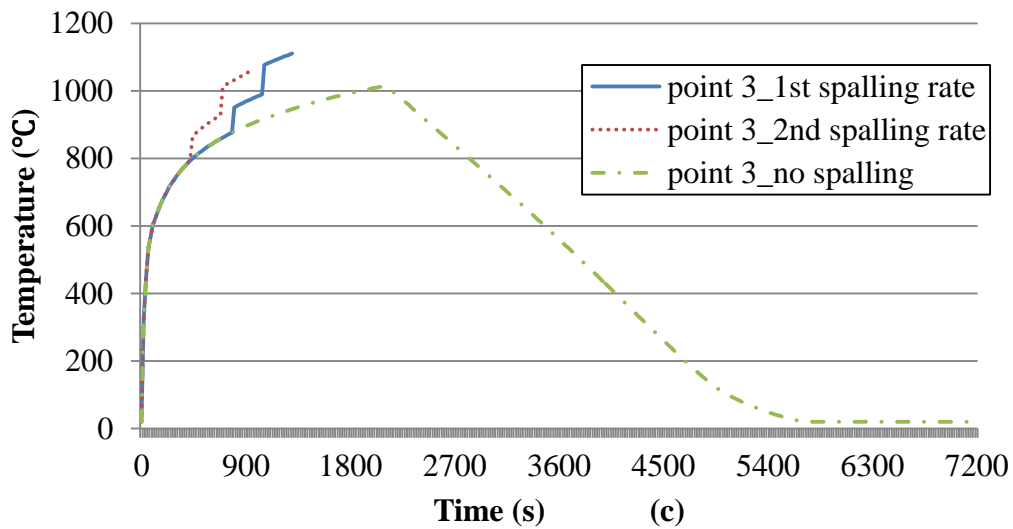
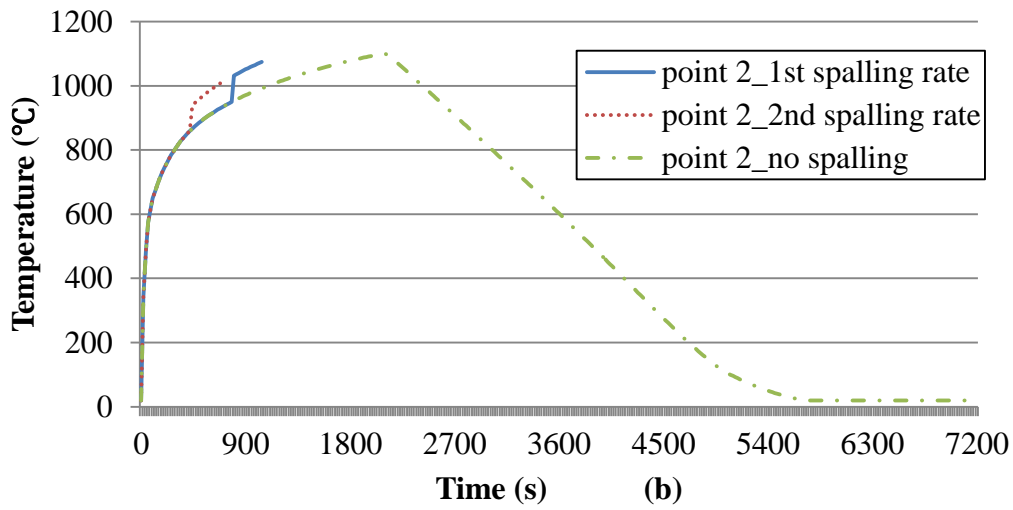
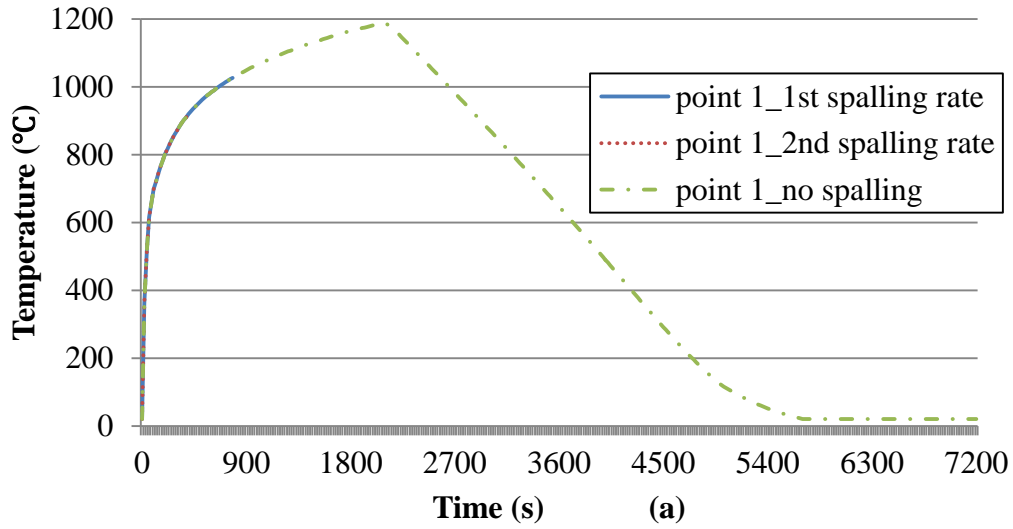


Figure 4-21 Nodal temperature comparison for Model 100 with all spalling rate cases exposed to fire II



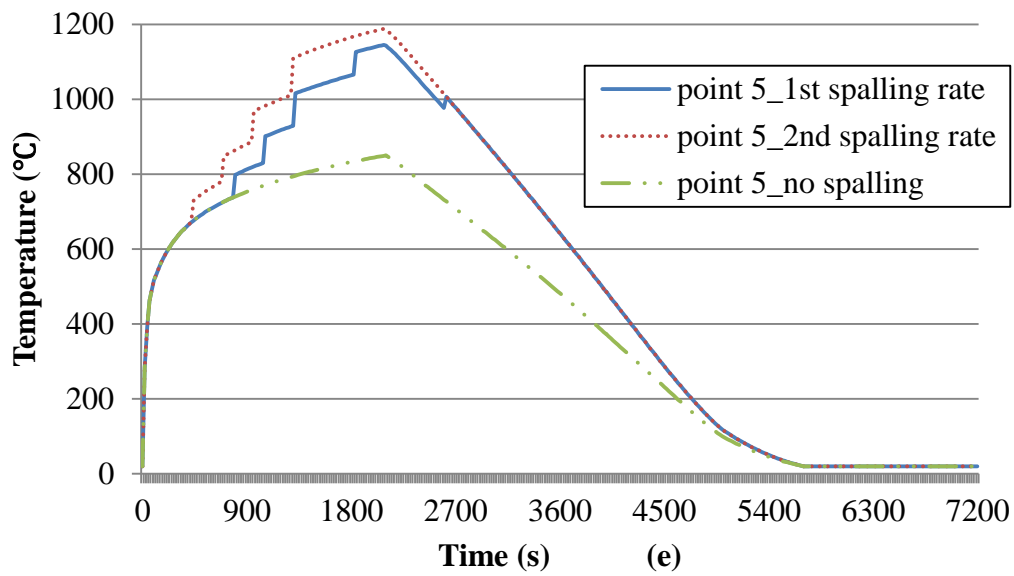
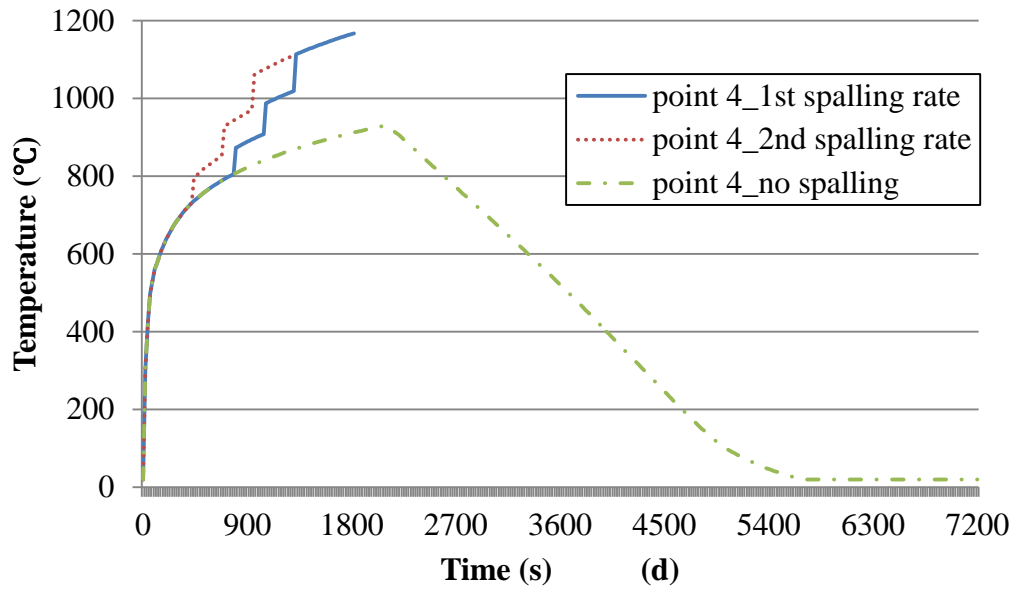
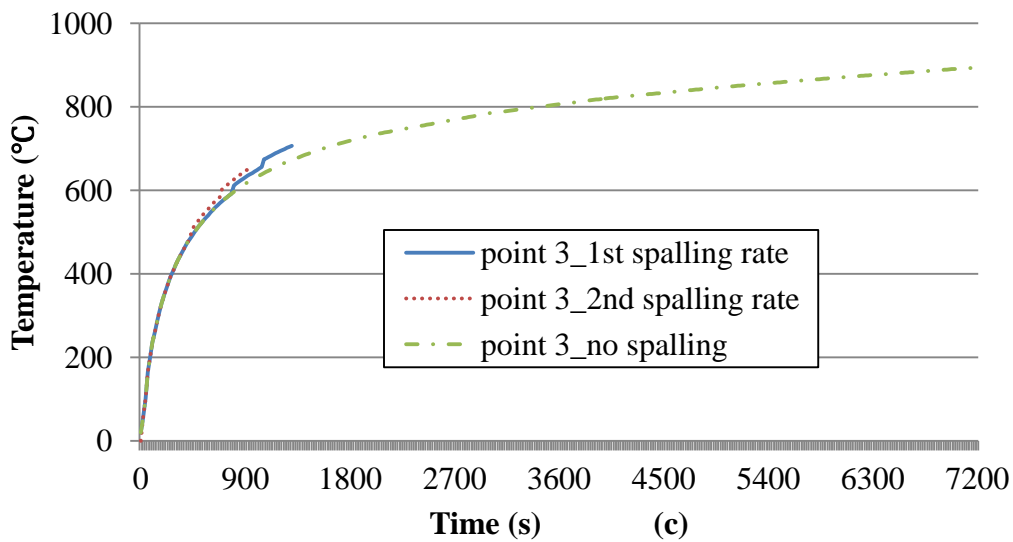
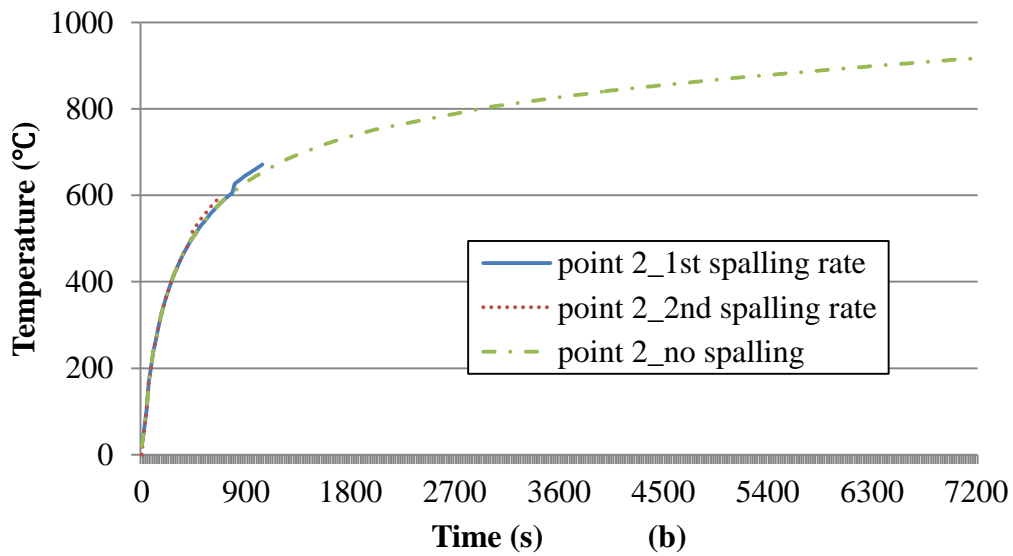
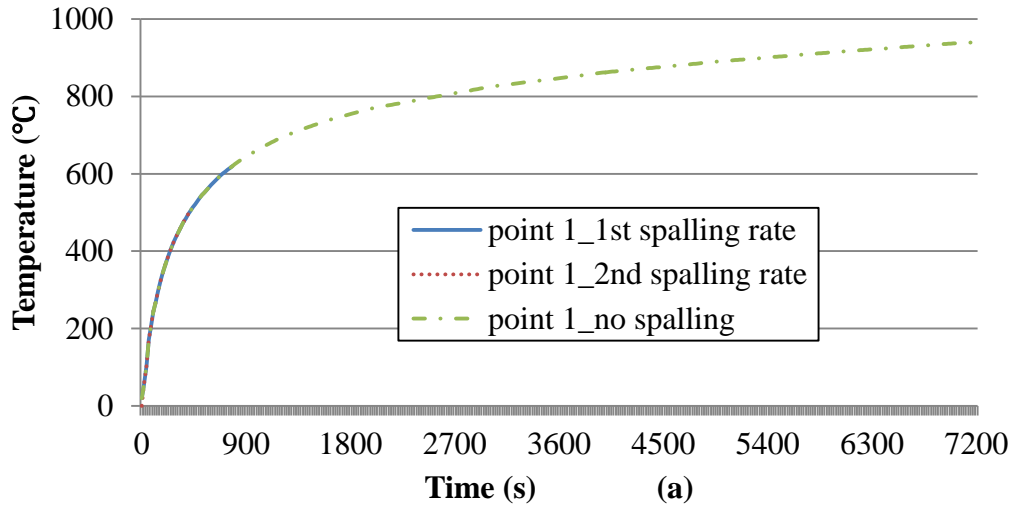


Figure 4-22 Nodal temperature comparison for Model 100 with all spalling rate cases exposed to Fire III



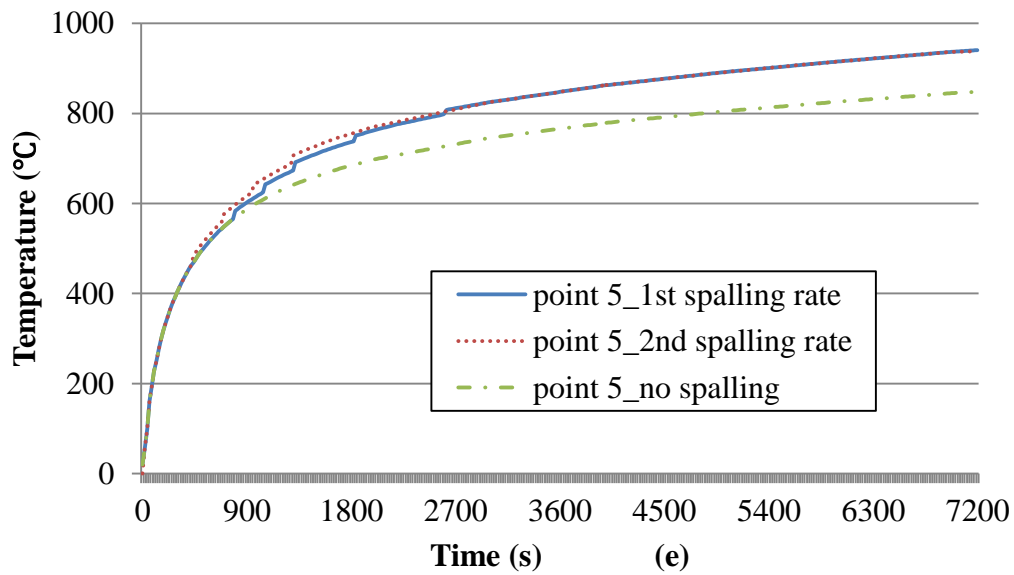
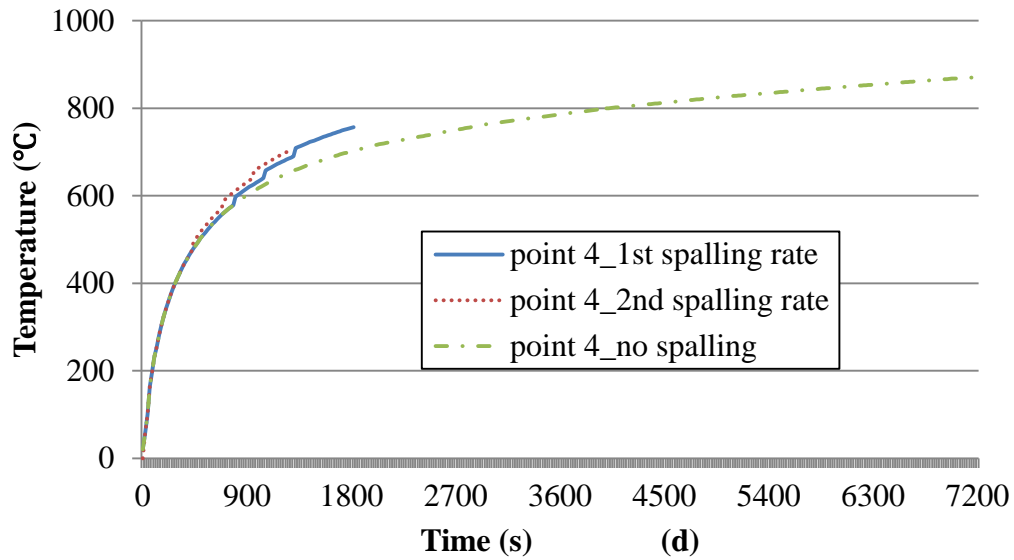
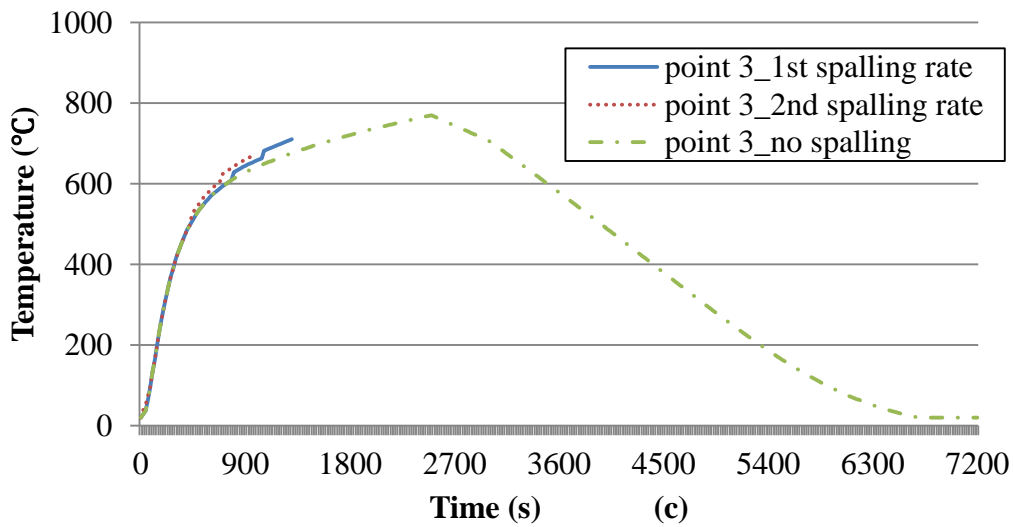
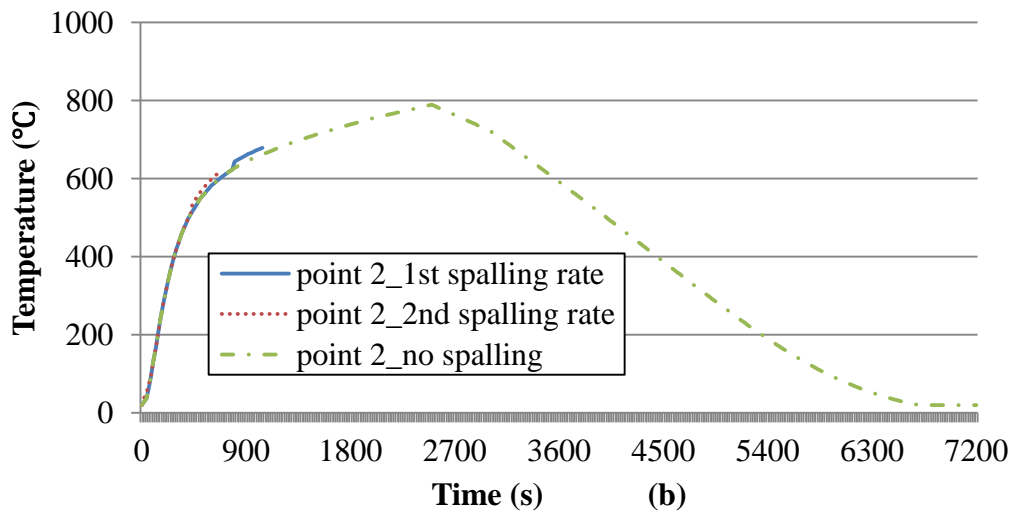
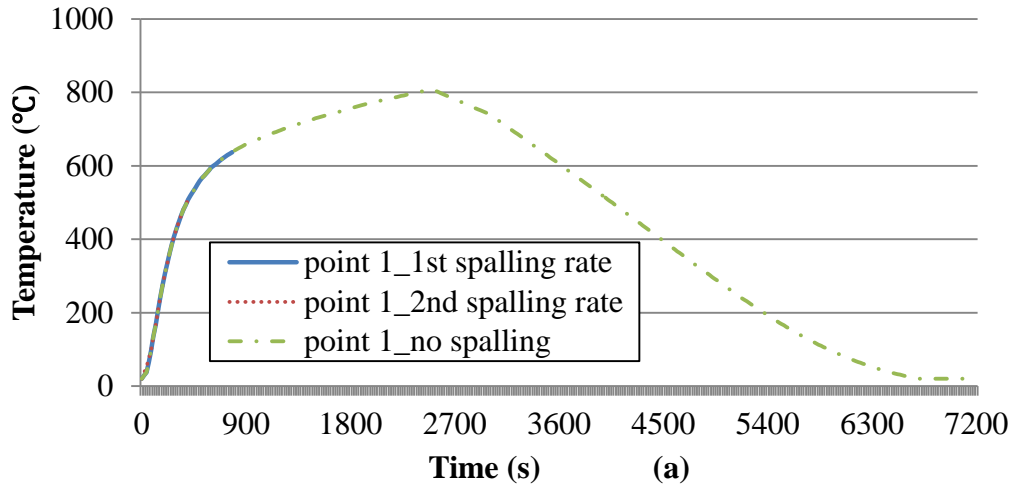


Figure 4-23 Nodal temperature comparison for Model 300 with all spalling rate cases exposed to Fire I



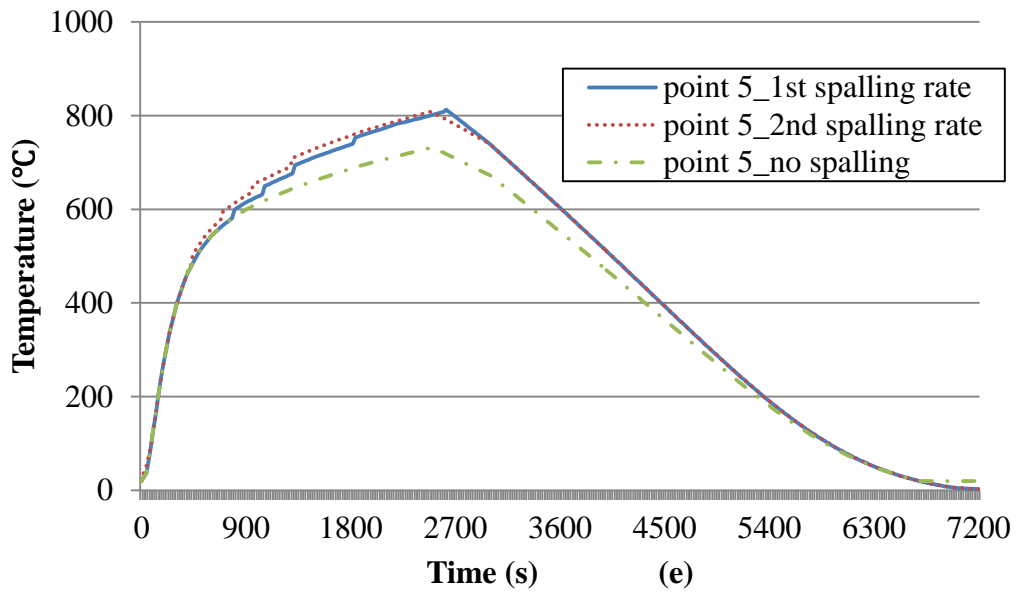
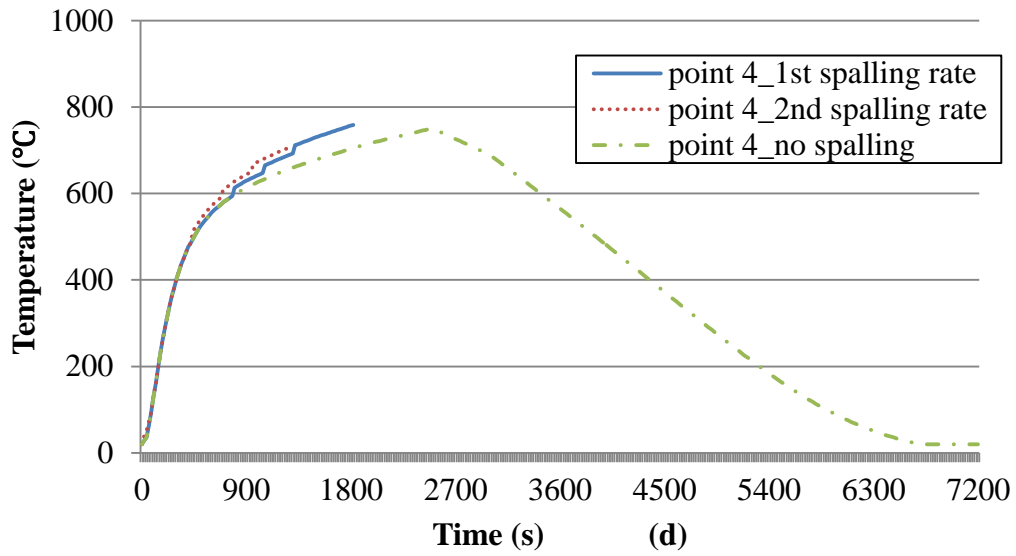
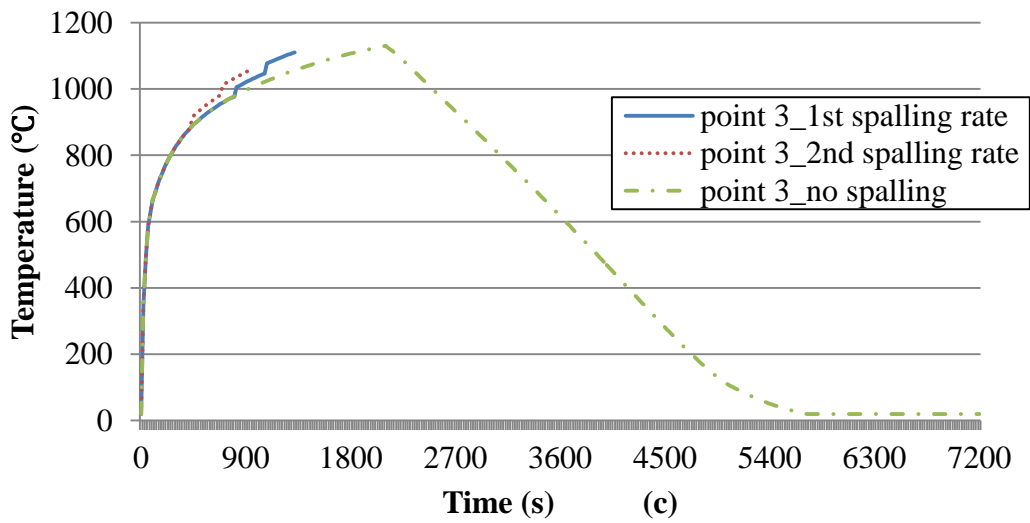
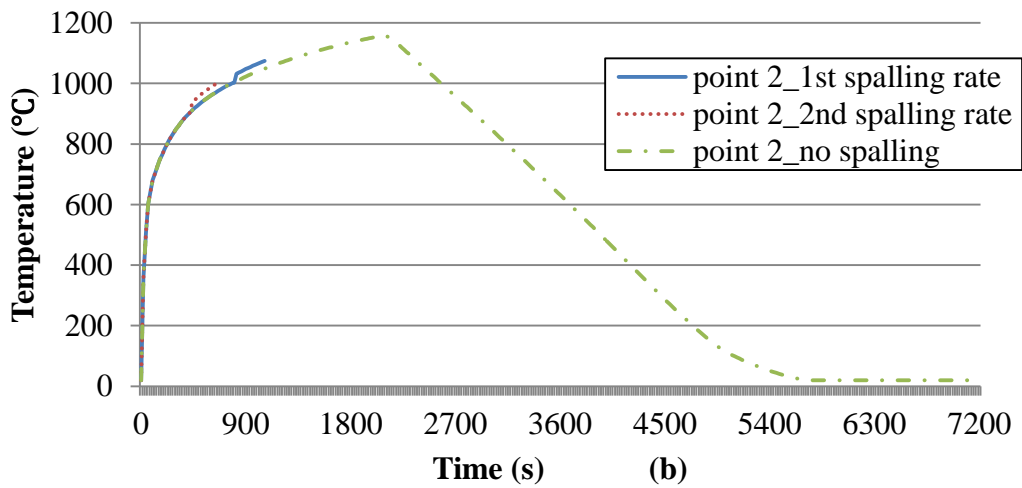
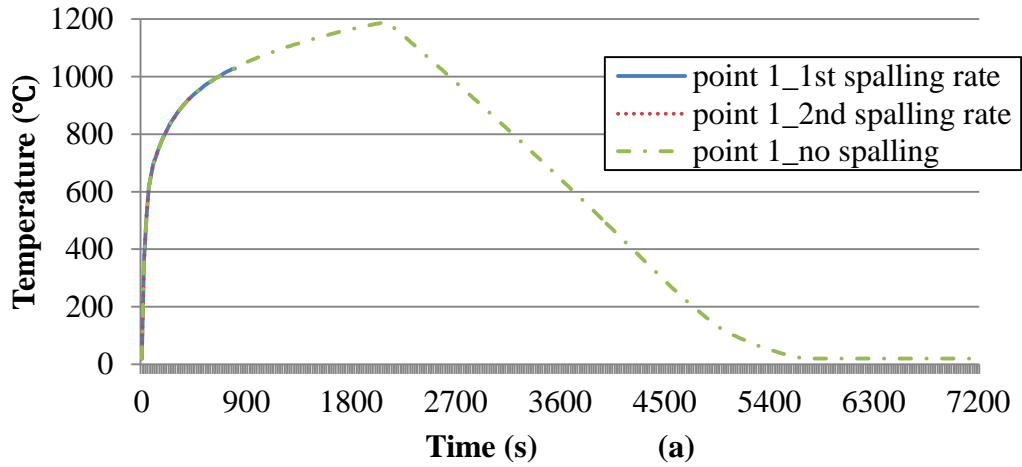


Figure 4-23 Nodal temperature comparison for Model 300 with all spalling rate cases exposed to fire II



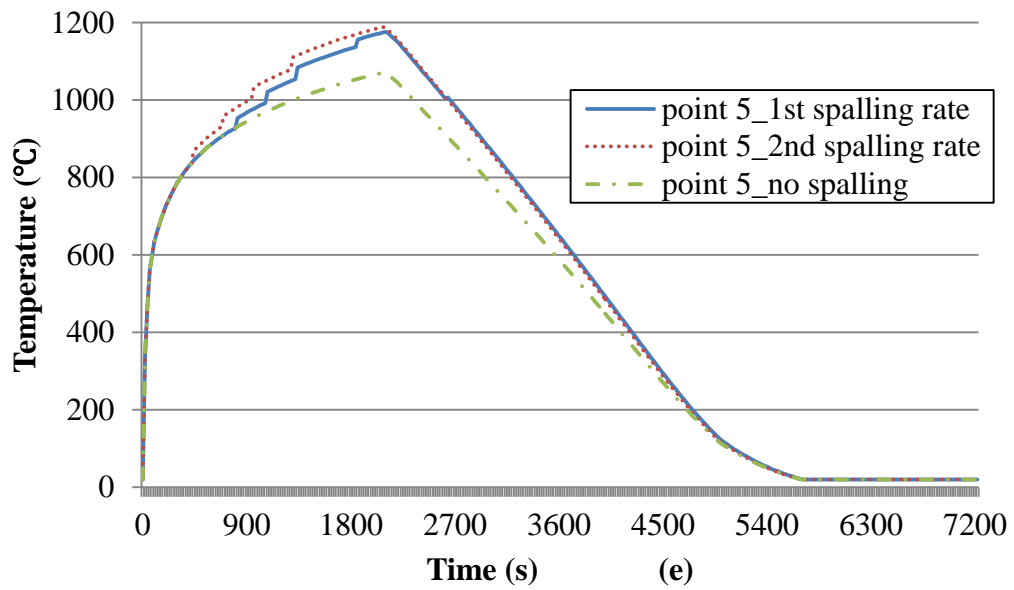
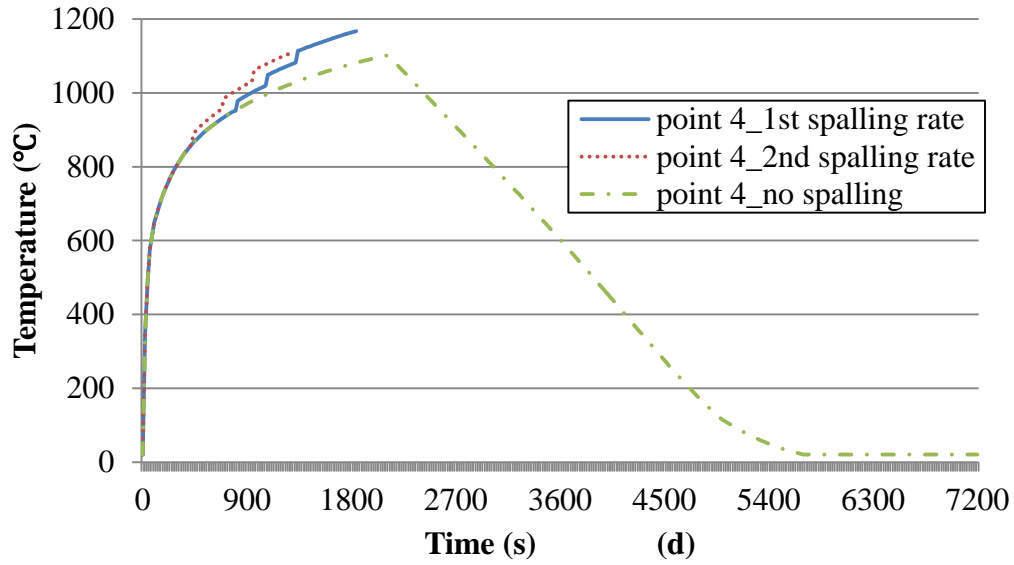


Figure 4-24 Nodal temperature comparison for Model 300 with all spalling rate cases exposed to fire III

5 Conclusions and Future Work

5.1 Introduction

5.2 Conclusions

Based on studying the results of research and theories, explosive spalling normally occurs within the first 30-40 minutes of fire exposure (Khoury, G. A.; Anderberg, Y.;, 2000). Moisture content, heating rate, fire profiles and strength and density of concrete are the critical parameters cause the occurrence of spalling, besides, specimen dimensions and shapes, type of aggregate and test methods should also be considered to avoid concrete spalling. Based on the results from modeling analyses, the following conclusions can be got:

- (1) Spalling phenomenon of high strength concrete influences distributions of temperature in a structural member against fires.
- (2) Type of fires a structural member exposed to have significant influence on spalling. Fire III possesses the highest maximum temperature and a rapidest heating rate at the early stage of fire, which leads to higher potential of occurring of severe spalling in high strength concrete members.
- (3) Reinforced high strength concrete members would fail if spalled off concrete covers, since steel is less stable than concrete in a fire environment and the resistant capacity would be weaken quickly.

5.3 Future Work

- (1) This paper carried out analyses based on two dimensional models, which are the idealized models taken from three dimensional specimens by assumption and approximation. Analyses of three dimensional models needed to simulate the spalling induced heat transfer procedure.
- (2) Only pure concrete models are presented in this paper, reinforced high strength concrete models needed to be introduced and the effects of reinforcements in spalling process would be discussed.
- (3) More accuracy approach of creating idealized models to simulate fire resisted performance of concrete members is still needed to be discussed. In this paper, linear approximation is the method of converting spalling volume to spalling rate, a more accuracy method needs to be discussed.
- (4) Spalling is not isotropic within a cross section, the method of converting irregular area into regular shape which can be calculated and applied needs analyses.

6 References

Connolly. (1995). *The Spalling of Concrete in Fires*. Aston University.

Copier, W. J. (1979). The Spalling of Normalweight and Lightweight Concrete on Exposure to Fire. *ACI Journal* , 219-236.

Diederichs, U; Jumppanen, U-M.; Schneider, U;. (1988). High Temperature Properties and Spalling Behavior of High Strength Concrete. *Fourth Weimar Workshop on High Performance Concrete: Material Properties and Design*, (pp. 219-235). HAB Weimar.

Dwaikat, M. B.; Kodur, V. K. R.;. (2009). Fire Induced Spalling in High Strength Concrete Beams. *Journal of Fire Technology* , 251-274.

Eurocode2. (1992). *Design of concrete structures, Part 1.2 Gneral rules—Structural fire design*.

Hertz, K. D. (1984). *Heat Induced Explosion of Dense Concretes*. Institute of Building Design.

Institution, B. S. (1985). Fire resistance. In *Structural use of concrete. Code of practice for special*. London.

Khoury, G. A.; Anderberg, Y;. (2000). *Concrete Spalling Review*. Swedish National Road Administration.

Kodur, V. K. (2000). Spalling in High Strength Concrete Exposed to Fire Concerns, Causes, Critical Parameters and Cures. *ASCE Structures Congress*. Philadelphia.

Kodur, V., & Sultan, M. (2003). Effect of temperature on thermal properties of high strength concrete. *Journal of materials in civil engineering* , 101-107.

Malhotra, H. L. (1984). *Spalling of Concrete in Fires*. London: Construction Industry Research and Information Association.

Meyer-Ottens, C. (1974). Behavior of Concrete Structural Members in Fire Conditions. Beton, Germany.

Meyer-Ottens, C. (1977). The Behavior of Concrete Structural Elements in Fires. Spalling of Normal Concrete Elements Under Fire Stress: Causes and Preventive Measures. *Building Research Establishment, Translation 2058* .

Meyer-Ottens, C. (1972). The question of spalling of concrete structural elements of standard concrete under fire loading. *Technical University of Braunschweig* .

Sanjayan, G., & Stocks, L. J. (1993). Spalling of High-Strength Silica Fume Concrete in Fire. *ACI Materials Journal* , 90, 170-173.

Schneider, U. (1988). Concrete at High Temperatures – A General Review. *Fire Safty Journal* , 13 (1), 55-68.

Shunan Bo

411 Webster St. Apt 301, Bethlehem, PA 18015

Tel.: (484)707-4533

Email: shunanbo@gmail.com

Education:

Lehigh University

Aug.2008 – May 2011

Master of Science, Structural Engineering

Harbin Institute of Technology

Sep. 2004 – Jul. 2008

Bachelor of Science, Geotechnical Engineering

Research Experience:

Finite Element Simulation of Fire Induced Spalling in High

Jan. 2010 – May 2011

Strength Concrete Slabs.

Fatigue Evaluation of the full scale orthotropic replacement

Jan. 2009 – Sep. 2009

deck for the Verrazano-Narrows bridge in New York City.